TURUN
YLIOPISTO
UNIVERSITY
OF TURKU

Additive manufacturing of polymer-based drug delivery systems

Effects of semi-solid ink composition and manufacturing process parameters on structural and drug release properties

Juuso Pohjola

TURUN YLIOPISTON JULKAISUJA – ANNALES UNIVERSITATIS TURKUENSIS
SARJA – SER. F OSA – TOM. 65 | TECHNICA – INFORMATICA | TURKU 2025

TURUN
YLIOPISTO
UNIVERSITY
OF TURKU

ADDITIVE MANUFACTURING OF POLYMER-BASED DRUG DELIVERY SYSTEMS

Effects of semi-solid ink composition and manufacturing process parameters on structural and drug release properties

Juuso Pohjola

TURUN YLIOPISTON JULKAISUJA – ANNALES UNIVERSITATIS TURKUENSIS
SARJA – SER. F OSA – TOM. 65 | TECHNICA – INFORMATICA | TURKU 2025

University of Turku

Faculty of Technology
Department of Life Technologies
Biotechnology
Doctoral Programme on Drug Research and Diagnostics (DRD)

Supervised by

Professor Tero Soukka, PhD
Department of Life Technologies
University of Turku
Turku, Finland

Mikael Stolt, DSc
Pharmaceutical Sciences
Bayer Oy
Turku, Finland

Mika Jokinen, DSc
DelSiTech Ltd
Turku, Finland

Reviewed by

Niklas Sandler, PhD
CurifyLabs Oy
Helsinki, Finland

Associate Professor Natalja Genina, PhD
Department of Pharmacy
University of Copenhagen
Copenhagen, Denmark

Opponent

Professor Hélder A. Santos, DSc
Department of Biomaterials &
Biomedical Technology
University Medical Center Groningen /
University of Groningen
Groningen, the Netherlands

ISBN 978-952-02-0386-3 (PRINT)
ISBN 978-952-02-0387-0 (PDF)
ISSN 2736-9390 (Print)
ISSN 2736-9684 (Online)
Painosalama, Turku, Finland 2025

UNIVERSITY OF TURKU
Faculty of Technology
Department of Life Technologies
Biotechnology
JUUSO POHJOLA: Additive manufacturing of polymer-based drug delivery systems: Effects of semi-solid ink composition and manufacturing process parameters on structural and drug release properties
Doctoral Dissertation, 189 pp.
Doctoral Programme on Drug Research and Diagnostics (DRD)
August 2025

ABSTRACT

Controlled release drug delivery systems enable the maintenance of drug levels within the therapeutic window for extended periods, thereby enhancing the treatment efficacy and patient compliance. However, there is a growing desire for further customization of drug products to meet the individual needs of patients. Various 3D printing techniques have emerged as potential manufacturing options that enable the personalization of the product size, shape, dosage, and drug release kinetics. In particular, the semi-solid extrusion (SSE) method has shown promise due to its versatility and compatibility with a wide range of materials and drugs. However, the process applies specific rheological requirements on the materials used, and optimization of the printing process is necessary for new formulations.

This thesis investigates the potential of SSE in the preparation of polymer-based drug delivery systems for the long-term macromolecule release. Extrudable inks containing biodegradable polymeric microspheres within a Carbopol hydrogel matrix were formulated, and their rheological properties and printability were assessed. Additionally, a solvent-based post-processing method was developed for tailoring the microstructure of the printed objects. Finally, microspheres encapsulating the model hydrophilic macromolecule drug fluorescein isothiocyanate-dextran (FITC-dextran) were formulated and incorporated into the inks, and drug release from the printed systems was studied *in vitro*. The results indicated that the microsphere concentration within the ink influenced its rheological properties and printability. Notably, the extrudate swell phenomenon was identified as a critical factor in the printing process, affecting both the final object resolution and suitable process parameters. Post-processing by exposure to solvent vapor caused progressive fusing of the particles, increasing the object density and mechanical strength. The release of FITC-dextran from the printed systems was affected by both the ink composition and the post-processing step, enabling different drug release profiles over durations of up to three months.

KEYWORDS: 3D printing, FITC-dextran, microsphere, PLGA, rheology, semi-solid extrusion, controlled release

TURUN YLIOPISTO
Teknillinen Tiedekunta
Bioteknologian laitos
Bioteknologia
JUUSO POHJOLA: Polymeeripohjaisten lääkeannostelujärjestelmien 3D-tulostus: Puolikiinteän musteen koostumuksen ja prosessiparametrien vaikutus rakenteellisiin ominaisuuksiin ja lääkeaineen vapautumiseen
Väitöskirja, 189 s.
Lääketutkimuksen ja diagnostiikan tohtoriohjelma (DRD)
Elokuu 2025

TIIVISTELMÄ

Kontrolloidusti lääkeainetta vapauttavat järjestelmät mahdollistavat pidempiaikaisen lääkeainepitoisuuksien ylläpitämisen terapeuttisella alueella, parantaen näin hoidon tehokkuutta ja noudattamista potilailla. Halu tuotteiden kustomointiin potilaiden yksilöllisten tarpeiden täyttämiseksi on kuitenkin kasvussa. Erilaiset 3D-tulostustekniikat ovat nousseet potentiaalisiksi valmistusmenetelmiksi mahdollistaen tuotteen koon, muodon, lääkeannoksen ja vapautumisnopeuden räätälöinnin. Erityisesti puolikiinteä ekstruusio (SSE) on osoittautunut lupaavaksi, sillä se on monipuolinen ja yhteensopiva laajan materiaali- ja lääkeainevalikoiman kanssa. Prosessi kuitenkin asettaa erityisiä reologisia vaatimuksia käytetyille materiaaleille, ja tulostusprosessin optimointi uusille formulaatioille on tarpeen.

Tässä väitöskirjassa tutkitaan SSE-menetelmän potentiaalia polymeeripohjaisten lääkeannosteluärjestelmien valmistamisessa makromolekyylien pitkäaikaista vapautusta varten. Ekstrudoitavia musteita valmistettiin lisäämällä biohajoavia polymeerisiä mikropartikkeleita Carbopol-hydrogeelimatriisiin, ja musteiden reologisia ominaisuuksia sekä tulostettavuutta tutkittiin. Lisäksi kehitettiin liuotinperusteinen jälkikäsittelymenetelmä tulostettujen kappaleiden mikrorakenteen räätälöimiseksi. Lopuksi, fluoreskeiini-isotiosyanaatti-dekstraani (FITC-dekstraani) -malliainetta kapseloitiin musteissa käytettäviin mikropartikkeleihin, ja lääkeaineen vapautusta tulostetuista kappaleista tutkittiin *in vitro*. Tulokset osoittivat, että musteen mikropartikkelipitoisuus vaikutti sen reologisiin ominaisuuksiin ja tulostettavuuteen. Erityisesti suulakepaisuma tulostusprosessissa vaikutti kriittisesti sekä lopullisen kappaleen tarkkuuteen että sopiviin prosessiparametreihin. Liuotinhöyrylle altistaminen jälkikäsittelyssä johti partikkelien progressiiviseen sulautumiseen ja siten kappaleen tiheyden ja mekaanisen lujuuden kasvuun. FITC-dekstraanin vapautuminen tulostetuista kappaleista riippui sekä musteen koostumuksesta että jälkikäsittelyvaiheesta, mahdollistaen erilaisten lääkeaineen vapautumisprofiilien aikaansaamisen jopa kolmen kuukauden ajalle.

ASIASANAT: 3D-tulostus, FITC-dekstraani, mikropartikkeli, PLGA, reologia, puolikiinteä ekstruusio, kontrolloitu vapautuminen

Table of Contents

Abbreviations

2PP	two-photon polymerization
3D	three-dimensional
3ITT	three-interval thixotropy test
ABS	acrylonitrile butadiene styrene
API	active pharmaceutical ingredient
ASTM	American Society for Testing and Materials
CA	cellulose acetate
CAD	computer-aided design
CLIP	continuous liquid interface production
CLSM	confocal laser scanning microscope
DCM	dichloromethane
DIW	direct ink writing
DLP	digital light processing
DMSO	dimethyl sulfoxide
DPE	direct powder extrusion
EE	encapsulation efficiency
EVA	poly(ethylene vinyl acetate)
FD	FITC-dextran
FDA	U.S. Food and Drug Administration
FDM	fused deposition modelling
FE-SEM	field emission scanning electron microscope
FFF	fused filament fabrication
FITC	fluorescein isothiocyanate
GMP	Good Manufacturing Practice
HME	hot-melt extrusion
HPMC	hydroxypropyl methylcellulose
ISO	International Organization for Standardization
IUPAC	International Union of Pure and Applied Chemistry
IVIVC	*in vitro-in vivo* correlation
LD	loading degree
LVR	linear viscoelastic region

MCC	microcrystalline cellulose
NaOH	sodium hydroxide
O-R-O	oscillation-rotation-oscillation (three-interval thixotropy test)
O/W	oil-in-water emulsion
PAM	pressure-assisted microsyringe
PAT	Process Analytical Technology
PBF	powder bed fusion
pbo	placebo
PBS	phosphate buffered saline
PCL	poly(ε-caprolactone)
PDLLA	poly(D,L-lactide)
PDMS	polydimethylsiloxane
PEA	poly(ester amide)
PEG	poly(ethylene glycol)
PETG	polyethylene terephthalate glycol
PGA	poly(glycolide)
PLA	poly(lactide)
PLGA	poly(lactide-co-glycolide)
PLLA	poly(L-lactide)
PLLGA	poly(L-lactide-co-glycolide)
PMMA	poly(methyl methacrylate)
POE	poly(ortho ester)
PU	polyurethane
PVA	poly(vinyl alcohol)
PVAc	poly(vinyl acetate)
PVP	poly(vinyl pyrrolidone)
RCF	relative centrifugal force
R-R-R	rotation-rotation-rotation (three-interval thixotropy test)
SEC	size exclusion chromatography
SLA	stereolithography
SLS	selective laser sintering
SSE	semi-solid extrusion
STL	stereolithography (file format)
THF	tetrahydrofuran
USP	United States Pharmacopeia
UV	ultraviolet
W/O	water-in-oil emulsion
W/O/W	water-in-oil-in-water double emulsion

Symbols

A	area
C	circularity
D	filament diameter
D_i	particle diameter i percentile
D_n	nozzle size parameter
D_p	physical nozzle diameter
E	extrusion factor
G'	storage modulus
G''	loss modulus
h	layer height
K	consistency index
L	perimeter
m	mass
M_0	initial weight average molecular weight
M_w	weight average molecular weight
n	flow index
P_r	printability index
Q	volumetric flow rate
S	extrudate swell ratio
t	time
$tan\ \delta$	loss factor
T_g	glass transition temperature
T_m	melting temperature
V	volume
$\dot{\gamma}$	shear rate
η	viscosity
η_a	apparent viscosity
ρ	density
σ	shear stress
σ_e*	ultimate compressive strength
σ_y	yield stress
ω	angular frequency

List of Original Publications

This dissertation is based on the following original publications, which are referred to in the text by their Roman numerals:

I J. Pohjola, M. Jokinen, T. Soukka, and M. Stolt. Polymer microsphere inks for semi-solid extrusion 3D printing at ambient conditions. *J. Mech. Behav. Biomed. Mater.*, 2024; 160: 106783.

II J. Pohjola, T. Soukka, M. Jokinen, and M. Stolt. Material extrusion 3D printing with polymer microsphere inks: Effects of solid volume fraction and extrudate swell on the resolution and suitable processing parameters. *CIRP J. Manuf. Sci. Technol.*, 2025; 60: 182–194.

III J. Pohjola, M. Jokinen, T. Soukka, and M. Stolt. Long-term controlled *in vitro* release of FITC-dextran using polymer-based drug delivery systems manufactured by semi-solid extrusion 3D printing. *Int. J. Pharm.*, 2025; 684: 126176.

1 Introduction

Many drugs suffer from limited efficacy due to factors such as poor solubility, instability, limited absorption, and a narrow therapeutic window.[1]–[4] Additionally, conventional therapeutic approaches frequently result in fluctuating blood plasma drug levels, which can reduce the treatment efficacy and increase the risk of adverse side effects.[1]

To maintain drug plasma levels within the therapeutic window for longer times, controlled release drug delivery systems have been developed.[5], [6] These systems often utilize biodegradable polymers, typically formulated as microparticle depots or implants, to protect the drug molecules from degradation and to regulate the drug release kinetics.[7] However, the development of such systems requires careful consideration of various aspects. For example, biological macromolecules often suffer from instability, as well as low diffusion in the polymer matrices, limiting the suitable processing and formulation method options.[8]–[10] To address the limitations associated with the current pharmaceutical treatments, the development of novel approaches is required.

3D printing has the potential to transform the pharmaceutical sector by providing enhanced flexibility and customization in drug formulation. These technologies enable the production of personalized dosage forms with tailored drug release profiles according to individual patient needs, thus addressing the shortcomings of traditional “one size fits all” approaches.[11]–[13] Among the various 3D printing techniques, semi-solid extrusion (SSE) stands out for its ability to create complex drug delivery systems with tailored release profiles while accommodating the use of traditional pharmaceutical grade excipients and thermolabile drugs. However, the inks used in the SSE process must meet specific rheological requirements, and printability remains a critical factor for the successful implementation of the technology.[12], [14]

The purpose of this thesis was to evaluate the potential of SSE 3D printing in the preparation of polymer-based drug delivery systems for long-term controlled release of macromolecule drugs. Inks composed of biodegradable polymeric microspheres within a hydrogel matrix were formulated to enable extrusion at ambient conditions, and their rheological properties were characterized. Ink behavior in the 3D printing

process was assessed with various methods, and printing process optimization was conducted. A solvent-based post-processing method was investigated to control the microstructure of the printed objects at low temperatures. Additionally, printed systems containing fluorescein isothiocyanate-dextran (FITC-dextran) -loaded microspheres were analyzed *in vitro* to gain insights on their degradation and drug release behavior for up to three months.

2 Review of the Literature

2.1 Controlled drug delivery

Drugs form an essential part of the modern medicine, playing a pivotal role in diagnosing, treating, alleviating, curing, or preventing diseases. While the terms "drug" and "drug product" refer to final products that consist of active pharmaceutical ingredients (APIs) and other materials, in this context, the term "drug" is also used to denote the API component to ensure consistency with the other terms.[15], [16]

Despite the advances in pharmaceutical science and the development of new drug products, traditional therapeutic approaches often encounter significant limitations. These limitations are due to the inherent characteristics of drugs and the complexities of human physiology. Challenges such as *in vivo* drug solubility, stability, and physical barriers to absorption can prevent drugs from reaching their target organs and causing their desired effects, leading to suboptimal treatment outcomes.[2]–[4] Moreover, conventional drug delivery systems typically result in fluctuating drug levels in the bloodstream, with concentrations peaking above the minimum effective concentration and then falling below it. This variability can reduce therapeutic efficacy, induce side effects, and necessitate frequent dosing, which may compromise patient compliance, especially in chronic conditions.[1], [10] It has been reported that the patient adherence to long-term medication reaches only 25–50% with diseases such as glaucoma and cardiovascular complications.[17]

Controlled release drug delivery systems offer an alternative approach that may overcome the limitations of traditional therapies. By ensuring the maintenance of constant drug plasma levels within the therapeutic window (**Figure 1**), these systems enhance the efficacy of the treatment, reduce dosing frequency, and improve patient compliance.[1] This approach also minimizes the risk of toxicity and the occurrence of adverse effects. Controlled release systems are designed to release the drug at a predetermined rate, thereby minimizing drug exposure to the biological environment. Such property becomes important, for example, with drugs that are rapidly metabolized and eliminated from the body. Additionally, these systems may also target drug release to specific sites within the body, minimizing exposure elsewhere and preventing unwanted effects on other organs.[5], [6]

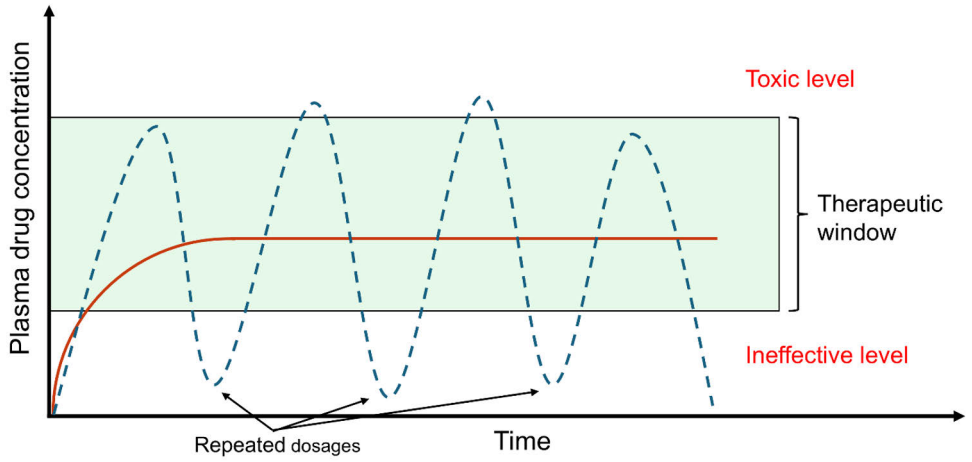

Figure 1. Fluctuating drug plasma concentrations (dashed blue line) are typically observed with traditional drug delivery systems, while controlled drug release systems (red line) maintain the drug plasma levels within a therapeutic window.

The evolution of controlled release drug delivery systems has been marked by significant technological advancements. The first sustained release formulation was introduced in 1952 by Smith, Kline & French (nowadays GlaxoSmithKline) for the 12-hour delivery of dextroamphetamine.[18] Since then, the field has seen remarkable progress with the development of various other systems, ranging from microspheres and drug-eluting implants designed for long-term drug delivery to "smart" polymers that respond to environmental changes.[7], [19]

Despite the advantages of controlled release systems, they are not without challenges. Issues such as patient variability, limited options for dose modification, dose dumping and a weak correlation between the *in vitro* and *in vivo* behaviors present significant obstacles.[15] Furthermore, not all drugs are suitable for controlled release formulations. These include drugs with a long half-life, as well as those that can induce resistance if their levels are maintained at constant levels. Additionally, drugs that require immediate effects may also not benefit from controlled release.[20] These considerations highlight the need for careful selection and design of controlled release formulations to ensure that they meet the specific therapeutic needs of patients.

2.1.1 Routes of administration

The route of drug administration refers to the way a drug enters the body, and selecting the appropriate route is crucial in pharmaceutical science.[21] This choice depends on factors such as the drug's physicochemical properties, convenience,

desired site of action, and whether local or systemic delivery is intended.[1], [22] Each route has its advantages and challenges that influence its suitability.[21], [22] Some of the most common routes are presented in this section.

Oral administration, which utilizes the gastrointestinal tract for drug absorption, is often preferred for its convenience and patient compliance.[2] However, it faces challenges such as first-pass metabolism, which can reduce the drug's bioavailability, as well as the harsh stomach environment that may degrade some drugs. Additionally, the selective permeability of the intestinal epithelium limits the absorption of larger macromolecules.[4], [21], [22]

Nasal and pulmonary routes provide alternatives for systemic delivery while also allowing for local effects. Common dosage forms for nasal administration include dry powders, suspensions, and emulsions, while pulmonary delivery typically uses gases and aerosols. Administration by either route often requires specific devices, such as pumps or inhalers.[23] Both routes avoid first-pass metabolism and enable rapid absorption, with nasal delivery being more suitable for hydrophobic drugs and peptides, while pulmonary delivery is generally limited to small molecules.[22], [24] An additional benefit of nasal administration is the possibility of delivering drugs to the central nervous system through the olfactory region.[24] However, active nasal clearance applies limitations to the drug absorption and bioavailability.[22] While both routes have high absorption rates, they also suffer from inconsistent administration methods among patients.[5], [23]

Topical administration means drug application to the skin, whereas transdermal delivery specifically targets absorption through the skin.[1], [22] Common transdermal dosage forms include gels, lotions, and creams, as well as topically administered solutions, suspensions, powders, and pastes.[23] Transdermal delivery offers good patient compliance and avoids the first-pass metabolism, but is typically limited to small hydrophobic drugs. To enhance the delivery of macromolecule drugs, techniques like microneedles and electroporation have been developed.[22], [25] However, the challenges of this route include low systemic delivery rates and variability, which can, however, be mitigated by specialized delivery patches.[23]

Parenteral administration encompasses routes outside the gastrointestinal tract, including intravenous, intramuscular, and subcutaneous injections.[23] Parenteral administration bypasses the first-pass metabolism, providing high bioavailability and rapid effects, making it ideal for drugs having poor oral bioavailability or instability in the gastrointestinal tract. However, it requires sterile conditions and suffers from decreased patient compliance.[21], [22], [25]

Although many implantable drug delivery systems are often parenterally administered, those administered via a surgical procedure make it reasonable to consider the implantation process separately.[26], [27] Implantation involves placing a drug delivery device directly into the body, often allowing for controlled release over

extended periods.[8] These combination devices are often made either from degradable or non-degradable polymers, and may also have additional device-related functionalities, for example in the case of orthopedics or cardiovascular treatments. Drug administration by implantation is particularly beneficial for localized treatment in cases where systemic drug delivery is ineffective or when the drug has a narrow therapeutic window.[8] The potential advantages of localized therapy over systemic therapy also include lower required doses, reduced systemic exposure, greater control over bioavailability, and the ability to directly target the site of action.[28] Such properties are particularly beneficial in the treatment of solid tumors and infections.[8] However, the surgical administration procedure and a commonly necessary implant removal are significant drawbacks.[29]

2.1.2 Release mechanisms

Drug release refers to the process by which drug molecules transition from the drug delivery system into the surrounding environment.[15], [30] This process is governed by various mechanisms, each with unique characteristics that influence the rate and pattern of drug release. Understanding these mechanisms is crucial for the design and development of effective drug delivery systems that can provide the desired release profiles. It is important to realize that while multiple mechanisms may be present, the rate-controlling process is typically considered the actual release mechanism.[30] Some of the typical mechanisms are presented below and illustrated in **Figure 2**.

Dissolution is the process whereby drug molecules dissolve in a solvent, typically water or bodily fluids, transitioning from a solid phase finally to the surrounding medium.[26], [31] In dissolution-controlled systems, as shown in **Figure 2a**, the drugs are either incorporated within polymeric materials having the desired solubility (monolithic or matrix systems) or coated by them (reservoir systems).[1] The dissolution of the polymer or drug acts as the rate-limiting step, enabling immediate[1], sustained, delayed, or pulsatile release. Factors influencing the dissolution rate include the matrix and the coating materials, system geometry, surface area, drug solubility, and the particle size of the drug.[6], [31] Many oral dosage forms such as tablets are dissolution-controlled drug delivery systems.[1], [20]

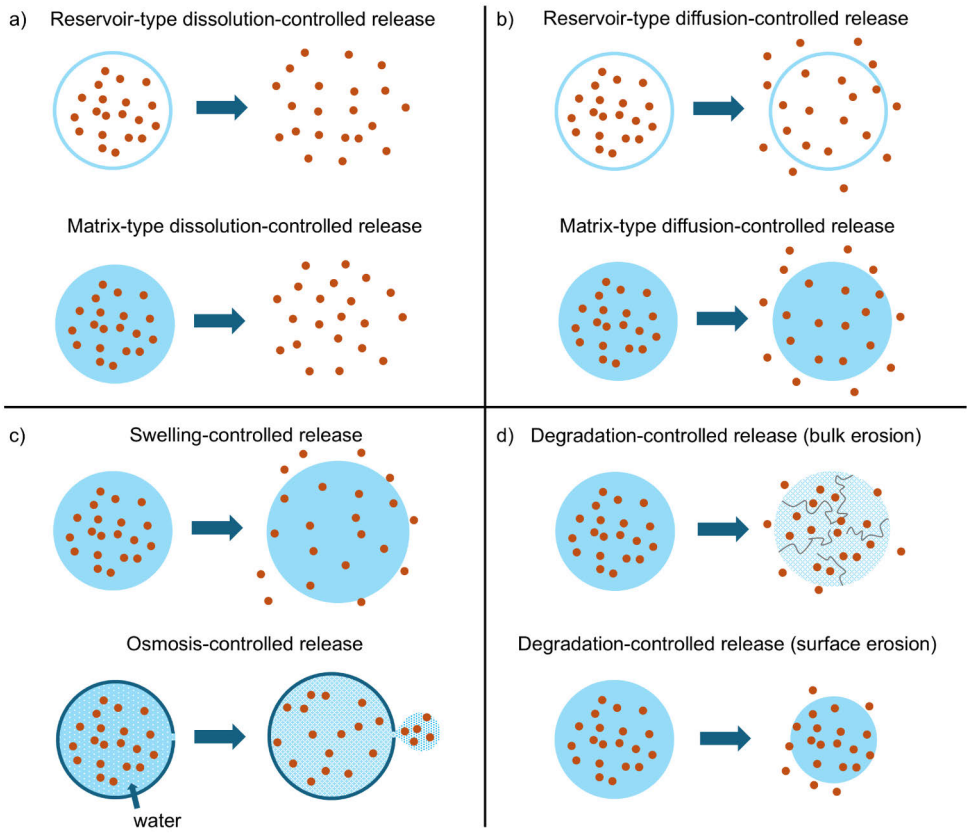

Figure 2. Illustration of typical drug release mechanisms. Dark orange dots represent the drug molecules, whereas the blue areas represent the (typically polymeric) drug delivery system. Of the chemically controlled release mechanisms in d), surface and bulk erosion types are illustrated, and they are discussed more in detail in the section 2.2.1.2.

In diffusion-controlled systems (shown in **Figure 2b**), drug release is driven by a concentration gradient within a non-dissolving matrix (monolithic systems) or through a membrane (reservoir systems).[1] The rate-controlling material is typically polymeric, and Fick's laws of diffusion govern the mass transport process of the dissolved drug molecules.[32], [33] Monolithic systems often exhibit an initial high release "burst" phase, followed by a decrease in release rate due to increased diffusion distance.[10], [26] In contrast, reservoir systems can achieve linear, zero-order release profiles by maintaining excess drug concentration.[32]

Water penetration-controlled systems, as illustrated in **Figure 2c**, can be further categorized into swelling-controlled and osmotically-controlled systems.[1] Swelling-controlled systems use hydrophilic polymers that swell upon contact with fluids, enhancing permeability and facilitating drug diffusion.[34] The release rate is

influenced by polymer chain relaxation and swelling.[10], [34] Osmotic systems leverage osmotic pressure to maintain constant drug release rates over extended periods by generating steady pressure upon exposure to an aqueous environment.[1], [10], [35]

Chemically controlled delivery systems utilize chemical reactions, such as polymer degradation or ion exchange[10], to regulate the drug release. These systems can be polymer-drug dispersion systems, where the drug is dispersed within a biodegradable polymer, or polymer-drug conjugate systems, where the drug is chemically linked to the polymer.[1], [36] In the case of dispersion systems (shown in **Figure 2d**), the release is governed by polymer degradation, and is influenced by factors such as pH, enzymes, and system design.[10], [37] This mechanism is particularly relevant for macromolecules, which suffer from poor diffusivity when compared to small-molecule drugs. In practice, both degradation and diffusion-controlled release may be present.[27] Moreover, the mass-loss of the polymer, erosion, may also promote diffusion by inducing porosity to the structure, in distinction to drug release without diffusion.[30]

2.1.3 Release kinetics

Understanding and predicting drug release kinetics under physiological conditions is essential for developing new drug delivery systems, optimizing their therapeutic efficacy, and ensuring patient safety. To achieve this, various mathematical models have been developed.[26] The models may be mechanistic, empirical, or semi-empirical, depending on whether they have real theoretical background or not.[15], [38] Empirical models are often simpler to implement, but they are not able to provide substantial information about the underlying release mechanisms.[26], [37] The vast variety in the different drug delivery systems makes it impossible to establish a universal model applicable to every case, necessitating the use of different models for the different types of systems.[39], [40]

Some of the most widely used models include the first-order, zero-order, Hopfenberg, Hixson–Crowell, Baker–Lonsdale, Korsmeyer–Peppas, Peppas–Sahlin, and Weibull models.[26] Some of these require specific properties from the delivery systems, such as a certain shape, microstructure, or degradation behavior[38], [40], while others are more general and do not have as strict requirements.[26], [39], [41] The models typically also have additional assumptions or limitations, such as a constant shape[26] of the delivery system or perfect sink conditions[40], making it necessary to consider their applicability carefully. However, an applicable model may give valuable information about the drug release kinetics and mass transport mechanisms, offering a tool for product development and quality control.[1], [26], [38]

2.1.4 *In vitro* drug release testing

In vitro drug release testing is essential in the development and evaluation of drug delivery systems. Conducted under laboratory conditions, these tests mimic the drug release process in the human body without the complexities of actual biological systems. *In vitro* testing is vital in the early stages of drug development, helping to select and optimize formulation candidates before progressing to more costly *in vivo* studies.[42] Additionally, it plays an important role in product quality control by monitoring batch-to-batch consistency and ensuring compliance with specifications.[15], [43] Mathematical models can be applied to the experimental release data as a way to quantify the release properties and to identify the release mechanisms. Multiple types of test methods have been developed for evaluating the drug dissolution or release from different drug delivery systems. These tests can be divided into compendial (official) and non-compendial (unofficial) methods.[15] Some of these are illustrated in **Figure 3** and presented below.

Compendial methods, as outlined in pharmacopeias, are standardized testing procedures widely recognized and accepted by regulatory authorities.[44] The United States Pharmacopeia (USP) categorizes dissolution apparatus into official types; USP I (basket), USP II (paddle) (shown in **Figure 3a** as an example), USP III (reciprocating cylinder), USP IV (flow-through cell) (**Figure 3b**), USP V (paddle over disk), USP VI (rotating cylinder), and USP VII (reciprocating disk), each designed for specific dosage forms and release mechanisms, although they have originally been developed for testing oral and transdermal dosage forms.[15] For instance, USP II is commonly used for testing solid oral dosage forms like tablets and capsules, while USP IV is often preferred for more complex dosage forms, including implants and drugs with low solubility.[45], [46] However, the initial intended use cases for the compendial methods leads into issues when testing novel dosage forms which do not fall into the typical categories.[47] These issues include high dissolution volumes, evaporation of the dissolution media, sample loss, and particle aggregation. Thus, compendial methods may be suboptimal for testing novel dosage forms.[43], [48]

Non-compendial methods, on the other hand, are developed to address the specific testing needs that compendial methods may not fulfill, especially for novel or specialized dosage forms such as nanoformulations[42].[49] The non-compendial methods include the common sample-and-separate, dialysis or membrane diffusion, and continuous flow methods. Each method has its unique setup and application based on the drug formulation.[50] A common aspect of the non-compendial methods is that despite their flexibility and simplicity, the non-standardized methodology dangers the reproducibility of the results.[45], [49]

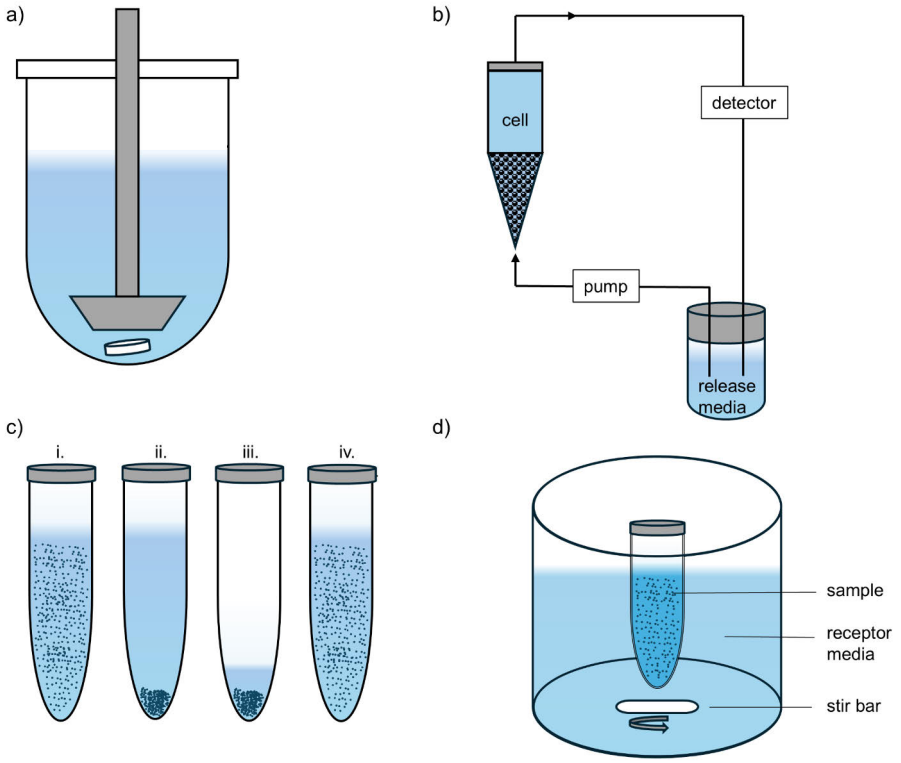

Figure 3. Illustration of some common *in vitro* test methods: a) USP II paddle method, b) USP IV flow-through cell, c) sample-and-separate, and d) dialysis. In c), a particulate sample is shown as an example (i.). After centrifugation (ii.) and supernatant extraction (iii.), equal volume of fresh media is added, followed by redispersing the sample (iv.).

The continuous flow method (**Figure 3b**) utilizes USP IV apparatus or its modification for mimicking the body's fluid flow by circulating the release media over the drug formulation, making it suitable for testing how drugs release under more dynamic conditions.[45], [50] This method, including the sampling procedure and change of the dissolution media, can be automated, but it can also be complex and costly due to the need for specialized equipment.[42]

Sample-and-separate methods, as illustrated in **Figure 3c**, involve simple setups where the drug formulation is placed in the release medium in a suitable container, and drug release is monitored over time. Drug concentration in the media is quantified after physically separating the sample from the media. Separation can be performed either manually or, in the case of particulate samples, by e.g. centrifugation.[48], [51] Typically, the separated sample is also returned, and fresh media is added to compensate the drawn sample volume. These methods are flexible and can be adjusted based on the formulation being tested, but may face challenges in the physical separation, as well as aggregation of particulate samples.[42], [50]

Dialysis and membrane diffusion methods (**Figure 3d**) utilize semi-permeable membranes to separate the drug formulation from the receptor media, i.e. that part of the release media which will be used for quantifying the drug concentration. These methods are useful for testing particulate dosage forms due to their convenient sampling procedures.[49] However, they may exhibit misleading release kinetics if the membrane influences drug diffusion. Additional challenges associated with the dialysis method include poor agitation inside the dialysis devices, which might promote particle aggregation. There is also a risk of violating the sink conditions. However, conducting the release study using a reverse dialysis method may help in avoiding these issues.[45], [50]

One of the fundamental aspects of *in vitro* testing is simulation of the drug release in biological conditions.[37] However, translating the *in vitro* results to the real *in vivo* environment may not be straightforward. The *in vitro-in vivo* correlation (IVIVC) aims to set a relationship between an *in vitro* property of the drug and the *in vivo* response through a mathematical model. For example, the *in vivo* drug plasma concentration can be compared to the amount of drug released *in vitro*.[51] Establishing a robust IVIVC is crucial for enhancing the utility of the *in vitro* studies, guiding formulation and process changes, and establishing clinically relevant specifications for the *in vitro* release.[42] Once validated, IVIVC can minimize the need for extensive human or animal studies, serving as a surrogate for bioequivalence studies.[49], [50] The U.S. Food and Drug Administration (FDA) defines four main IVIVC levels, ranging from Level A point-to-point correlations to Level D rank order comparisons between *in vitro* and *in vivo* release profiles.[45] Setting the IVIVC for novel non-oral drug delivery systems poses significant challenges due to their complex nature, as well as the lack of standardized *in vitro* release testing methods.[49], [52] Accurate simulation of physiological variables, such as body temperature, pH, metabolism, and the specific conditions at the administration site, is necessary to achieve *in vivo* relevance and to ensure the predictive accuracy of the *in vitro* tests.[37] Moreover, tissue responses, such as fibrous encapsulation may affect drug release *in vivo*, necessitating careful consideration in IVIVC establishment.[43] These challenges have been recognized, but current guidance from the regulatory authorities remains limited.[45], [47]

2.2 Polymer-based controlled drug delivery systems

The therapeutic benefit of a drug is closely linked to how it is formulated and delivered within the body.[5] Polymers are employed in drug delivery systems due to their ability to modulate the pharmacokinetics of drugs, for example, to achieve controlled drug release. In addition, polymers may serve as carriers that protect drugs

from premature degradation and improve drug solubility and bioavailability.[1]. This section presents important polymer-based controlled drug delivery systems as well as the common materials used in the field.

2.2.1 Materials in polymer-based controlled drug delivery

Although the incorporation of bioactive molecules into polymeric materials was first described in the 1950s, the initial application was for agricultural purposes. The medical applications were realized later in the 1960s, starting the history of polymer-based drug delivery systems. Since then, their use has evolved greatly, and they have become an essential part of modern pharmaceutical development.[5] Polymers used in controlled drug delivery systems can be broadly classified based on their origin (natural or synthetic) and their stability (biodegradable or non-degradable).[53] Natural polymers, such as proteins and polysaccharides, have a long history in medical applications but may suffer from batch-to-batch variability and potential immunogenicity. Synthetic polymers, on the other hand, offer consistency and can be tailored to possess the desired properties.[27], [54] This section presents typical polymers used in controlled release applications, with an emphasis on materials intended for long-term drug delivery. The polymers are categorized based on their stability.

2.2.1.1 Non-degradable polymers

Despite the current interest towards degradable polymers, the non-degradable options have remained a viable choice for several applications, especially for those where durability, good mechanical properties, or controlled drug release over months or years is desired.[37], [55] Due to their inert nature, non-degradable polymers often lead to diffusion-controlled drug release where the drug release kinetics are affected by the design of the drug delivery system, the permeability of the polymer, and the solubility of the drug.[56] However, there are also great differences. Some polymers are extremely hydrophobic whereas the others are hydrophilic and prone to swelling. The physical and mechanical properties range from soft and flexible to rigid and brittle, with certain materials also exhibiting tailorable properties. Some materials are thermoplastic and heat-processable, while others can undergo chemical crosslinking. This variation in properties has led to the development of drug delivery systems that range from non-implantable to implantable systems and from short-term to long-term release applications.[37], [57] Typical non-degradable polymers used in controlled drug delivery systems are presented in **Table 1**.

Table 1. Characteristic information of common non-degradable polymers used in controlled drug delivery.

Polymer	Structure	Properties	Applications	Reference
Poly(ethylene vinyl acetate) (EVA)	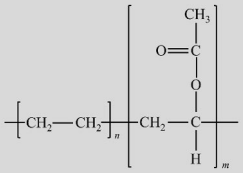	• Modifiable by tailoring the copolymer ratio • Good thermal processability • Suitable for small molecule drugs and macromolecules	• Implantable systems • Long-term release	[37], [55], [57]
Polydimethylsiloxane (PDMS)		• Exceptional flexibility • Compatibility with hydrophobic drugs • Possibility for zero-order release • Crosslinkable	• Reservoir and matrix-type devices • Long-term release	[37], [57]
Poly(methyl methacrylate) (PMMA)	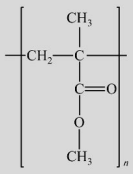	• Excellent biocompatibility • Hard, rigid, and brittle	• Prosthetic and orthopedic devices • Particulate drug delivery systems • Combination products (e.g. antibiotic-eluting bone cement) • Long-term release	[58], [59]
Poly(vinyl alcohol) (PVA)*	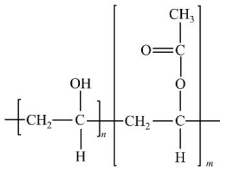	• Modifiable by tailoring the degree of hydrolysis • Hydrophilic and water-soluble • Good film-forming properties • Low protein adsorption	• Implantable and non-implantable medical devices and drug delivery systems • In combination with other polymers • Short and mid-term release	[60]–[62]
Polyurethane (PU)	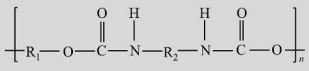	• Modifiable by tailoring the composition and ratio of soft and hard segments • Strong and moldable	• Medical devices and combination products	[37], [63]

*Partially hydrolyzed form of PVA is illustrated

2.2.1.2 Biodegradable polymers

Since the 1960s, biodegradable polymers have revolutionized the field of drug delivery by offering new approaches to controlled drug release.[5] They are particularly valued for their ability to break down into non-toxic, natural byproducts within the body, thereby eliminating the need for surgical removal of the drug delivery system after releasing the drug. This enhances the convenience from the patient's perspective, but also reduces the healthcare costs.[64] In addition, these polymers offer the flexibility to achieve different release profiles and they can also be fabricated into various delivery systems such as implants, *in situ* forming implants, microspheres, and nanoparticles.[27]

According to the International Union of Pure and Applied Chemistry (IUPAC), the term "biodegradable" refers to the chemical breakdown of the material due to cellular or *in vivo* biological actions, leading to its eventual elimination from the body. However, many polymers used in drug delivery systems are in fact "degradable", meaning that although they are cleaved by hydrolysis or enzymatic activity, the processes do not necessarily occur due to biological actions.[65] For simplicity, here all degradable polymers are called as "biodegradable", regardless of the actual process of degradation. Examples of the labile bonds present in common biodegradable polymers are ester, amide, or anhydride bonds.[37], [65] "Erosion" is another frequently encountered term, and it means the physical mass loss of the material, often occurring after degradation, thus distinguishing from the chemical degradation process.[27], [53]

Biodegradable polymers can be categorized into bulk-degrading and surface-degrading types (**Figure 2**).[37] Surface degradation occurs when water penetration into the polymer is slower than the erosion rate, confining degradation to the outer surface. Such a behavior is typical for highly hydrophobic polymers. Surface degradation is often desirable for its reproducibility and the potential for zero-order drug release, but also because it can protect water-labile drugs until their release. Bulk degradation, on the other hand, occurs when water penetrates the matrix at a higher rate than the erosion takes place, leading to a more homogeneous degradation throughout the material.[65] This mechanism is typical for many biodegradable polymers used in controlled drug delivery.[53]

Despite their advantages, biodegradable polymers may have limitations, such as suboptimal drug release rates and uncontrollable kinetics, which can hinder the performance of drug delivery systems.[53], [65] This is often the case with the commonly used polymers, which will be presented below. The biodegradation can be influenced by various factors such as the polymer composition, crystallinity, molecular weight, size and shape of the drug delivery system, and the physicochemical environment, which brings versatility to the designing of these systems but also increases the complexity of the development work.[27], [54]

Additionally, the degradation process might produce acidic byproducts that could cause local irritation, bringing another factor to consider.[53] However, due to the aforementioned benefits, the use of biodegradable polymers and the development of novel drug delivery systems is well justified. Typical biodegradable polymers used in controlled drug release applications are presented in the following text.

Poly(esters) are the cornerstone of biodegradable polymers for drug delivery applications, offering biocompatibility and controlled degradation. They are hydrophobic and bulk-degrading polymers, and their degradation is based on hydrolytic cleavage of the ester bonds.[64] The synthesis of poly(esters) through ring-opening polymerization or condensation polymerization, along with their low toxicity, has facilitated their commercial availability and broad application in the biomedical field and drug delivery systems. These applications range from particulate systems to implants, and from small molecules to macromolecules.[27], [65], [66] Among these polymers, poly(lactide) (PLA), poly(glycolide) (PGA), poly(lactide-co-glycolide) (PLGA), and poly(ε-caprolactone) (PCL) represent the most extensively studied and utilized materials in the field. These polymers are presented in **Table 2**.

Despite their widespread use, poly(esters) present challenges, including the release of acidic degradation products that can lead to local irritation and potentially affect the stability of encapsulated therapeutics.[53], [67] This is the case especially with the faster degrading polymers. The release of acidic degradation products also leads to an autocatalytic effect, where the interior part of larger objects degrades faster due to the more acidic microclimate.[27] However, there are strategies to control the local pH levels, for example by adding buffering agents to the formulation.[54] Alternatively, these drawbacks can possibly be avoided by selecting other biodegradable polymers, some of which are presented in **Table 3**. These materials may offer the much-desired surface degradation property, resulting in a zero-order release profile, as well as wide options for tailoring the properties through chemical conjugation or by adjusting the monomer composition.[53], [68]

Table 2. Characteristic information of common biodegradable poly(esters) used in controlled drug delivery.

Polymer	Structure	Properties	Applications	Reference
Poly(lactide) (PLA)	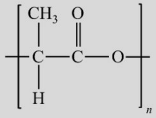	• Depending on the enantiomeric forms (D and L) of the monomer ○ poly(L-lactide) (PLLA) is highly crystalline with melting temperature (T_m) ≈ 170 °C ○ racemic poly(D,L-lactide) (PDLLA) is amorphous with glass transition temperature (T_g) ≈ 55–60 °C • Long degradation time (> 1 year)	• Controlled release systems • Films • Tissue engineering scaffolds	[27], [53], [63]
Poly(glycolide) (PGA)	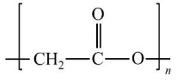	• High crystallinity • Good mechanical strength • Degrades faster than PLA • High T_m (>200 °C) • T_g ≈ 35–40 °C • Poor solubility in organic solvents	• Sutures • Orthopedic implants • Tissue engineering scaffolds	[53], [63]
Poly(lactide-co-glycolide) (PLGA)	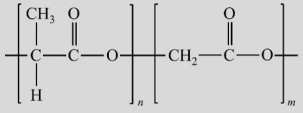	• Affected by the copolymer composition and the end-group capping • Adjustable degradation times from days to years • Typically exhibits a triphasic release profile	• Controlled release systems • Sutures • Tissue engineering scaffolds	[53], [54], [63], [65], [67]
Poly(ε-caprolactone) (PCL)	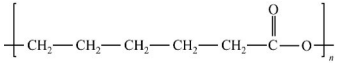	• Low T_g (≈ -60 °C) and T_m (≈ 60 °C) • Long degradation time (>2 years) • High elasticity • Permeable to small molecule drugs	• Tissue engineering scaffolds • Implantable systems for long-term drug release • Blended with other polymers	[54], [63], [65]

Table 3. Characteristic information of other common biodegradable polymers used in controlled drug delivery.

Polymer	Structure*	Properties	Applications	Reference
Poly(ortho ester) (POE)	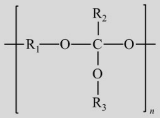	• Surface degrading • Tunable properties • Good processability	• Controlled release systems (especially class IV POE)	[27], [53], [65], [69], [70]
Poly(anhydride)	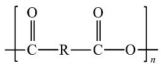	• Surface degrading • Adjustable degradation times • Poor mechanical properties • High T_m	• Controlled release systems	[27], [53], [63], [65]
Poly(phosphoester)	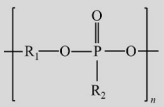	• Backbone similarity to DNA/RNA • Modifiable by tailoring the R group composition • Fast degradation	• Drug delivery systems • Tissue engineering scaffolds	[53], [63], [65]
Poly(ester amide) (PEA)	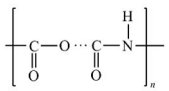	• Good mechanical properties • Adjustable degradation times • Possibility for chemical conjugation	• Drug delivery systems • Tissue engineering scaffolds • Films and coatings	[65], [68], [71]
Poly(phosphazene)	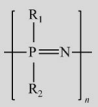	• Modifiable by tailoring the size chain composition	• Drug delivery systems • Tissue engineering scaffolds	[27], [53], [63], [72]
Poly(carbonate)	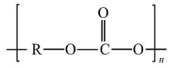	• Surface degrading • Slow degradation • Properties depend on composition	• Drug delivery systems • Tissue engineering scaffolds	[63], [65]

* Example structures of the different polymer types are illustrated.

2.2.2 Long-term controlled release systems

The efficacy and safety of many drugs have been enhanced by using systems that precisely control their release rate, timing, and target site within the body.[22] For example, micro- and nanoparticle systems, hydrogel-based matrices, and implants are available for long-term controlled release applications, particularly for those requiring sustained therapeutic levels or localized site-specific activity.[10] However, the development of a delivery system for a certain therapeutic agent requires careful consideration. The parameters to consider are related either to the formulation or the drug molecule. Formulation-related parameters include, for example, the route of administration, carrier and matrix material properties, and desired drug release kinetics, whereas drug-related parameters include the drug properties and regulatory aspects.[1] For example, large molecules, such as proteins and peptides, often suffer from poor biostability, limited diffusivity, and instability[8], [9] at harsh conditions, applying restrictions to their processability and release performance.[10] This section presents two common, often polymeric, drug delivery systems capable of achieving long-term controlled drug release: microparticle depots and implant systems. These systems have shown great promise for the delivery and release of macromolecules, as well as other molecules that suffer from insufficient delivery to the target site.[27]

2.2.2.1 Microparticle depots

Microparticles are particles with diameters in a micrometer range, although in pharmaceutical applications the size range typically falls below 100 µm.[73] They are often spherical, allowing for the use of the terms microsphere or microcapsule, depending on the particle structure.[9] However, non-spherical particles are not uncommon either.[73] Microparticles generally consist of a polymeric matrix in which the drug is either dispersed or dissolved, or alternatively the drugs are encapsulated within a polymeric shell.[27], [74] The polymer component controls the drug release, typically from weeks to months, by gradual degradation, by acting as a diffusional barrier, or a combination of both.[9], [73] With their micrometer range particle size, microparticles enable administration through various routes such as oral or pulmonary.[73] However, to achieve long-term controlled release, the injectable parenteral (subcutaneous or intramuscular) depot formulations have been a common approach, especially in the case of macromolecules[29].[54], [75] Administration by injection enables easy dosage adjustment, avoids surgical procedures and can be conducted without anesthesia, increasing the convenience and patient acceptance.[64], [74] Due to their non-retrievable nature, microparticle formulations have greatly benefitted from the application of biodegradable polymers.[29]

Microparticles can be produced through various methods, each with distinct advantages and challenges. Common techniques include emulsification-solvent

evaporation, spray drying, and coacervation. Some of these are presented below and illustrated in **Figure 4**.

Emulsification-solvent evaporation method is valued for its simplicity and versatility in creating single or multiple emulsions by using solid and/or liquid phases, depending on the drug solubility.[76], [77] In a typical single emulsion process (**Figure 4a**), the drug and the polymer are dissolved in an organic phase, which is dispersed in a larger volume of a continuous aqueous phase that typically contains a surfactant for stabilization, forming an oil-in-water (O/W) emulsion. After emulsification, the solvent evaporates, hardening the microparticles, which are then separated by, e.g., centrifugation, washed, and often finally freeze-dried. Double emulsion process (**Figure 4b**), on the other hand, is typically used for encapsulating hydrophilic drugs. In this method, the drug is first dissolved in an aqueous solvent, which is then dispersed in the organic phase to form a primary water-in-oil (W/O) emulsion. Next, the second emulsion is created similarly to the single emulsion process, yielding a water-in-oil-in-water (W/O/W) emulsion.[73], [77], [78] Typical process parameters include the drug, polymer and surfactant components, volumes and concentrations[79] of the different phases, and the time and intensity of the emulsification process.[76] Despite the versatility of the emulsification methods, they suffer from limited scalability, non-uniform particle size, and challenges in removing the toxic solvents.[76]–[78]

In spray drying, the drug and polymer are dissolved in a volatile organic solvent, which is then atomized (**Figure 4c**). The atomized fluid is subjected to a drying gas, usually at elevated temperature, leading to solvent evaporation and hardening of the particles.[9], [27] The particles are finally separated from the gas. This method is particularly useful for the encapsulation of hydrophobic drugs, although hydrophilic drugs can also be encapsulated by atomizing an emulsion.[27], [76] Spray dying can be carried out as a continuous process in an industrial scale.[80] Easy control over the process parameters, such as the flow rate and inlet temperature, enables convenient control over the product properties. However, the method may suffer from a low yield, high operating temperatures, and complications in the product separation.[76]

Coacervation, also known as phase separation, is based on controlling the solubility of the polymer to initiate the formation of the microparticles (**Figure 4d**).[9], [76] This can be achieved by various means such as changing the temperature, pH and ionic strength of the system, adding other polymers, or by using an organic nonsolvent.[9], [27] In the process, the drug is dissolved, suspended, or emulsified in a polymer solution, which is then exposed to coacervating agents to form a polymer coating around the core.[27], [64] For example, the drug can be emulsified in the polymer phase, which is then mixed with an organic non-solvent in which the polymer has negligible solubility. The solvent is extracted from the polymer (coacervate) phase, leading to hardening of the polymer.[76] Coacervation is

especially useful for encapsulating hydrophilic drugs, as their partitioning into an external aqueous phase can be avoided. However, the method is sensitive to process parameter changes, and residual coacervating agents can be a significant drawback.[64], [80]

To overcome the limitations of conventional preparation methods, novel approaches such as membrane emulsification and droplet microfluidics have been developed. In membrane emulsification (**Figure 4e**), the droplets are generated by forcing the polymer solution though a microporous membrane. Droplet microfluidics, as illustrated in **Figure 4f**, employs precise control over the flow of solutions within microchannels and microchips with specific designs, allowing for the controlled generation of droplets with a desired structure, one at a time.[9], [80], [81] These advanced methods provide better control over the particle size, morphology, and drug encapsulation, enhancing the efficiency of microparticle preparation.[9]

Several factors influence the drug release from microparticles, including the particle porosity, molecular weight of the polymer, and size of the particles. Typically, the drug release rate increases when the porosity of the particles increases, the molecular weight of the polymer decreases, and when the size of the particles decreases.[79] The release is primarily governed by drug diffusion from the polymer matrix and the matrix erosion. Common microparticle formulations, especially those containing macromolecules, typically exhibit a triphasic release profile characterized by an initial burst release, a lag phase, and a final release phase. This behavior can limit the treatment efficacy and is a notable drawback of microparticle systems.[9], [64], [67]

Despite these challenges, several microparticle products have received clinical approval. Examples of marketed polymeric microparticle products are listed in **Table 4**, illustrating the diverse range of therapeutics that can be delivered and released over varying durations. Microparticle formulations are prominent in parenterally administered controlled release systems, with 14 clinically approved products as of 2021.[9], [64] Most formulations are based on PLGA, although other polymers are also under investigation.[29], [65]

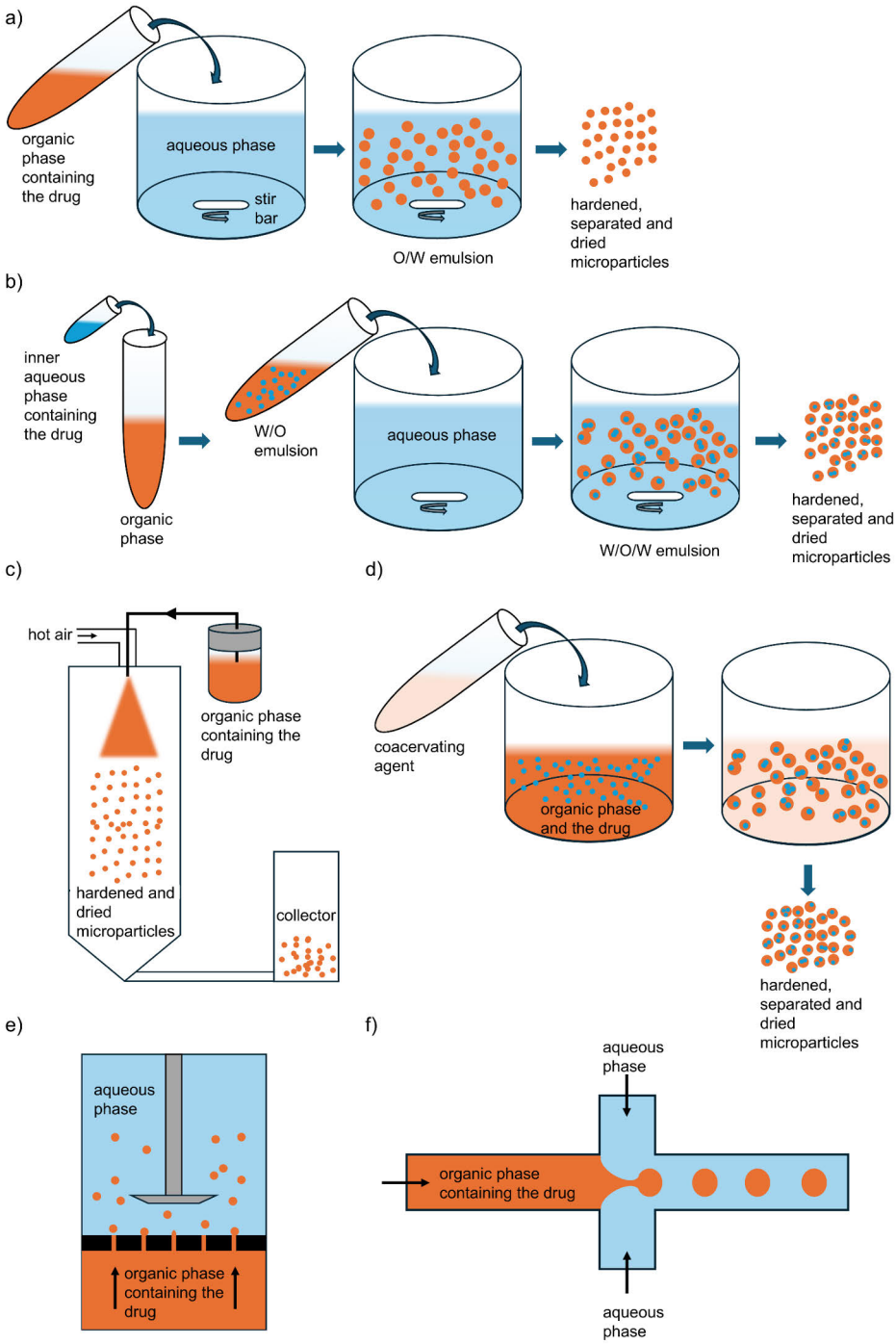

Figure 4. Principles of common methods for manufacturing drug-loaded microparticles: a) single emulsion, b) double emulsion, c) spray drying, d) coacervation, e) membrane emulsification, and f) droplet microfluidics.

Table 4. Examples of marketed polymer microparticle drug delivery systems.

Product	Polymer	Drug	Indication	Duration	Reference
Lupron Depot®	PLGA/PLA	Leuprolide acetate	Prostate cancer, breast cancer, ovarian cancer, endometrial cancer, endometriosis, infertility, benign prostatic hypertrophy	1, 3, and 4 months	[9], [54], [65], [67]
Lupron Depot-PED®	PLGA/PLA	Leuprolide acetate	Central precocious puberty	1 and 3 months	[9]
Trelstar® Depot	PLGA	Triptorelin pamoate	Prostate cancer	1 and 3 months	[9], [54], [82]
Sandostatin® LAR Depot	PLGA–glucose	Octreotide acetate	Acromegaly, tumor-associated diarrhea and flushing episodes	1 month	[9], [54], [83]
Risperdal® Consta®	PLGA	Risperidone	Schizophrenia	2 weeks	[54], [65]
Vivitrol®	PLGA	Naltrexone	Alcohol dependency, opioid dependency	1 month	[9], [54], [82]
Bydureon®	PLGA	Exenatide	Type 2 diabetes	1 week	[9], [67], [84]
Zilretta®	PLGA	Triamcinolone acetoamide	Osteoarthritis pain of the knee	3 months	[9]
Arestin®	PLGA	Minocycline HCl	Periodontitis (adjunct therapy)	3 weeks	[54]

2.2.2.2 Implant systems

Implant systems offer a unique approach to controlled drug release. They are either matrix or reservoir type of systems, and encountered in various forms such as gels, pellets, rods, films, plugs, or discs.[22], [56] Implant systems can be administered parenterally using specialized devices or through surgical implantation, often under anesthesia.[26], [27] Non-degradable implants may necessitate a second surgical procedure for removal, reducing the patient comfort, although their retrievable nature may also be an advantage over microparticle depots.[29] In addition, there are injectable *in situ* forming implants which transform from liquid to solid or semisolid depots by different mechanisms such as thermal gelation or ionic crosslinking. Such systems can form their shape based on the site of administration while avoiding a surgical implantation procedure.[64]

Implants are typically designed for sustained drug release over extended periods, often ranging from months to years.[26], [57] Their localized long-term drug delivery makes them a feasible choice for applications such as contraception, ophthalmology,

and cancer treatment.[85] Additionally, drug-eluting implants may also possess other functionalities, such as in cardiovascular treatments and orthopedic applications. In these cases, they are referred to as combination devices.[28] **Figure 5** presents two well-known implantable polymeric drug delivery systems, Jadelle®[86] and Gliadel® wafer[85], as examples. They are also included in **Table 5**, along with other clinically approved polymer-based drug-releasing implants.

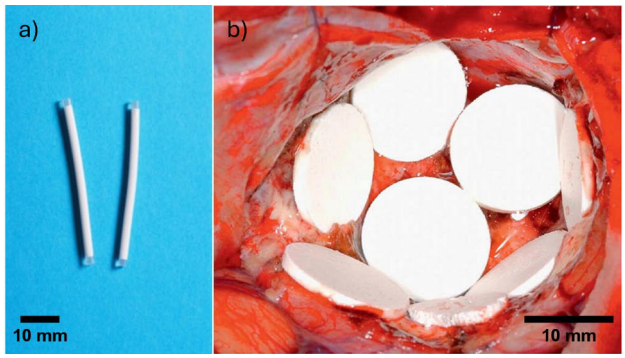

Figure 5. Photographs of a) Jadelle® and b) Gliadel® wafer implants. Figure b) is adapted from [85] with permission from Elsevier.

Table 5. Examples of marketed implantable polymeric drug delivery systems.

Product	Type	Polymer	Drug	Indication	Duration	Reference
Jadelle®	Rod	PDMS/ methylvinyl-siloxane	Levonorgestrel	Prevention of pregnancy	5 years	[5], [8], [86]
Gliadel® wafer	Disc/ wafer	Poly-anhydride*	Carmustine	Newly diagnosed or recurrent malignant glioma (adjunct to surgery and radiation)	2–3 weeks	[5], [54], [87]
Zoladex®	Rod	PLGA	Goserelin acetate	Breast and prostate cancer	3 months	[29], [54]
Vitrasert®	Intra-ocular insert	PVA/EVA	Ganciclovir	Cytomegalovirus retinitis	8 months	[8], [33]
Implanon®	Rod	EVA	Etonogestrel	Prevention of pregnancy	3 years	[8], [88]
Eligard®	*In situ* forming implant	PLGA	Leuprolide acetate	Advanced prostate cancer	1, 3, 4, and 6 months	[27], [54], [67]

*Poly(1,3-bis(p-carboxyphenoxy)propane-co-sebacate)

The choice of an implant manufacturing method depends on the characteristics of the drug and the desired properties of the final implant. Typical manufacturing methods include extrusion, injection molding, compression molding, and solvent casting, each with its unique advantages and challenges.[8], [64]

Extrusion involves forcing molten or plasticized polymer with molecularly dispersed or suspended drug through a nozzle, followed by cooling and cutting. This scalable method allows for controllable process parameters and is solvent-free but may not be suitable for thermally sensitive drugs due to high operating temperatures and potential thermo-oxidative or thermomechanical degradation.[64]

Injection molding utilizes high pressure and temperature to transfer the plasticized material into a mold, enabling the manufacturing of complex shapes as the material cools. Like extrusion, injection molding is a solvent-free method but shares the same limitations regarding thermally sensitive materials. Additionally, the temperature in injection molding is often higher than that in the extrusion process.[64]

Compression molding is performed by mixing the polymer and drug in a mold and then applying pressure while maintaining the temperature slightly above the glass transition temperature (T_g) of the polymer to create an implant with the mold's shape. The relatively low fabrication temperature is beneficial for maintaining the activity of sensitive drugs. However, due to potential inhomogeneous drug distribution, there can be significant variability in drug release.[8], [64]

Solvent casting involves dissolving the polymer in a volatile solvent, with dissolved or dispersed drug. The viscous solution or dispersion is then placed into a mold having the desired geometry and maintained at a controlled temperature to allow slow evaporation of the solvent. Finally, the implants are, for example, punched from the dried part. This method is suitable for heat-sensitive drugs due to the low processing temperatures. However, it can result in the formation of a porous structure, poor mechanical properties, and inhomogeneous drug distribution.[8], [64]

Drug release from implants is not only affected by the material and geometry of the system, but also by several other factors. The level of drug loading and the localization of the drug greatly influence the resulting drug release behavior.[8], [64] For example, high drug concentrations can disrupt the continuity of the polymer matrix, allowing for increased diffusion. Factors such as porosity, pore interconnectivity, and tortuosity also affect the release rates, with a higher number of short diffusional pathways facilitating drug release. With biodegradable systems, the microstructure often changes during the degradation, leading to change in the diffusivity and drug release, as opposed to the stable non-degradable systems.[8] The microstructure may also be tailored with different types of additives, increasing the possibilities of controlling the drug release behavior.[64] In addition to the system's microstructure, the characteristics of the drug, such as the solubility and hydrophilicity, also influence the release. The affinity between the drug and the

polymer also plays an important role, since higher affinity slows down the diffusional movement of the drug.[8] Thus, optimization of the product performance and treatment efficacy is a complex task requiring careful consideration.

2.3 Additive manufacturing in the preparation of polymer-based drug delivery systems

Additive manufacturing, also known as three-dimensional (3D) printing, rapid prototyping, or solid freeform fabrication, is an innovative technology that fabricates objects based on digital models by selectively adding material, usually in a layer-by-layer fashion.[11], [89] In this context, the more commonly used term "3D printing" is used due to its wide recognition.[90] 3D printing encompasses various processing technologies, some of which are presented in section 2.3.2. Despite this diversity, the typical process workflow is similar.[12]

The process often begins with designing a three-dimensional object using a computer-aided design (CAD) software. The output file, typically in STL format, describes the external surface of the 3D model. The STL file is then subjected to a slicing procedure, where the model is expressed as a stack of cross-sectional slices with specified thicknesses. These slices are read by the 3D printer, and the product is manufactured by selective addition of material one layer at a time.[12], [91] According to the International Organization for Standardization/American Society for Testing and Materials standard (ISO/ASTM 52900), material addition can be achieved using various methods.[89]

The history of 3D printing began in 1981 with Dr. Kodama's attempt to create 3D objects by selectively curing photosensitive resins using ultraviolet (UV) light.[11] This eventually led to the development of stereolithography (SLA), a technique involving layer-by-layer curing of polymeric liquid precursors.[92] Other manufacturing methods were subsequently developed in the late 1980s and early 1990s, including selective laser sintering (SLS), fused deposition modeling (FDM), and binder jet printing. Since then, 3D printing has found applications across various disciplines, from arts to engineering and pharmaceutics. The potential of additive manufacturing in the pharmaceutical field was first demonstrated in the early 1990s, and in 2015, Spritam® (Aprecia Pharmaceuticals), a levetiracetam-containing rapidly disintegrating tablet for the treatment of epileptic seizures, became the first 3D printed drug to receive FDA approval.[11], [92], [93]

2.3.1 Advantages of 3D printing in drug formulation and delivery

3D printing has emerged as a highly promising technology in the pharmaceutical sector, offering flexibility and customization in the preparation of drug formulations and various delivery systems. One of the most significant advantages is the ability to produce personalized dosages for individual patients. This is particularly important for drugs with a narrow therapeutic window, such as the orally administered anticoagulant warfarin, which is used for the prevention of venous thromboembolism and prevention and treatment of the thromboembolic complications associated with atrial fibrillation. In the case of warfarin, tailored dosing is crucial to achieve the patient-specific therapeutic efficacy while avoiding adverse effects, such as major bleeding.[11], [94]–[96]

Additionally, the flexibility in dosing is beneficial for pediatric and geriatric patients, who differ significantly from the general population.[92] Beyond dosage control, pediatric pharmacotherapy presents unique challenges, such as the need for oral formulations that are palatable and easy to administer. Through 3D printing, it is possible to prepare innovative dosage forms with appealing shapes and flavors for children.[11], [92]

The flexibility in design also provides control over drug release behavior through the adjustment of factors such as size, shape and internal geometry of the product, enabling the creation of dosage forms that release the drug at an optimal rate for each patient's specific needs.[11], [92] Controlling the shape of the manufactured object becomes essential also in the preparation of medical devices and drug delivery systems according to the patient's anatomy.[92] An additional benefit of 3D printing is the ability to incorporate multiple drugs to the same product. This approach to polypharmacy can overcome the poor compliance often observed in patients who need to take multiple individual drugs.[11], [92]

The possibility for a high level of customization marks a significant difference to the traditional drug delivery systems, which are often made in a "one size fits all" fashion. These systems fail to control the dose regimen based on individual differences such as age, weight, sex, genetics and lifestyle, potentially leading to underdosing, overdosing, and negative side effects.[12], [13] Overall, 3D printing has been seen as an enabling technology for the customization of medication according to the needs of individual patients, also known as personalized medicine.[11], [92]

The flexibility of 3D printing contrasts sharply with conventional pharmaceutical manufacturing, which often involves multiple production steps and numerous operators for these processes.[97] 3D printing supports point-of-care production, enabling rapid, decentralized manufacturing of unstable drugs with short half-lives to meet immediate patient needs. This capability reduces reliance on suppliers and allows for a quick response to both patient and market demands.[11]

Despite these advantages, 3D printing faces limitations, including lower throughput compared to traditional methods and higher costs for certain raw materials.[97]–[99] While 3D printing excels in small-scale, customized manufacturing, the limited regulatory framework and lack of standardized analytical practices for 3D printed products hinder the broader adoption of these technologies. As with other pharmaceutical products, the safety and functionality of 3D printed systems must be ensured, necessitating the development of robust quality control measures.[100], [101] These technical and regulatory limitations are further discussed in section 2.3.5. Overall, a deeper understanding of various 3D printing methods is essential for critically assessing their potential applications in personalized medicine and beyond.

2.3.2 3D printing techniques with clinical relevance

3D printing encompasses a variety of techniques, each distinguished by unique material usage, deposition technology, and layer formation mechanisms. As described in the ISO/ASTM 52900 standard, 3D printing technologies are categorized into seven main groups: binder jetting, material extrusion, material jetting, powder bed fusion (PBF), vat photopolymerization, sheet lamination and directed energy deposition.[89], [90] However, within the pharmaceutical field, only some of these technologies have received substantial attention. The relevant techniques are binder jetting, material extrusion, material jetting, powder bed fusion, and vat photopolymerization.[14] These different technologies and their subcategories are presented below, illustrated in **Figure 6**, and summarized in **Table 6**. However, the focus will be on the semi-solid extrusion process, which is presented in section 2.3.3.

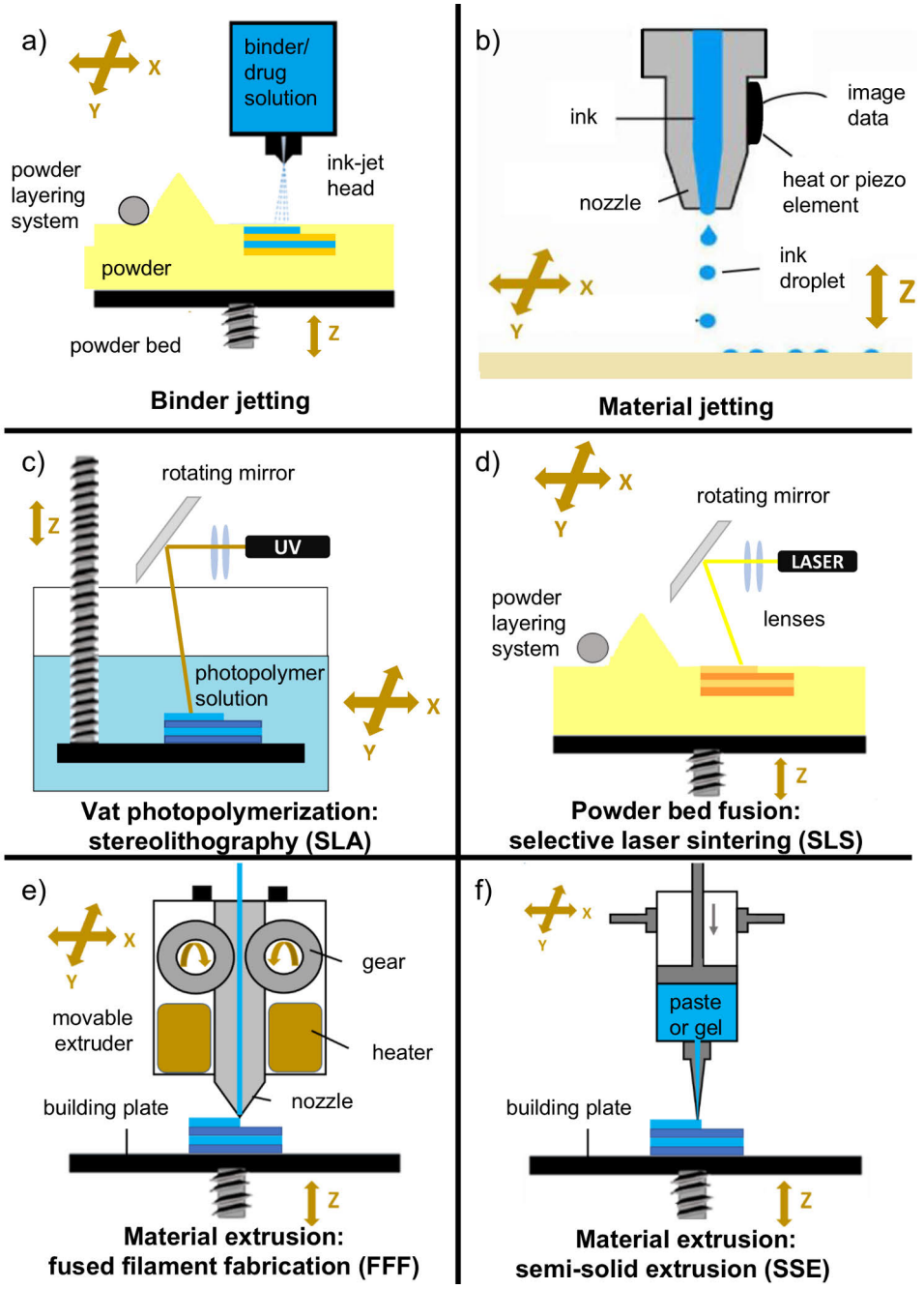

Figure 6. Illustration of commonly used 3D printing technologies in the pharmaceutical field. Some methods are illustrated based on specific subcategories. Adapted with permission from [12].

TABLE 6. Characteristics of clinically relevant 3D printing categories.

Method	Principle	Materials	Resolution	Advantages	Disadvantages	Reference
Binder jetting	Selective spreading of a binding liquid on powder	• Powder: any type • Liquid: various drugs, solvents, and binders	100–150 µm	• Material selection • Allows manufacturing of complex features	• Need for post-processing such as drying and removal of unbound powder	[12], [102], [103]
Material jetting	Selective deposition of liquid droplets	Excipients (including polymers and solvents) and drugs	~50 µm	• Flexibility in dosage and drug release control • High resolution	• Support material required for overhang structures • Limitations in suitable formulations	[12], [57], [90], [91], [103]
Vat photo-polymerization	Selective crosslinking of polymer resin by exposure to high energy light	Photocrosslinkable resin (possibly containing a drug), and photoinitiatior	From <100 nm to 100 µm, depending on the method	• Low processing temperature • High resolution	• Post-processing: removal of excess resin and supports, and curing • Resin toxicity • Possible reactions with the drug	[12], [57], [90], [91], [98], [104], [105]
Powder bed fusion	Selective fusion of powder by laser	Metal, polymer, or ceramic powder	~100 µm	• Moderately high resolution and accuracy • Good repeatability • Solvent-free method	• High operating temperature • Need for post-processing such as the removal of unbound powder	[12], [57], [90], [106]
Material extrusion	Selective extrusion of material through a nozzle	Excipients (including polymers) and drugs	~100 µm, depending on, e.g., the nozzle size	• Simplicity and flexibility • Compatibility with a wide range of materials (especially SSE) • Low processing temperature (SSE)	• Low resolution • Rheological requirements • High temperature (FFF) • Drying and solvent removal (SSE)	[12], [14], [64], [103], [107], [108]

2.3.2.1 Binder jetting

Binder jetting technology (**Figure 6a**), also known as drop-on-solid or drop-on-powder, is based on ink-jet printing technology. It involves spreading a thin layer of powder material onto a build platform, followed by the selective deposition of a liquid binder onto the powder bed through a nozzle moving across the x–y axis. The liquid binds or solubilizes the particles, depending on its composition, solidifying the layer. The build platform is then lowered, a new layer of powder is applied on top of the previous one, and the cycle is repeated until the desired 3D object is formed. Post-printing steps may include the removal of unbound powder, as well as drying to improve the mechanical strength and to eliminate the residual solvents.[90], [102], [109]

The resolution of the product is influenced by various factors such as the liquid's viscosity and droplet size, as well as the powder characteristics like particle size, flowability, and wettability. Printing speed and the distance from the powder bed also play critical roles.[12] Typically, droplet sizes range from 80 to 90 μm, with printed features achieving a thickness of 100–150 μm, depending on the materials and parameters used.[103]

Binder jetting offers several advantages, including high compatibility with various pharmaceutical excipients and drugs, as well as the ability to modify product composition by using different excipients in different layers. However, it also has drawbacks, such as the frequent use of toxic solvents, the need for precise control over raw materials, the requirement for post-processing, and the relatively poor mechanical strength of porous objects.[12], [102] Binder jetting has been successfully applied in the fabrication of oral dosage forms like Spritam® and various controlled release formulations.[102], [103]

2.3.2.2 Material jetting

Material jetting typically employs ink-jet printing technology to deposit small droplets of solutions, suspensions, or molten materials (**Figure 6b**).[90] The droplets are deposited onto a substrate, where material solidification occurs through processes such as cooling, curing, or solvent evaporation. Deposition can be performed on top of the previous layers to create a 3D shape. Additionally, a secondary support material may be required for overhang structures. Droplet generation can be continuous, where a stream of ink is ejected and broken into droplets, or on-demand, where droplets are generated only as needed. The positioning of droplets is precisely controlled, enabling the creation of detailed structures with high resolution.[57], [91], [103]

In the pharmaceutical field, the "ink" is often a solution or suspension containing the drugs and the excipients.[12] The physical properties of the ink, such as viscosity

and surface tension, are crucial for ensuring successful droplet formation and deposition onto the substrate. A typical droplet volume is in the picolitre range, enabling a spatial resolution in the range of tens of micrometers.[57], [103]

Material jetting, and specifically the subcategory ink-jet printing, has found applications in the fabrication of drug delivery systems with personalized dosages and complex drug release profiles, including transdermal microneedles, drug-releasing implants, and tablets. In addition to the versatility of the process, its scalability is an advantage for the industrial-scale production of pharmaceuticals.[57] The limitations of the method are often related to the need for precise tailoring of the ink formulation to ensure product quality and to prevent nozzle clogging during the process.[103]

2.3.2.3 Vat photopolymerization

Vat photopolymerization processes create solid objects from a bath (vat) of liquid photopolymer resin through the selective application of high-energy light. Photoinitiators are used in the process to generate reactive species that cause polymer chain growth under light irradiation, solidifying the resin layer-by-layer.[91], [98] In many current systems, the light is projected from below the object through a laser-transparent resin bath, and after the layer is completed, the support platform rises one step to create space for the next layer.[110] The resins typically contain methacrylates or acrylic esters, although the exact chemical compositions of commercial resins are often secret.[98]

Vat photopolymerization has several subcategories, including SLA, digital light processing (DLP), continuous liquid interface production (CLIP), and two-photon polymerization (2PP). While SLA (illustrated in **Figure 6c**) involves a UV laser to selectively cure the photopolymer resin, DLP uses a digital mirror device to project light and solidify the entire layer simultaneously, enabling a higher production rate. CLIP is an advanced form of vat photopolymerization that utilizes an oxygen-permeable membrane to create an inhibition zone for the curing, enabling a continuous process and the formation of products without distinguishable layers. These methods have an impressive resolution in the range of tens of micrometers. However, in terms of achievable resolution, the 2PP process outperforms all other methods. 2PP utilizes a femtosecond laser beam and a two-photon absorption process to initiate polymerization in a highly confined region, enabling approximately 100 nm resolution. Unfortunately, 2PP is currently only suitable for manufacturing small objects.[98], [105], [110]

In addition to its high resolution, vat photopolymerization operates at low temperatures, making it advantageous for incorporating heat-sensitive drugs.[11] However, the requirement for post-processing steps, such as washing and post-

curing, to remove the residual solvents and improve the mechanical integrity, is a characteristic disadvantage of the vat photopolymerization processes. Additionally, these methods bear risks regarding chemical reactions between the polymer and the drug, degradation of the drug due to light exposure, and potential cytotoxicity of the commercial resins and photoinitiators. These drawbacks limit the use of vat photopolymerization in the medical field.[12], [57], [103], [105] Still, it has been employed in a wide range of biomedical and pharmaceutical applications, including the fabrication of tablets, microneedles, and implants.[57], [105]

2.3.2.4 Powder bed fusion and selective laser sintering

PBF is a family of 3D printing techniques that create 3D objects by selectively fusing regions of a powder bed.[91] Among these techniques, SLS (**Figure 6d**) stands out for its versatility and capability to process a wide range of materials, including various thermoplastic polymers. It operates by directing a laser at specific areas on a pre-heated powder bed in an inert atmosphere, causing selective sintering of the material. After each layer is sintered, the build platform lowers, and a new powder layer is spread. Unfused powder acts as support for the structure being built, enabling the production of complex geometries without additional support structures. Post-processing involves cooling the material, cleaning the product, and potentially reusing the unsintered powder.[92], [106] The particle size of the powders is typically 20–60 µm, and both particle size and size distribution significantly affect the process.[57]

The advantages of SLS include a moderate resolution of around 100 µm, as well as good reproducibility. The method is also solvent-free, eliminating the need for a drying step. However, the high processing temperature may lead to degradation of drugs, limiting the use of the technique in pharmaceutical applications.[57], [90] In addition, removal of the unsintered powder is necessary.[12]

SLS has been explored for various pharmaceutical applications, including the production of tablets[111] and drug delivery systems with customizable release profiles[112]. The technique's ability to fabricate complex structures with high drug loading and good mechanical strength makes it a potential option for pharmaceutical applications and personalized medicine.[12], [57]

2.3.2.5 Material extrusion

Material extrusion has been the most widely studied 3D printing category, with a growing interest also in the pharmaceutical field.[91], [107], [108] These methods are characterized by the direct deposition of materials through a nozzle or orifice to construct three-dimensional objects layer-by-layer. Material extrusion methods can

be primarily categorized based on the state of the material being extruded, i.e., whether the material requires melting prior to extrusion or whether it can be extruded in a semi-solid state. The most notable subcategories are fused filament fabrication (FFF) and semi-solid extrusion (SSE).[12], [90] The FFF process is presented below, and section 2.3.3 is dedicated to the SSE process.

FFF, also known as FDM, is a 3D printing technology that involves melting, extrusion, and layer-by-layer deposition of thermoplastic polymers to produce solid objects. The process, as illustrated in **Figure 6e**, begins with feeding a thermoplastic filament into the extrusion head of the 3D printer, where it is melted and then deposited onto a build platform following a predetermined nozzle pathway. After deposition, the material cools and solidifies. Once the layer is completed, the next one is extruded on top of the previous layer.[92], [113] Key parameters that must be controlled during the FFF process include the infill density, print speed, layer height, and temperatures of the nozzle and the build plate. These parameters collectively determine the resolution, porosity, and the mechanical properties of the final product.[12], [57], [103]

A variety of filaments made from thermoplastic polymers, such as PVA, PLA, PCL, PU, polyethylene terephthalate glycol (PETG), acrylonitrile butadiene styrene (ABS), and nylon, are commercially available for FFF. However, pharmaceutical grade options are not widely available, and currently, no commercial filaments with incorporated drugs exist.[12] Thus, hot-melt extrusion (HME) is commonly used to prepare filaments of biocompatible and/or pharmaceutical grade thermoplastic polymers, either with or without drugs.[57], [91], [98] However, many pharmaceutical grade polymers that could be processed by HME lack other properties required for a successful FFF process, thus limiting their use.[98] For instance, the filaments must withstand certain mechanical loads during printing, as well as possess suitable rheological properties to enable extrusion through small nozzles. In some cases, brittleness and poor surface quality have been observed in filaments prepared by HME, especially with high drug loadings. However, the properties may be tailored with the addition of certain excipients such as plasticizers.[114], [115]

FFF offers several advantages, including the ability to customize the shape, size, and density of the product, as well as the potential to fabricate various solid dosage forms with high drug loading efficiencies.[57], [97], [98] Additionally, FFF systems are generally inexpensive, and the process is relatively simple. However, the use of this technique is limited by the risk of thermal degradation of sensitive drugs, the high anisotropy in the mechanical properties, and the potential need for post-processing, such as polishing.[90], [113] Another significant drawback of FFF is the relatively poor resolution, which can reach 50–100 µm but is highly dependent on the nozzle diameter and layer height.[12], [98] The requirement for the filament preparation beforehand is another possible limitation, which has led to the development of the

direct powder extrusion (DPE) method, allowing pellets or powders to be directly printed using a screw-based extrusion system.[57]

FFF has been applied in the manufacturing of a wide range of dosage forms, including single-component and multi-layered tablets for immediate and controlled drug release, orodispersible films, intrauterine devices, scaffolds, and implants.[97], [113] The technology allows for the modification of drug release profiles by altering the product geometry and combining different drugs or polymers in a single dosage form using a dual extrusion system.[57], [113]

2.3.3 Semi-solid extrusion 3D printing

SSE 3D printing, also known by various other names such as pressure-assisted microsyringe (PAM), robocasting, and direct ink writing (DIW), differs from the FFF method by employing semi-solid feedstock materials. These inks are extruded, often without substantial heating, through a nozzle and deposited in sequential layers. Upon extrusion, they harden through different mechanisms, enabling the construction of three-dimensional objects. The process is illustrated in **Figure 6f**. SSE has become an increasingly studied method in the pharmaceutical field, offering several benefits over other 3D printing methods.[12], [14]

2.3.3.1 Process characteristics

In SSE, the feedstock material is often in the form of a gel or paste and is contained in a syringe. Inks can be extruded through various systems, including pneumatic, mechanical, or solenoid-based mechanisms. Pneumatic systems utilize pressurized air to extrude the material. While this method is suitable for extruding high-viscosity materials, the characteristic delay before flow initiation can limit the accuracy of the process. Mechanical systems often employ pistons or screws to generate the necessary mechanical force for flow. Piston-based systems provide high control over the material flow, whereas screw-based systems offer better spatial control and extrusion of materials with higher viscosities. Solenoid systems, on the other hand, apply electrical pulses to a valve below the syringe, enabling controlled extrusion of sub-microliter volumes of low-viscosity materials.[14], [116]

Selecting the appropriate nozzle size is critical for achieving successful extrusion and the desired resolution; smaller nozzles allow for higher precision but may lead to inconsistent flow or clogging with high-viscosity inks or inks containing solid components.[14] Consequently, the resolution of the SSE process is typically limited to hundreds of micrometers.[117] The positioning of the nozzle is another critical factor, as improper distances can hinder material adhesion or cause flow

inconsistencies.[14], [116] Additionally, the nozzle travel speed must be synchronized with the extrusion rate to prevent under-extrusion or over-extrusion.[14]

In SSE, the solidification of the extruded material can occur through various mechanisms, such as solvent evaporation, crosslinking, or crystallization, depending on the printed materials and process characteristics.[117] A post-printing drying step is typically necessary to ensure proper solidification and structural integrity of the object. However, this step may introduce challenges, such as shrinking or deformation of the structure.[12] Furthermore, the use of solvents in the formulations requires careful consideration due to potential toxicity, which could impact the safety of the final product.[103]

SSE offers flexibility in designing drug delivery systems, enabling the creation of complex designs with varied infill patterns and compartmentalization to achieve tailored drug release profiles.[12] The low extrusion temperatures make it suitable for thermolabile materials and drugs, positioning it as a promising approach in the fields of pharmaceuticals and tissue engineering.[14], [116]

2.3.3.2 Material requirements

A variety of pharmaceutical grade materials, including drugs and excipients, can be used in the SSE process by incorporating them into the extrudable inks. This approach allows for high drug loading and the combination of multiple drugs in a single dosage form. However, the inks must meet specific requirements, particularly regarding their rheological properties.[14], [118] These are commonly analyzed with a rheometer in rotational mode or by small-amplitude oscillatory measurements.[107], [119] Some common rheological tests are illustrated in **Figure 7** and discussed below.

Viscosity determines the stress required for ink extrusion. Low viscosity allows for easy extrusion but may result in poor shape retention after exiting the nozzle. Conversely, high viscosity improves shape retention but restricts the material flow. Therefore, non-Newtonian shear-thinning behavior is desirable, as illustrated in **Figure 7a**. This property ensures that the ink remains stationary in the container until sufficient force is applied, enabling consistent flow even through small nozzles. Equally important is the recovery of viscosity after a reduction in the shear stress, i.e., when the ink has been extruded through the nozzle.[14], [107] This phenomenon is often time-dependent, as illustrated in **Figure 7d**, and in that case known as thixotropy. A rapid recovery of viscosity to the initial level facilitates the shape retention of the printed object.[120]

The viscoelastic properties of the ink significantly impact its behavior in the SSE process. Viscoelasticity encompasses both viscous and elastic behavior, characterized by the storage modulus (G') and loss modulus (G''). The storage modulus reflects the elastic energy stored during deformation, while the loss

modulus measures the dissipated energy.[118], [119] The combined effect of these factors determines how the ink behaves in different situations, with examples shown in **Figure 7b** and **Figure 7c**. If the storage modulus dominates, the ink exhibits gel-like elastic behavior, which is beneficial for post-extrusion stability. In contrast, a dominating loss modulus indicates that the ink behaves as a viscoelastic liquid.[119], [120]

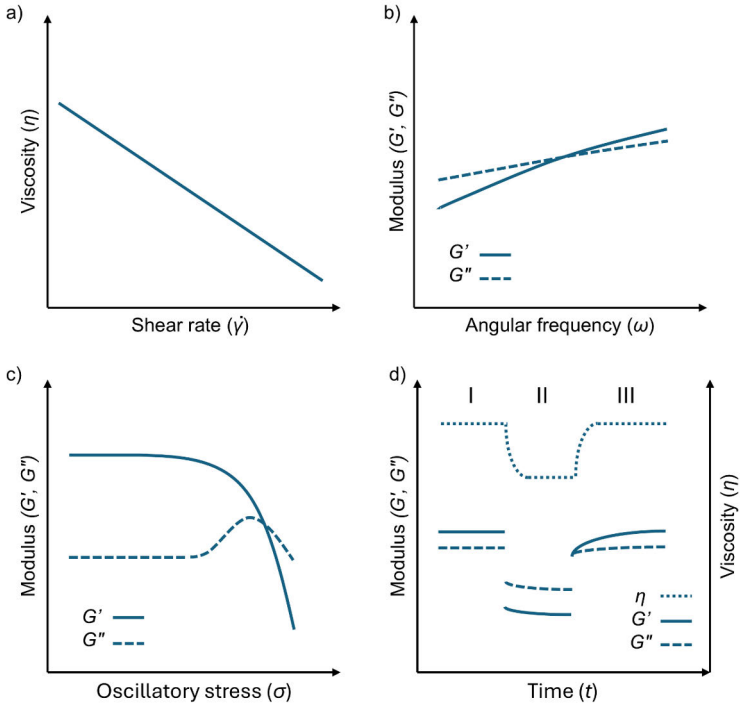

Figure 7. Illustration of common rheological tests used in ink characterization. In a), the shear rate sweep shows a non-Newtonian shear-thinning behavior, resulting in decreasing viscosity with increasing shear rate. In b), the oscillatory frequency sweep illustrates the change in viscoelastic moduli and the transition from a viscoelastic solid to a viscoelastic liquid as the frequency decreases. The yield stress determination is shown in c), illustrating both the yield and flow points. The viscosity recovery determination, shown in d), can be conducted using rotational or oscillatory methods, or a combination of both, by altering between high and low shear rates or oscillatory strains at specific intervals.[118], [119], [121], [122]

Yield stress (**Figure 7c**) describes the material's ability to resist deformation. Below the yield stress, the material behaves as an elastic solid, recovering its original shape upon removal of the stress. When the applied stress exceeds the yield stress, the storage modulus shows a decreasing trend. If the loss modulus exceeds the storage modulus at a "flow point," significant deformation occurs. A high yield stress is

crucial for ensuring ink homogeneity[120], shape retention after extrusion, and the ability to support overlying layers.[118], [119] However, excessively high yield stress may hinder the initiation of material flow.[107]

Similarly to viscosity recovery, a rapid recovery of the viscoelastic moduli (**Figure 7d**) after deformation is essential for ensuring adequate shape retention. From the viscoelasticity perspective, this means that after deforming the material, the storage modulus should quickly rise above the loss modulus, causing a transition in the material's behavior from fluid-like to viscoelastic solid.[118], [119]

2.3.3.3 Printability assessment methodologies

Printability is a general term used to describe the ink's ability to be printed into constructs with adequate quality. It is related to the rheological properties of the ink, which, together with the used process parameters, determines the outcome of the process. However, there is currently no standardized methodology for assessing printability. Various methods, either qualitative or quantitative, have been proposed in the literature, highlighting the complexity of the topic. The methods typically evaluate the extrudability and filament formation of the ink, as well as the shape fidelity of the printed construct.[118], [123] Some common methods are presented in **Figure 8** and discussed below.

Extrudability is determined by the ink's viscosity and shear-thinning behavior, allowing it to be extruded through the nozzle without damaging the ink components or the extrusion system.[14], [120] Extrudability can be assessed through rheological analysis, as well as by simply mapping the achievable flow rates at different pressures using a pneumatic 3D printer.[123] Such analysis can also reveal important information about the inks' homogeneity, as fluctuating material flow rates may indicate the presence of aggregates.[118]

In addition to being extrudable, the ink should form a uniform and smooth filament without breaking into droplets or becoming granular (**Figure 8a**). This behavior is related to the ink's shear-thinning and viscosity recovery properties. It can be evaluated by extruding a filament and then categorizing its shape, often qualitatively, either before or after deposition onto a substrate.[123]

The evaluation of extruded and deposited lines is a common approach to studying the printability and shape fidelity of the ink (**Figure 8b**). Typically, the width of the line is measured and compared to the nozzle size to determine the degree of spreading.[118], [120] Alternatively, parallel lines are printed with decreasing spacing, and their merging is studied. This analysis can be used to evaluate factors such as ink composition, concentration, and degree of crosslinking, all of which affect the ability to produce fine details and sharp angles. Ideally, the viscosity of the ink would recover quickly after deposition, and the yield stress or storage modulus

would be sufficiently high to prevent deformation by gravity or surface tension. In addition to the ink's rheological properties, process parameters such as printing speed, pressure, temperature, and nozzle offset from the substrate influence the line formation.[118], [123]

Another approach, as illustrated in **Figure 8c**, involves printing grid-like structures with alternating line directions that are perpendicular to each other to assess ink stabilization and shape fidelity. The resulting pore shapes can be evaluated semi-quantitatively by calculating a printability index (P_r). Perfectly square pores have a P_r value of 1, while values below 1 indicate spreading of the material and the formation of round pores. Over-gelation and the formation of irregular pores result in P_r values above 1.[118], [120]

Spreading and deformation of the material are also crucial when printing structures with multiple layers. As more layers are added, the stress applied to the lower layers increases, applying higher demands on the ink to ensure proper shape fidelity compared to depositing single lines. The ink's suitability for manufacturing of multi-layered structures has been evaluated, for example, by printing three-dimensional objects and comparing their heights to the original design values. This test avoids the effects of the substrate, which are known to affect the spreading of the material.[118], [123]

The ability to produce structures with defined porosity or overhangs is crucial for several applications. In these cases, preventing the filament's collapse due to gravity is essential. The ability to resist deformation by gravity can be quantitatively evaluated by depositing a filament over an array of pillars with increasing distances (illustrated in **Figure 8d**) and measuring the deflection of the filament or the area below it. Alternatively, the breaking of the filament upon deposition over gaps of different lengths can be assessed. The yield stress and storage modulus of the ink are critical in counteracting the effects of gravity, thereby influencing the outcome of the tests.[118], [123]

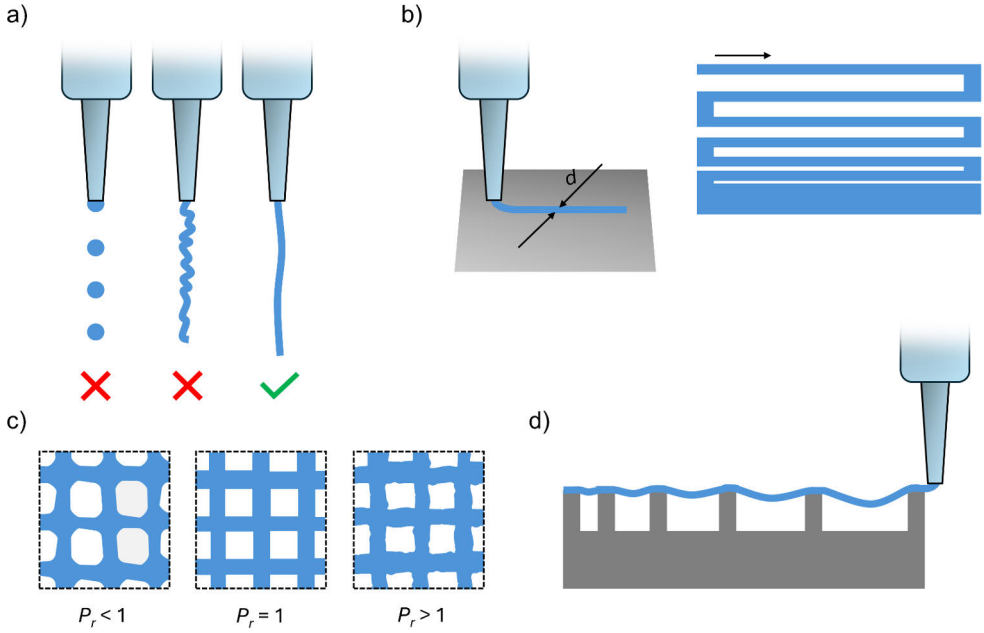

Figure 8. Illustration of common printability assessment methods. The filament formation test is presented in a), while filament spreading can be evaluated by measuring b) the diameter of the filament or the fusing of parallel lines, or alternatively by c) printing a grid structure and analyzing the pore shape. The filament deflection test is illustrated in d), showing the process of printing filament over gaps of different lengths.

2.3.3.4 Drug delivery applications

Due to its low processing temperature and compatibility with a wide range of materials, SSE has become the most widely utilized 3D printing method in tissue engineering, where ensuring the viability of the cells within the ink is essential.[120] In contrast, SSE still lacks widespread adoption in the pharmaceutical field, although several studies have demonstrated its significant potential for the cost-efficient preparation of small batches of customized dosage forms, such as pediatric formulations.[11], [12], [14] **Table 7** lists examples of polymer-based drug delivery systems manufactured by SSE 3D printing. The majority of systems reported in the literature are various types of tablets, although drug delivery devices ranging from patches to scaffolds have also been developed.[12], [14]

Table 7. Examples of polymer-based drug delivery systems prepared by semi-solid extrusion 3D printing. Solvents are excluded from the material list.

Type	Materials	Drug	Reference
Immediate release tablet	Poly(vinyl alcohol)-poly(ethylene glycol) graft copolymer (PVA-PEG) and polyvinylpyrrolidone-vinyl acetate copolymer (PVP-PVAc)	Levetiracetam	[124]
Immediate release tablet	Hydroxypropyl-β-cyclodextrin, hydroxypropyl methylcellulose (HPMC), PVP, sodium carboxymethylcellulose, and croscarmellose sodium	Carbamazepine	[125]
Extended-release tablet	HPMC	Theophylline	[126]
Extended-release tablet	HPMC, lactose, microcrystalline cellulose (MCC), and PVP	Glipizide	[127]
Chewable tablet	Sucrose, pectin, maltodextrin, flavorings, and colorants	Isoleucine	[128]
Chewable tablet	Gelatin, HPMC, and reduced starch syrup	Lamotrigine	[129]
Polypill	PVP, lactose, D-mannitol, sodium starch glycolate, HPMC, cellulose acetate (CA), and PEG	Aspirin, hydrochlorothiazide, pravastatin, atenolol, and ramipril	[130]
Polypill	PVP, PEG, HPMC, CA, D-mannitol, croscarmellose sodium, MCC, sodium starch glycolate, sodium chloride, and tromethamine	Nifedipine, captopril, and glipizide	[131]
Self-nanoemulsifying tablet	Capryol 90, octanoic acid, PEG, and Poloxamer 188	Dapagliflozin propanediol monohydrate	[132]
Orodispersible film	Hydroxypropyl cellulose	Warfarin	[133], [134]
Orodispersible film	Maltodextrin, sorbitol, and hydroxyethyl cellulose	Benzydamine hydrochloride	[135]
Patch	PCL and PLGA	5-fluorouracil	[136]
Microneedle patch	Sodium alginate, hydroxyapatite, and anhydrous calcium chloride	Glucose-responsive releasing insulin	[137]
Controlled release device	Silopren UV LSR 2030	Prednisolone	[138]
Scaffold	PDMS (vinyl terminated), methyl modified silica, methylhydrosiloxane-dimethylsiloxane copolymer (trimethylsiloxane terminated)	Metronidazole	[139]

2.3.4 Design considerations for 3D printed drug delivery systems

To ensure the successful adoption of 3D printing in the manufacturing of polymer-based drug delivery systems, several design considerations must be addressed to optimize the efficacy, safety, and manufacturability of these systems. A crucial factor to consider is the drug molecule itself, as it may impose fundamental limitations on the formulation, design, and manufacturing process to ensure the stability and proper drug release behavior.[11], [140]

Another vital aspect is the intended administration route. Each route presents unique challenges and requirements, influencing the choice of materials, geometry, and manufacturing method. For example, transdermal microneedle patches designed for localized delivery necessitate specific shapes for effective skin penetration.[92], [140]

The geometry of the drug delivery system significantly impacts the drug release profile. Complex three-dimensional structures can control the release kinetics through factors such as surface area, pore architecture, and wall thickness, enabling programmed release profiles such as pulsatile or sustained release.[57], [140] However, the geometric design and strand orientation can also affect the mechanical properties of the printed object. Support structures may be necessary for complex constructs, leading to a trade-off between functionality and simplicity.[141]

Accurate delivery of the target dose is critical, especially in personalized medicine, where dosing varies among patients.[110], [142] Process parameters such as print speed, nozzle size, and layer thickness can be adjusted to achieve the desired dosage precision. However, enhanced precision often comes at the cost of decreased process throughput. For example, smaller nozzles and lower layer heights improve resolution but can significantly extend the production time.[12], [14], [141]

Material selection is another essential component of product design, as the polymers used in drug delivery must possess specific rheological and mechanical properties for effective processing and post-administration performance. When considering tissue contact of these systems, biocompatibility and toxicity are also important factors. Furthermore, material characteristics, such as degradation behavior and crystallinity, influence the drug release rates.[57]

When considering the scalability of the process, the choice of 3D printing technology is important. A fundamental question is whether the technology can provide reasonable throughput to meet market demands. The selected process must consistently produce high-quality products while maintaining flexibility, being operator-friendly, and complying with regulatory requirements.[140]

2.3.5 Regulatory aspect and future perspectives

Currently, 3D printing in the pharmaceutical field is predominantly in the research phase.[110] Although the technology has demonstrated significant potential to transform drug delivery through preclinical and clinical studies, widespread clinical application has yet to be achieved.[101], [143], [144] Furthermore, the existing focus appears to be primarily on oral administration, with other delivery systems receiving less attention. The primary objective of utilizing 3D printing in the manufacturing of drug delivery systems is to overcome the limitations of traditional methods, such as limited tailorability.[142] Thus, much of the technology's potential remains untapped.

Despite its promise, several technical limitations hinder the implementation of 3D printing for the manufacturing of drug delivery systems. Achieving high resolution in printed products is a critical challenge, as is the need for thorough post-processing to ensure quality and consistency. Variability in the appearance and performance of finished products necessitates further process development and research into suitable raw materials.[11], [107] This is also linked to concerns about quality control, as the safety and efficacy of 3D printed products must be ensured.[12] It has been envisioned that integration of Process Analytical Technology (PAT), such as non-destructive in-line measurements, into the 3D printing process could significantly improve the quality control capabilities.[14], [100]

Another factor contributing to the slow adoption of 3D printing in the pharmaceutical field is the lack of Good Manufacturing Practice (GMP) compliant equipment. Most commercial 3D printers do not meet the stringent requirements set by regulatory bodies, complicating the integration of this technology into pharmaceutical manufacturing.[14], [100], [101]

Furthermore, the regulatory framework surrounding 3D printed drug delivery systems is still under development. The diversity of printing methods and materials presents challenges in establishing clear guidelines.[12], [98] Additional complexity arises from the various scenarios in which 3D printing could be used, ranging from the development stage in the industry to point-of-care applications.[12], [100], [103], [145] In 2017, the FDA issued guidance on technical considerations for additive manufactured medical devices. However, this guidance did not specifically address drug delivery systems.[14] Nevertheless, it underscored the necessity for tailored regulatory pathways that reflect the unique characteristics of each technology and product. Regulatory considerations must encompass various aspects, including material selection, manufacturing processes, and sterilization protocols, to ensure the safety and efficacy of 3D printed pharmaceuticals.[12], [110]

As the technology matures and regulatory frameworks are established, the potential for personalized medicine and novel drug delivery solutions will continue to expand, potentially transforming the pharmaceutical field.[57], [92], [98]

3 Aims of the Study

The overarching aim of this thesis is to enhance the versatility of 3D printing within the pharmaceutical sector, specifically regarding systems for macromolecule delivery and release, by facilitating the 3D printing of widely used medical materials under ambient conditions. The research presented in this thesis focuses on extrusion-based 3D printing, including the evaluation of suitable materials and processing parameters for the preparation of drug delivery systems.

The main objectives of the study were:

I To develop an extrusion-based 3D printing method and ink formulation that enable room-temperature processing of thermoplastic polymers.

II To evaluate the relevant material and process-related factors affecting the success of the 3D printing process.

III To enhance the resolution of the semi-solid extrusion 3D printing process by modifying the ink composition.

IV To tailor the microstructure, mechanical properties and drug release rate of the printed systems by developing a low-temperature post-processing method.

4 Materials and Methods

The materials and methods used in this thesis are briefly summarized here. More detailed information is available in the original publications (**I-III**). Electron microscopy (publications **I-III**) was conducted at the Materials Research Infrastructure (MARI) in the Department of Physics and Astronomy at the University of Turku, Finland. Confocal microscopy (publication **III**) was performed at the Cell Imaging and Cytometry Core, Turku Bioscience Centre, Turku. 3D printing (publications **I-III**) was conducted at Brinter AM Technologies Ltd., Turku.

4.1 Materials

PLGA polymers (Resomer® RG 502 H, Resomer® RG 504, and Resomer® RG 756 S), and PVA (M_w 13,000–23,000, 87–89% hydrolyzed) were purchased from Sigma-Aldrich (Espoo, Finland). Carbopol® Ultrez 10 NF was received as a sample from IMCD Nordic (Malmö, Sweden).

Poly(L-lactide-co-glycolide) (PLLGA, lactide:glycolide ratio = 75:25) microspheres were purchased from Rimless Industry Co., Ltd (Changchun, China) and PMMA microspheres were purchased from Cospheric LLC (California, USA).

Fluorescein isothiocyanate-dextran (FD, FITC-dextran 40 kDa), sodium azide (NaN_3, ≥99.5%), and phosphate buffered saline-Tween® (PBS-Tween, pH 7.4, 0.05% Tween® 20) tablets were purchased from Sigma-Aldrich (Espoo, Finland)

Acetone (≥99.5%), dichloromethane (DCM, ≥99.5%), dimethyl sulfoxide (DMSO, ≥99.8%), tetrahydrofuran (THF, ≥99.9%), and sodium hydroxide (NaOH, 1 M) were purchased from Sigma-Aldrich (Espoo, Finland). Ultrapure water (>18.2 MΩ cm^{-1}) was generated with a Milli-Q® IQ 7000 water purification system (Millipore SAS, Molsheim, France).

4.2 Microsphere preparation

Single emulsion solvent evaporation method[146] was used in the preparation of FD-loaded PLGA microspheres at room temperature (publication **III**). The oil phase was prepared by dissolving PLGA (Resomer® RG 502 H, Resomer® RG 504, or Resomer® RG 756 S) in DCM and FD in DMSO, followed by mixing the solutions.

The oil phase was emulsified for 1 min in 1% (w/v) PVA aqueous solution using an Ultra-Turrax® T25 digital homogenizer (IKA®-Werke GmbH & Co. KG, Staufen, Germany) equipped with an 18-mm dispersing tool, followed by solvent evaporation overnight. Different stirring rates were selected based on preliminary screening (data not shown) with the aim of obtaining similar particle size distributions for the different formulations. Microspheres were separated and washed with MilliQ water by centrifugation at 4,000 RCF for 5 min using an Eppendorf 5804 R centrifuge (Eppendorf AG, Hamburg, Germany). Microspheres were vacuum dried overnight in a SalvisLab Vacucenter VC50 (Renggli AG, Rotkreuz, Switzerland) vacuum drying oven at room temperature. Placebo microspheres were prepared from RG 504 by following the same protocol, but without FD. The microspheres are hereinafter abbreviated according to the polymer used and the presence of the drug [(FD or placebo (pbo)], e.g., $RG504_{FD}$. The abbreviations are collected in **Table 8**. The FD-loaded microspheres were protected from light during every manufacturing step, while being stored, and during further processing.

Table 8. Emulsification parameters used in the preparation of different microsphere formulations. Reprinted from publication **III** with permission from Elsevier.

Abbreviation	Polymer	Model drug	Stirring rate (rpm)
$RG502H_{FD}$	RG 502 H	FD	3,000
$RG504_{FD}$	RG 504	FD	4,000
$RG504_{pbo}$	RG 504	-	4,000
$RG756S_{FD}$	RG 756 S	FD	5,000

4.3 Microsphere characterization

4.3.1 Process yield

The yield of the microsphere manufacturing process was quantified by weighing the microspheres after drying (publication **III**).

4.3.2 Size and morphology

Microsphere particle size and size distribution were analyzed in liquid mode using a PSA 1190 L/D particle size analyzer (Anton Paar, Graz, Austria) equipped with a Small Volume Unit (SVU) (publications **I** and **III**). Microspheres were dispersed in water for the analysis, and Mie theory[147] was used for particle size calculation, utilizing the characteristic refractive index and absorbance coefficient values of the

microsphere matrices. Volume mean diameter *D[4,3]*, volume percentiles, and span[148] values were collected. The analysis was performed in triplicate.

Microsphere morphology was analyzed using an Apreo S field emission scanning electron microscope (FE-SEM) (Thermo Fisher Scientific, Brno, Czech Republic) (publications **I** and **III**). Samples were attached on aluminum stubs and coated with either gold (publication **I**) or platinum (publication **III**). Imaging was conducted using a 2 kV acceleration voltage and detection of secondary and backscattered electrons.

4.3.3 Drug content

The amount of encapsulated FD within the microspheres was quantified by dissolving a known amount of microspheres in DMSO and extracting the drug by adding PBS-Tween (publication **III**). The resulting polymer precipitate was separated by centrifugation at 20,000 RCF for 15 min using an Eppendorf 5424 centrifuge (Eppendorf AG, Hamburg, Germany), and the FD concentration in the supernatant was determined by absorbance measurement at 487 nm with a Victor Nivo plate reader (Perkin Elmer, Pontyclun, UK). Drug loading degrees (LD) and encapsulation efficiencies (EE) were calculated (n = 3) with the following equations:

$$LD = \frac{m_{encapsulated\ drug}}{m_{encapsulated\ drug} + m_{polymer}} \cdot 100\% \quad (1)$$

$$EE = \frac{m_{encapsulated\ drug}}{m_{total\ drug\ added}} \cdot 100\% \quad (2)$$

The distribution of FD within the microspheres was analyzed using confocal laser scanning microscopy (CLSM) imaging with an LSM 880 (Zeiss, Oberkochen, Germany) (publication **III**). Imaging was conducted using 488 nm argon light excitation and 493–564 nm bandpass filters for emission. Transmitted light images were also captured by the system. The captured images were processed with ImageJ® software (version 1.53q, National Institutes of Health, Bethesda, Maryland, USA).

4.4 Ink formulation

Carbopol gel was prepared (publications **I**, **II**, and **III**) by suspending Carbopol® Ultrez 10 NF in Milli-Q® water at a 0.5% (w/v) concentration. The gel was formed by adjusting the pH of the suspension to 7.0 ± 0.2 by gradual addition of NaOH. The gel was mixed for 2 × 1 min with SpeedMixer™ DAC 400.1 FVZ (Hauschild GmbH

& Co. KG, Hamm, Germany) at 1,200 rpm while measuring the pH between the mixing periods.

Inks were prepared by mixing the microspheres with the gel at concentrations ranging from 0% to 60% (vol). Material densities (1.34 g/cm^3 for PLGA 50:50, 1.30 g/cm^3 for PLGA 75:25 and PLLGA[149], [150], 1.19 g/cm^3 for PMMA, and 1.00 g/cm^3 for Carbopol gel) were used for volumetric conversions. In publication **I**, the PLLGA60 ink was discarded from further processing due to its high viscosity, whereas in publication **III**, a couple of drops of water was added to some of the inks to reduce their viscosity. The inks were mixed using a SpeedMixer™ at 1,600 rpm for 2 min and loaded into plastic syringes, followed by degassing through centrifugation at 2,880 RCF for 5 min in an Eppendorf 5804 R. The degassed inks were then mixed by manual pumping between two connected syringes.

The inks are later abbreviated by the name of the polymer and the volume percentage of microspheres within the ink (**Table 9**). For example, the PLLGA45-RG504$_{FD}$5 ink contains 45% (vol) PLLGA microspheres and 5% (vol) FD-loaded RG 504 microspheres.

Table 9. Composition and abbreviations of the prepared inks.

	Microsphere component 1		Microsphere component 2		
Ink	**Formulation**	**% (vol)**	**Formulation**	**% (vol)**	**Publication**
PLLGA0	PLLGA	0	-	-	**I, II**
PLLGA10	PLLGA	10	-	-	**I, II**
PLLGA20	PLLGA	20	-	-	**I, II**
PLLGA30	PLLGA	30	-	-	**I, II**
PLLGA40	PLLGA	40	-	-	**I, II**
PLLGA50	PLLGA	50	-	-	**I, II**
PLLGA60	PLLGA	60	-	-	**I**
RG504$_{FD}$50	RG504$_{FD}$	50	-	-	**III**
RG504$_{pbo}$45-RG502H$_{FD}$5	RG504$_{pbo}$	45	RG502H$_{FD}$	5	**III**
RG504$_{pbo}$45-RG504$_{FD}$5	RG504$_{pbo}$	45	RG504$_{FD}$	5	**III**
RG504$_{pbo}$45-RG756S$_{FD}$5	RG504$_{pbo}$	45	RG756S$_{FD}$	5	**III**
PLLGA45-RG504$_{FD}$5	PLLGA	45	RG504$_{FD}$	5	**III**
PMMA45-RG504$_{FD}$5	PMMA	45	RG504$_{FD}$	5	**III**

4.5 Ink characterization

The rheological behavior of the inks containing PLLGA microspheres was characterized in publication **I** using an MCR 702e MultiDrive™ rheometer (Anton Paar, Graz, Austria) equipped with a serrated 20 mm parallel plate setup (gap = 1 mm). Measurements were conducted in triplicate at 25 °C after preshearing in steady-state rotational mode (0.1 1/s for 60 s), followed by a 1 min stabilization time. A solvent trap and silicone oil cover were used to prevent sample drying.

An oscillatory strain amplitude sweep (0.001–1,000%) was conducted at a frequency of 1 Hz to determine the linear viscoelastic region (LVR), with the yield strain (γ_y) taken from the point where the storage modulus (G') value decreased by 5% from its linear range value. The yield stress (σ_y) was determined from an oscillatory stress amplitude sweep (0.1–1,000 Pa) at 1 Hz frequency. A crossover point of G' and G'' was determined as the yield point.

Apparent viscosities were measured using shear rate ramps (0.01–100 1/s) in rotational mode, with 60 s timeout for each point. The true viscosities were calculated after applying the Weissenberg-Rabinowitsch correction[151], [152] to the experimental data, after which the Herschel–Bulkley model[118] was used to determine the yield stress (σ_y), flow index (n) and consistency index (K):

$$\sigma = \sigma_y + K\dot{\gamma}^n \tag{3}$$

Model fitting was conducted in Origin (version 2022, OriginLab Corporation, Northampton, Massachusetts, USA), which was also used for graphing.

An oscillation-rotation-oscillation (O-R-O) three-interval thixotropy test (3ITT) [120], [122] was chosen to characterize the viscosity recovery behavior. The first interval was conducted in oscillatory mode (60 s time sweep with 0.01% amplitude at 1 Hz frequency), while the second interval was conducted in rotational mode (steady-state rotation with a shear rate of 10 1/s for 10 s). The third interval was again conducted in oscillation mode (t = 180 s), during which the change in G' and G'' values was monitored. Additional samples (n = 1) were tested in rotation-rotation-rotation (R-R-R) mode using shear rates of 0.1, 10, and 0.1 1/s for the first, second, and third intervals, respectively.

4.6 3D printing & post-processing

4.6.1 Printing process

Object design and STL file generation were performed using SolidWorks CAD-software (v. 2021, Dassault Systèmes, SolidWorks Corporation, Waltham, Massachusetts, USA) (publications **I**, **II**, and **III**).

Semi-solid extrusion 3D printing was conducted with the Brinter® One (Brinter AM Technologies Ltd., Turku, Finland) using a progressive cavity technology-based Rotary Tool (Brinter AM Technologies Ltd., Turku, Finland) and the compatible accessories (publications **I**, **II**, and **III**). System operation and object slicing were performed using the embedded software.

Tool pressure was set to 300 mbar in all studies, and Nordson EFD Optimum® SmoothFlow™ Tapered Tips (Elgood Oy, Vantaa, Finland) with various internal diameters were used. Printing was conducted at room temperature on glass slides, unless otherwise stated, with the print speed (v) set to 5 mm/s. The different sample types are presented in **Figure 9** along with their characteristic parameters. Other parameters, such as physical nozzle size (D_p), nozzle size parameter (slicer value, D_n), layer height (h), and extrusion factor (E), were varied.

The printed samples intended for further post-processing and/or characterization were vacuum dried overnight at room temperature (publications **I**, **II**, and **III**).

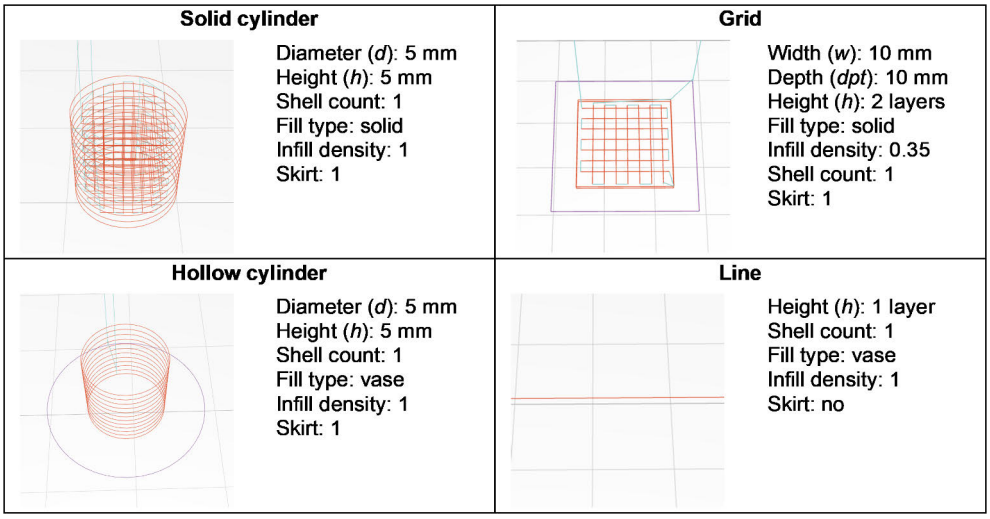

Figure 9. Different sample types and their characteristic slicing settings. The line shape was generated by manually modifying the G-code within the slicing software. Reprinted from publication **II** with permission from Elsevier.

4.6.2 Printability assessment & material flow optimization

Publication **I** focused on simple printability demonstration of the PLLGA inks with the solid cylinder models. In the tests, D_p = 410 µm and h = 328 µm were used. In publication **II**, a more comprehensive printability assessment was conducted using the PLLGA inks for all sample types presented in **Figure 9**. These methods are described below.

Filament formation tests and filament diameter analysis were conducted by extruding the inks through nozzles of different sizes from heights of 20 mm and 10 mm, respectively, while capturing images with the printer's embedded camera. Image acquisition was followed by qualitative assessment of filament quality or measurement of filament diameter through image analysis using ImageJ® software (version 1.53q). The extrudate swell ratio S[153] was determined from 10 parallel measurements as the ratio of the measured filament diameter D to the nozzle diameter D_p:

$$S = \frac{D}{D_p} \tag{4}$$

In the other printability assessment tests, D_p was 410 µm.

The printability index (P_r)[154, 155] values were obtained by photographing the grid structures prepared with different layer heights. The circularity (C) of the pore geometry was derived from the pore perimeter (L) and area (A) using the following equation:

$$P_r = \frac{\pi}{4} \cdot \frac{1}{C} = \frac{\pi}{4} \cdot \frac{1}{4 \cdot \pi \cdot \frac{A}{L^2}} = \frac{L^2}{16A} \tag{5}$$

The areas and perimeters were obtained from 10 parallel measurements using image analysis with ImageJ®.

A modified filament collapse test[156] was performed by depositing a single filament over a custom-made block containing 10 mm wide pillars separated by gaps of 5–30 mm in 5 mm increments. Different D_n and h values were used in the analysis. In the test, E = 0.79 was applied to correct the flow rate for a filament with a round cross-section instead of a rectangular one. The maximum span lengths over the different gaps were recorded for three parallel samples.

Material flow optimization focused on the visual assessment of the effects of different printing parameters and extrudate swell on the resulting object quality. Solid and hollow cylinders were printed with varying D_n, h, and E values.

In publication **III**, the inks were formulated using PLGA, PLLGA and PMMA microspheres. In this case, printability was evaluated by manual extrusion through

nozzles of different sizes. For the actual 3D printing, D_p = 580 µm and h = 290 µm were used.

4.6.3 Post-processing

In publications **I** and **III**, the dried samples were sintered using solvent vapor[157]. In this step, the samples were enclosed in a polymeric jar while being elevated from the bottom. A solvent or solvent mixture was poured into the bottom of the jar and the system was sealed for varying durations (1–24h). For sintering structures composed mainly of PLLGA and PMMA microspheres, acetone was used (publications **I** and **III**), whereas a 1:3 acetone:water mixture was used for sintering samples containing 45–50% (vol) of PLGA microspheres (publication **III**). The different sintering conditions were chosen with the aim of achieving similar sintering behavior for the different materials. After sintering, the samples were vacuum dried overnight at room temperature. The efficiency of solvent removal during vacuum drying has been studied in publication **III** supplementary material.

4.7 Characterization of the printed samples

The printed samples were photographed immediately after preparation (publications **I** and **II**), as well as after drying (publications **I**, **II**, and **III**).

4.7.1 Shrinkage

In publications **I** and **II**, the solid cylinders (printed using D_n = 410 µm and h = 328 µm) were used for shrinkage determination (n = 3) after calculating their volumes based on dimensional measurements taken with a caliper. In publication **I**, the analysis was conducted for the sintered samples made from the PLLGA50 ink by comparing the volumes of the sintered samples (V_{final}) to their initial volumes before sintering ($V_{initial}$). Volumetric shrinkage was calculated using the following equation:

$$Shrinkage = \left(1 - \frac{V_{final}}{V_{initial}}\right) \cdot 100\% \quad (6)$$

In publication **II**, the analysis was conducted for the dried samples made from PLLGA inks with different microsphere concentrations. Sample volumes (V_{print}) were compared to the theoretical print volumes (V_{theor}), and the volumetric shrinkages were calculated using the following equation:

$$Shrinkage = \left(1 - \frac{V_{print}}{V_{theor}}\right) \cdot 100\% \quad (7)$$

4.7.2 Porosity

The porosities of the samples were analyzed before and after sintering (publications **I** and **III**) using the following equation:

$$Porosity = \left(1 - \frac{m_{print}/V_{print}}{\rho_{print}}\right) \cdot 100\ \% \quad (8)$$

where m_{print} is the weight of the sample and ρ_{print} is the theoretical density of nonporous dry ink. For the density calculations, a density value of 1.41 g/cm^3[158] was used for the Carbopol polymer. The densities of the microspheres have been presented earlier.

The internal structure of the solid cylinder samples made from PLLGA50 ink (n = 1) was analyzed in publication **I** using micro-computed tomography (μCT). The imaging was conducted with a Phoenix Nanotom S (GE Sensing & Inspection Technologies GmbH, Wunstorf, Germany) using the following parameters: 60 kV voltage, 240 μA current, 1,440 projections, an exposure of 4 × 500 ms/projection, and a voxel size of 3 μm. The data were processed with ImageJ® software (version 1.54f) using automatic brightness/contrast adjustment and threshold functions before calculating the area percentages of the porous and solid phases.

4.7.3 Morphology

The printed samples (n = 1) were imaged with the FE-SEM following the same protocol as in the microsphere characterization, with the exception of adding Pelco® colloidal graphite (Ted Pella Inc., Redding, California, USA) during sample mounting. In publications **I** and **III**, the analysis was conducted on solid cylinder samples before and after the sintering by imaging their surface or cross-section. Prior to cross-sectional analysis, samples were manually cut with a scalpel. In publication **II**, the analysis was conducted on the dried solid and hollow cylinders without sintering.

4.7.4 Drug distribution

CLSM was used in publication **III** to analyze the drug distribution within the post-processed solid cylinder samples.

4.7.5 Mechanical strength

The mechanical strength of the printed PLLGA50 structures was investigated before and after sintering through compression testing (publication **I**). The samples (n = 3) were analyzed at a compression speed of 1 mm/min using an Instron 5943 universal testing system equipped with a 500 N load cell. Ultimate compressive strength values were determined from the first observed clear peaks in the stress-strain plots.

4.8 *In vitro* testing

In vitro studies were conducted in publication **III** for the microspheres and printed samples. Briefly, approximately 50 mg of the microspheres or a printed sample was immersed in 20 mL of PBS-Tween (pH 7.4) containing 0.02% (w/v) NaN_3 and placed in a shaking water bath (Model 1092, GFL Gesellschaft für Labortechnik GmbH, Burgwedel, Germany) at 37 °C and 100 rpm. Prior to placement in the shaker, the printed samples were briefly subjected to vacuum to ensure the penetration of the dissolution medium into the structures. The efficiency of the process has been studied in publication **III** supplementary material through dye staining testing.

4.8.1 Drug release

The amount of released FD was quantified at predetermined intervals by withdrawing 1.3 mL of the dissolution medium (n = 3), followed by centrifugation at 20,000 RCF for 5 min using an Eppendorf 5424. Then, 1.0 mL of the supernatant was collected for analysis, and an equal volume of fresh buffer was added to the tube. The mixture was vortexed before returning the contents to the original sample. The FD concentration was quantified from the extracted supernatant with a plate reader against a calibration curve using fluorescence analysis (excitation filter: 480/30 nm, emission filter: 530/30 nm). The percentage of FD released during the first day was determined as the burst fraction. Sink conditions were maintained throughout the study.

4.8.2 Mass loss

Mass loss was monitored for the samples printed from $RG504_{FD}50$ ink (n = 3). At predetermined intervals, the samples were taken, rinsed briefly with water, and vacuum dried at room temperature. The weights of the dry samples were compared to the initial weights measured before the start of the *in vitro* test.

4.8.3 Polymer degradation

The degradation study was conducted for different microspheres (PMMA excluded) and 3D printed samples made from $RG504_{FD}50$ ink through sampling at predetermined intervals (n = 1). The microspheres were separated from the dissolution medium by centrifugation at 4,000 RCF for 5 min in an Eppendorf 5804, followed by resuspension in water and repetition of the separation process. The 3D printed samples were rinsed with water after removing the dissolution medium. Samples were vacuum dried overnight at room temperature and dissolved in THF at a concentration of 0.5 mg/mL. For comparison, pure PLGA polymers and PLLGA microspheres were also analyzed.

Size exclusion chromatography (SEC) was used to analyze the molecular weight and molecular weight distribution of the samples. The system consisted of a model 515 HPLC Pump, 2707 Autosampler, 2414 Refractive Index Detector, PLgel column set (Agilent) (5 µm Guard 50 mm x 7.5 mm x 5 µm and 5 µm MIXED-C 300 mm x 7.5 mm x 5 µm) and a separate Mistral™ model 886 column thermostat (Spark Holland BV, Emmen, Netherlands). Polystyrene standards were used for calibration. Column and detector temperatures were set to 40 °C and 30 °C, respectively. A flow rate of 1 mL/min and an injection volume of 100 µL were used. Instrument operation and data collection were conducted via Empower software (Waters Corporation). The weight average molecular weights (M_w) after degradation were compared to the initial values (M_0) of the pure PLGA polymers or the PLLGA microspheres. The values were not corrected using the Mark–Houwink equation parameters, as only relative changes were monitored.

4.8.4 Morphological changes

Morphological changes occurring during the *in vitro* study were analyzed using the 3D printed samples made from $RG504_{FD}50$ ink (n = 1). At predetermined intervals, the samples were collected, rinsed with water, and vacuum dried. The surface and cross-section of the samples were imaged with FE-SEM, as previously described.

4.9 Statistical analysis

The results are presented as mean ± standard deviation. Statistical analysis was conducted using Minitab® software (versions 20–22, Minitab Inc., State College, Pennsylvania, USA). One-way analysis of variance (ANOVA) was performed, followed by Tukey's post-hoc test when statistically significant differences were observed. Statistical significance was determined as $p \leq 0.05$.

5 Results and Discussion

There is a growing interest in the use of biological macromolecules, such as proteins and peptides, in the pharmaceutical field.[159] To achieve long-term controlled release of these molecules, a common approach has been to use PLGA microspheres. [76], [160] However, for the preparation of personalized medicine, 3D printing has shown great promise[12], [14], making it reasonable to combine these different technologies.

In this thesis, PLGA microspheres containing the model hydrophilic macromolecule drug fluorescein isothiocyanate-dextran (40 kDa) were formulated and used in semi-solid extrusion 3D printing for the fabrication of controlled release drug delivery systems. The influence of post-processing on drug release and object degradation was assessed *in vitro*. The rheological behavior of different extrudable inks was first evaluated using commercial PLLGA microspheres. The PLLGA microsphere-based inks were also employed to optimize the SSE printing process and to evaluate the effects of ink formulation and post-processing conditions on the resulting structures.

5.1 Microsphere characterization

When considering the administration[67], drug release rate[77], or the rheological behavior[161], [162] of microspheres, their size and size distribution are critical factors. The PLLGA microspheres were used in publications **I**, **II**, and **III**, while the PMMA microspheres and the FD-loaded or placebo PLGA microspheres were used in publication **III**. In the preparation of the PLGA microspheres, different processing conditions were applied during the emulsification process to achieve similar particle sizes across all microspheres. As the molecular weight of the polymers increased (RG 502 H < RG 504 < RG 756 S), higher stirring rates were required to obtain similar particle sizes. This can be attributed to the increased viscosity along increase in the molecular weight of the polymer.[163]

The volume-weighted particle size distributions are presented in **Figure 10**, while **Table 10** lists the characteristic values of the different microspheres. All microspheres exhibited nearly identical size distributions, confirming the suitability of the chosen processing parameters. However, FE-SEM (**Figure 11**) analysis revealed differences among the microspheres. The PMMA microspheres had <5 µm

flakes attached to their surfaces, causing the small secondary peak in **Figure 10**. Additionally, open pores were observed on the surfaces of the FD-loaded microspheres. Given that FD has poor solubility within the PLGA matrix, these pores likely resulted from the heterogeneously distributed FD (**Figure 12)**, which partially dissolved in the external aqueous media during manufacturing. A more uniform FD distribution in PLGA microspheres was achieved by Mao *et al.*[146] at lower drug concentrations, indicating that the drug loading should be considered when optimizing formulations. Furthermore, the higher polymer concentration and smaller batch size in the study of Mao *et al*. may have led to faster microsphere hardening, limiting the FD separation.

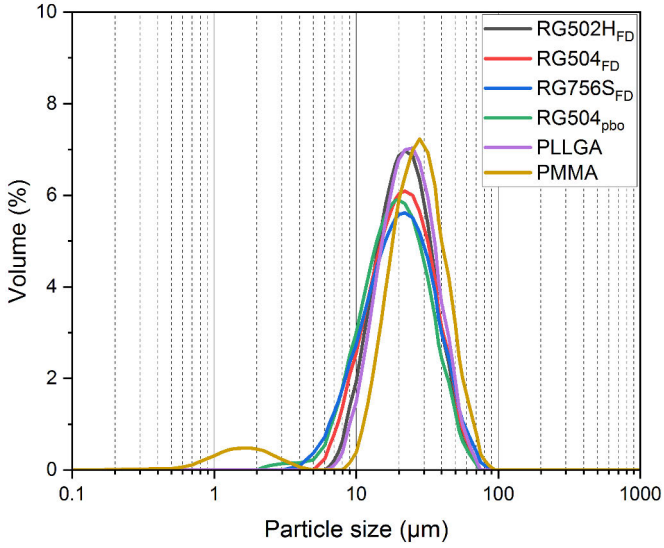

Figure 10. Volume-weighted particle size distributions of the different microspheres used in the thesis. Reprinted from publication **III** with permission from Elsevier.

Table 10 shows that the polymer influenced the drug loading degree and encapsulation efficiency. Both RG504$_{FD}$ and RG756S$_{FD}$ had an EE of approximately 75% and an LD of approximately 2.2% (wt), while RG502H$_{FD}$ showed EE less than 60% and an LD around 1.7% (wt). The lower viscosity of RG 502 H may have facilitated faster FD diffusion before microsphere hardening, resulting in reduced encapsulation efficiency. Overall, the data indicates good manufacturing repeatability and a high yield over 90%.

Table 10. Characteristic values* of the microspheres used in the thesis. Results are shown as mean ± standard deviation, when applicable**. Reprinted from publication **III** with permission from Elsevier.

Microsphere	D_{10} (µm)	D_{50} (µm)	D_{90} (µm)	Mean *D[4,3]* (µm)	Span	LD (%)	EE (%)	Yield (%)
$RG502H_{FD}$	11.4 ± 0.0	20.8 ± 0.0	36.9 ± 0.0	23.9 ± 0.0	1.2 ± 0.0	1.7 ± 0.1	58.5 ± 2.1	92
$RG504_{FD}$	10.3 ± 0.3	20.6 ± 0.5	39.0 ± 1.3	24.1 ± 0.7	1.4 ± 0.0	2.2 ± 0.1	76.9 ± 2.2	93 ± 1
$RG756S_{FD}$	8.8 ± 0.0	19.4 ± 0.0	38.9 ± 0.1	23.1 ± 0.0	1.6 ± 0.0	2.2 ± 0.2	75.6 ± 7.4	92
$RG504_{pbo}$	8.5 ± 0.4	17.6 ± 0.8	34.2 ± 1.6	20.7 ± 0.9	1.5 ± 0.0	N/A	N/A	91 ± 1
PLLGA	12.1 ± 0.1	21.9 ± 0.2	38.8 ± 0.4	25.1 ± 0.2	1.2 ± 0.0	N/A	N/A	N/A
PMMA	12.0 ± 0.0	25.0 ± 0.1	45.0 ± 0.1	28.0 ± 0.1	1.3 ± 0.0	N/A	N/A	N/A

* Volume-weighted particle size distribution values are shown. D_i represents the diameter below which *i*% of the particle population falls.

** Results were obtained by triplicate analysis from three parallel batches with $RG504_{FD}$ and $RG504_{pbo}$, and from a single batch with the rest of the microspheres. This is because only single batches of $RG502H_{FD}$ and $RG756S_{FD}$ were prepared.

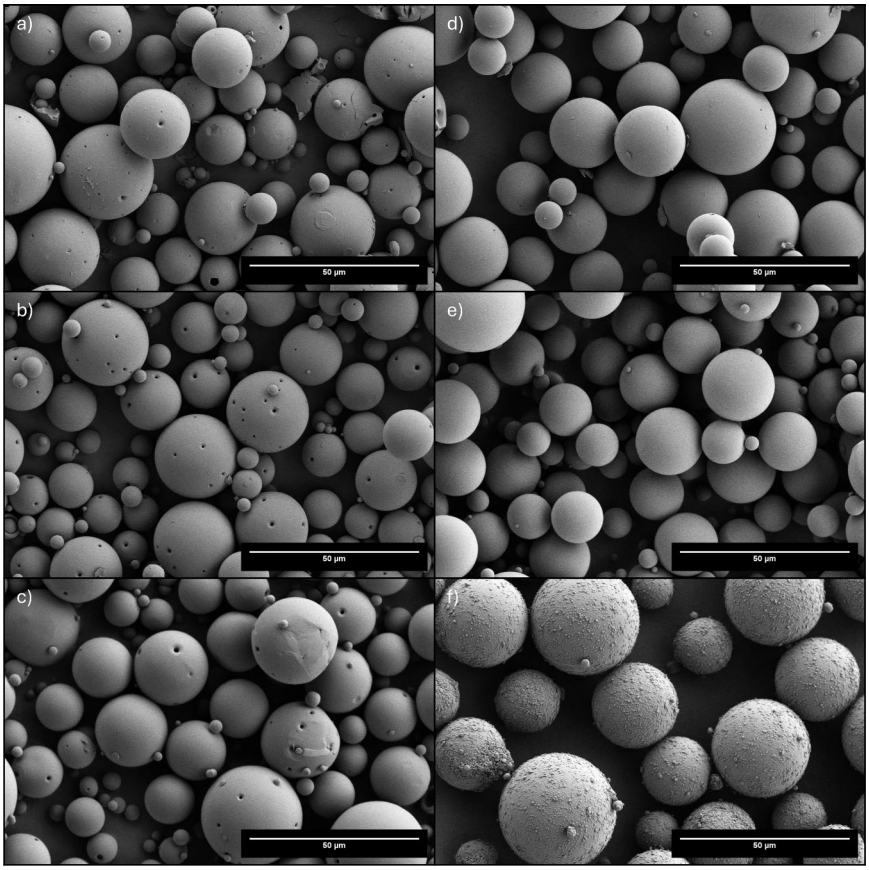

Figure 11. Representative FE-SEM images of the studied microspheres: a) RG502H$_{FD}$, b) RG504$_{FD,}$ c) RG756S$_{FD}$, d) PLLGA, e) RG504$_{pbo}$, and f) PMMA. Scale bars are 50 µm. Reprinted from publication **III** with permission from Elsevier.

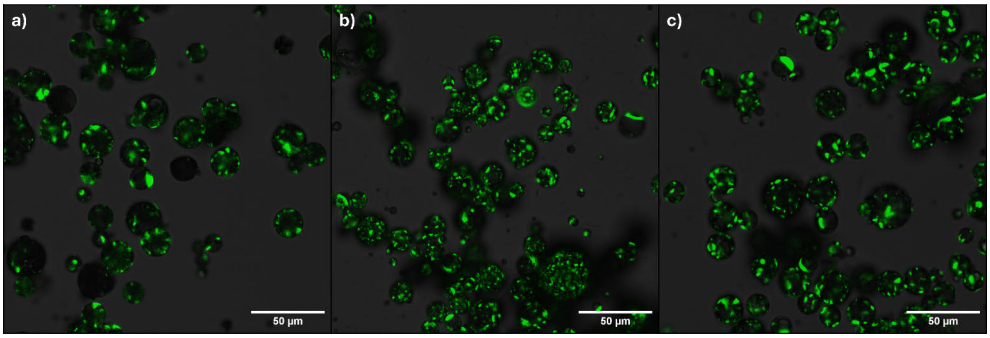

Figure 12. CLSM images of a) RG502H$_{FD}$, b) RG504$_{FD}$, and c) RG756S$_{FD}$ microspheres, showing the distribution of FD (green) in the (black) polymer matrix. The contrast between the dark grey background and the polymer matrix was created by applying an overlay of the transmitted light images with 10–15% opacity on the CLSM images. The black particles were not within the focal plane, thus lacking the fluorescence signal. Scale bars are 50 µm. Reprinted from publication **III** with permission from Elsevier.

5.2 Ink characterization

Carbopol microgels are highly effective rheology modifiers widely used in various pharmaceutical applications[158], [164]. Additionally, they have been demonstrated to be 3D printable.[165] For these reasons, Carbopol gel was selected as the ink matrix to achieve the desired rheological properties at a minimal concentration of 0.5% (w/v). This formulation allowed for the printing of constructs composed primarily of polymeric microspheres. In publication **I**, PLLGA microspheres were incorporated into the gel to achieve final microsphere concentrations ranging from 0% to 60% (vol), and the rheological properties of the inks were evaluated. Typically, the viscosity of the ink increases with the solid volume fraction. In this study, the highest particle concentration was close to the 64% theoretical random packing density of monodisperse spheres. Although the particles used were polydisperse, allowing for higher packing densities[166], [167], the ink with 60% (vol) microsphere content became too viscous for the experimental setup. Consequently, the maximum microsphere concentration was limited to 50% (vol).

Previous studies have shown that inks containing over 60% (vol) solids can still be extrudable.[168] However, the ink formulation method used in this thesis was based on an assumption that the microspheres were solid, potentially leading to an underestimation of their volume fraction due to the porosity within the particles. This observation aligns with the findings in publication **III**, where porosity was detected in the particles (**Figure 11**), necessitating the addition of water during the ink preparation. Furthermore, it is known that the maximum flowable particle volume fraction is influenced not only by the size distribution but also by the frictional interactions between particles.[162] These results suggest that the number of contact points among the solid components should not be excessively high for the ink to maintain smooth flowability.

The rheological analysis focused on assessing the relevant properties for an extrusion-based printing process, including viscosity, viscoelasticity, shear-thinning behavior, yield stress, and viscosity recovery. The results of this analysis are presented in **Figure 13** and **Table 11**.

The linear viscoelastic behavior is presented in **Figure 13a**, showing that all inks possess a linear region where $G' > G''$. This means that within a certain strain amplitude range, the inks behave as viscoelastic solids, characterized by a loss factor ($tan\ \delta$) < 1, which is essential for extrusion-based printing.[14], [118] This behavior is attributed to the elastic properties of Carbopol microgel.[164], [169]. Upon increase in the strain amplitude over a critical value (yield strain, γ_y), a decrease in G' is observed due to the slippage of the microgel particles past one another. Eventually, G' falls below G'' at a crossover point where the viscous behavior becomes dominant. When the microsphere concentration within the ink increases, both G' and G'' also increase. The inks containing 30–50% (vol) particles exhibit G' values within the range of 10^3

to 10^5 Pa, which is considered suitable for the SSE process.[14] However, higher microsphere concentrations lead to a decrease in the γ_y, resulting in a narrower linear viscoelastic region (LVR). At the same time, an increase in the *tan δ* values is observed, which can be attributed to the stiffening effect and the increased number of contact points between the solid particles, causing particle slippage at lower strains.[161], [170] The decreased elasticity is further reflected in the reduced type III overshoot peaks in the G'' curves near the crossover points, a phenomenon resulting from energy dissipation of the elastic component during deformation and rearrangement.[169], [171]

The oscillatory stress amplitude curves obtained from the yield stress analysis (**Figure 13b)** show similar linear regions and crossover points as those observed in the LVR analysis. However, when the viscoelastic moduli are plotted as a function of the shear stress (σ) amplitude, the linear ranges between the different inks are comparable. Similarly, the yield stress σ_y values derived from the crossover points ranged from approximately 220 to 360 Pa, with only PLLGA50 exhibiting a σ_y greater than 300 Pa. A high yield stress is generally considered beneficial for maintaining post-printing shape fidelity[118], [120]; however, no clear numerical requirements have been established. The results suggest that the yield stress is less responsive to changes in the microsphere concentration compared to the yield strain.

The flow curves in **Figure 13c** show typical shear-thinning behavior for all inks. At lower shear rates, the curves are overlapping, but at higher shear rates (above 1 1/s), they begin to diverge. To quantify this behavior, the Herschel–Bulkley model (**Equation 3**), which is known to effectively characterize Carbopol gels[158], [169], was applied. The obtained parameter values are summarized in **Table 11**. In general, the model fit the experimental data well, with R^2 values exceeding 0.996 for all samples. Consistent with the oscillatory yield stress analysis, the fitted values from the Herschel–Bulkley model indicated minimal effects of microsphere concentration on the yield stress, with all values falling within the range of 100–160 Pa. Notably, the yield stress values derived from the Herschel–Bulkley model were approximately half of those obtained from the oscillatory tests. This is due to the fact that the crossover point in oscillatory tests represents the material's flow stress, which is above the real yield point.[172]

The consistency index (K) is related to the viscosity of the ink.[121] The K values show only small differences when the microsphere concentration remains below 40% (vol). In contrast, the consistency index of PLLGA50 is significantly higher ($p < 0.05$), which is also seen in the slightly higher viscosity values, although this type of comparison is limited to inks with otherwise comparable Herschel–Bulkley model parameters. Higher viscosity is typically expected for inks with higher solid fractions.[166] However, the differences in the viscosities are small, and more pronounced differences have previously been reported in glass powder-containing

hydrogel inks by Nan *et al*.[170] According to their findings, viscosity increases due to the formation of a percolating particle network within the ink. They observed significant viscosity changes when the particle concentration increased from 25% to 35% (wt), whereas for the PLLGA inks, this effect appears to occur only above a 40% (vol) particle concentration. These differences may be attributed to the varying particle shapes, since the glass powder used in Nan *et al.*'s study was likely nonspherical due to mechanical grinding. In contrast, spherical PLLGA particles have limited capacity for structural organization within the ink, thereby reducing their impact on viscosity or shear-thinning at low shear rates.[173], [174] Additionally, the Carbopol microgel matrix may restrict the contact formation between the microspheres, leading to a decreased effect of particle concentration on viscosity. Such an effect has been reported by Sato *et al.*[173] in different aqueous inks. They observed only minor effects of silica particles on the ink viscosity and attributed it to the low particle interaction, the high viscosity of the ink matrix, and the alignment of matrix molecules during flow. Moreover, the presence of solid particles may lead to shear localization in smaller volumes, resulting in more pronounced shear-thinning.[161], [175], [176]

The flow index (*n*) describes the shear-thinning behavior of the ink: the lower the *n*, the higher the degree of shear-thinning.[121] Characteristically to Carbopol gels, the flow index values of all inks are in the range of 0.35 to 0.50.[158], [164], [169] However, the *n* appears to increase with rising microsphere concentration, indicating that inks with higher microsphere fractions are less shear-thinning. This variation in the *n* values is responsible for the divergence of the curves in **Figure 13c** at high shear rates. A similar effect has been observed in non-Brownian limestone suspensions by Wilms *et al.*[176]. They attributed the phenomenon to increased interparticle friction at higher solid fractions, resulting in a higher flow index for strongly shear-thinning phases. The behavior of the PLLGA microsphere-based inks aligns with the hypothesis of Wilms *et al.*, as the effect becomes more pronounced at higher particle concentrations. However, Sato *et al*.[173] studied aqueous xanthan solutions containing silica particles and noted that the increase in the flow index with the addition of solid particles could be attributed to reduced structural complexity. Their findings indicated that the effects of silica particles were evident even at concentrations below 10% (vol), differing from the observations with PLLGA microsphere inks. Therefore, the contact formation and interparticle friction among the particles is the more probable explanation for the reduced shear-thinning behavior. Overall, the differences in the rheological behavior of the inks under continuous flow are less pronounced than when the inks are at rest (as shown in **Figure 13a** and **Figure 13b**). This suggests that the incorporation of polymeric microspheres into the Carbopol gel enhances the stiffness of the ink without significantly affecting its flow properties.

The three-interval thixotropy test (3ITT) graphs are presented in **Figure 13d** and **Figure 13e**. Initially, the O-R-O method (**Figure 13e**) was selected as it simulates the extrusion process, where the ink is at rest in the barrel (interval I), then subjected to continuous flow (interval II), and finally returns to a resting state after extrusion (interval III). Typically, the viscosity (or G' and G'') levels at the beginning of the third interval are lower than those during the first interval, and recovery towards the initial values is observed.[14], [120], [155] However, while the viscoelastic moduli in the first interval are comparable to those observed in the LVR analysis (**Figure 13a**), the values at the beginning of the third interval are higher than the initial ones and exhibit a time-dependent decrease until stabilization. After 60 seconds of recovery, the G' values exceeded 120% of the initial values for all inks. This behavior was unexpected, although similar atypical recovery has been reported for other systems.[170], [177] Since all inks exhibited this behavior, it is likely a characteristic of the Carbopol matrix. A probable explanation is the elastic deformation of the microgel particles during the second interval, resulting in a stiffer gel structure. This is supported by the observation that the torsional force of the plate geometry was not released after the second interval, leading to residual stress and stored elastic energy. Carbopol gels are known to retain residual stresses after deformation, complicating the rheological analysis. Additionally, the long stabilization times associated with the characteristic long relaxation times of Carbopol gels[158], [178] make it challenging to avoid this phenomenon. Faster stabilization was observed in the inks with higher microsphere concentrations, likely due to decreased elasticity and the release of residual stress as the microgel particles slip into lower-energy positions.

Due to the limitations of the O-R-O method, the 3ITT was also conducted in a rotational mode (R-R-R) with shear rates of 0.1, 10, and 0.1 1/s for the first, second and third intervals, respectively. When transitioning to the high shear rate phase (interval II in **Figure 13d**), the viscosities decreased by approximately two decades, but also recovered over 80% within the first 4 seconds of the third interval. After 30 seconds, all inks had recovered more than 88% of their initial viscosities. The inks containing up to 30% (vol) microspheres achieved almost complete recovery of 98%, while the inks with higher microsphere concentrations exhibited recoveries between 89% and 95%. The reduced recovery in the inks with higher solid fractions may be attributed to stronger structural organization during the second interval. Alternatively, slight loss of sample or edge fracture during the second interval could also affect the recovery. Overall, the inks demonstrated good viscosity recovery over 80%, which has previously been considered a requirement for the successful manufacturing of multi-layer structures.[122] The immediate dominance of G' over G'' in **Figure 13e** further supports the inks' potential for 3D printing. However, shape distortion after printing is also influenced by the overall viscosity of the ink[179], indicating that multiple factors must be considered.

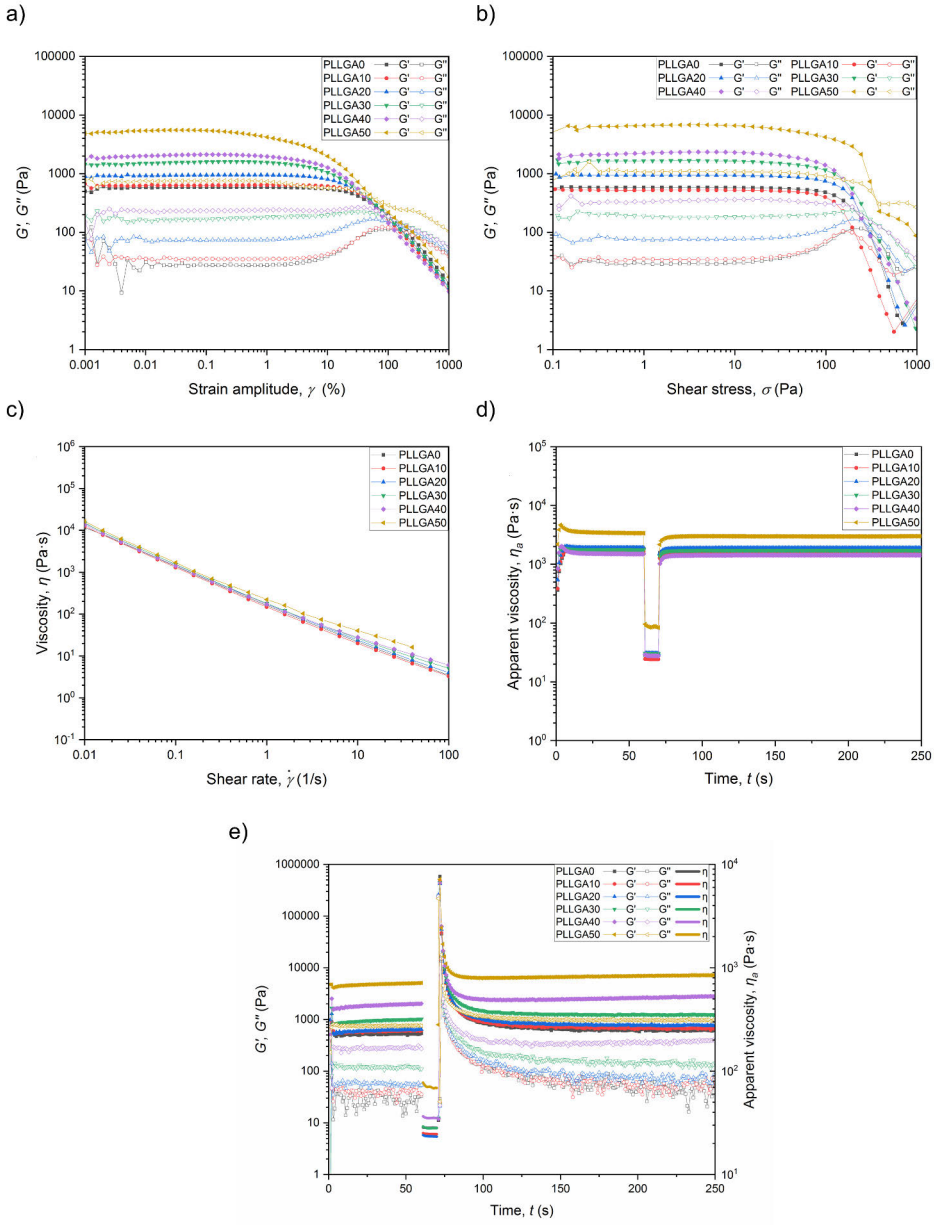

Figure 13. Representative graphs from the rheological analysis of inks with different PLLGA microsphere volume percentages: a) linear viscoelastic region (LVR) determination, b) oscillatory yield stress determination, c) flow curve analysis, and 3ITT viscosity recovery testing in d) R-R-R mode and e) O-R-O mode. In c), the final data points for PLLGA50 were discarded due to edge fracture and loss of the sample between the rheometer plates at high shear rates. Adapted from publication **I** with permission from Elsevier.

TABLE 11. Collection of the determined rheological values of the inks with different PLLGA microsphere volume percentages, presented as mean ± standard deviation. Statistically significant differences ($p < 0.05$) are indicated by different letters in the superscripts. Adapted from publication **I** with permission from Elsevier.

Test	LVR[i]				Yield stress (oscillatory)[ii]	Flow curve			3ITT[iii]	
Factor	γ_y (%)	G'_{LVR} (Pa)	G''_{LVR} (Pa)	$tan\ \delta_{LVR}$ (-)	$\sigma_{y,\,osc}$ (Pa)	$\sigma_{y,\,HB}$ (Pa)[ii]	K (Pa·s^n)	n (-)	G' recovery (%)	η recovery (%)
PLLGA0	7.9 ± 0.8 ^{a}	581 ± 7 ^{a}	28 ± 0 ^{a}	0.05 ± 0.00 ^{a}	290 ± 7 ^{a}	118 ± 3 ^{a,b}	47 ± 0 ^{a}	0.35 ± 0.00 ^{a}	130 ± 5 ^{a,b}	98
PLLGA10	10.4 ± 0.9 ^{b}	623 ± 12 ^{a}	35 ± 0 ^{a}	0.06 ± 0.00 ^{a,b}	222 ± 18 ^{b}	113 ± 4 ^{a}	28 ± 3 ^{a}	0.43 ± 0.01 ^{b,c}	132 ± 1 ^{a,b}	98
PLLGA20	4.1 ± 0.3 ^{c}	972 ± 36 ^{a,b}	76 ± 3 ^{a}	0.08 ± 0.00 ^{b}	274 ± 2 ^{a}	135 ± 3 ^{a,b,c}	41 ± 1 ^{a}	0.40 ± 0.01 ^{b}	136 ± 2 ^{a,b}	98
PLLGA30	1.4 ± 0.1 ^{d}	1,718 ± 134 ^{b,c}	198 ± 28 ^{a,b}	0.12 ± 0.01 ^{c}	278 ± 18 ^{a}	141 ± 4 ^{b,c}	45 ± 3 ^{a}	0.46 ± 0.02 ^{c}	134 ± 4 ^{a,b}	98
PLLGA40	1.0 ± 0.2 ^{d}	2,435 ± 326 ^{c}	330 ± 94 ^{b}	0.13 ± 0.02 ^{c,d}	234 ± 1 ^{b}	126 ± 1 ^{a,b}	44 ± 2 ^{a}	0.50 ± 0.01 ^{d}	129 ± 4 ^{a}	95
PLLGA50	0.2 ± 0.0 ^{d}	6,066 ± 708 ^{d}	892 ± 131 ^{c}	0.15 ± 0.01 ^{d}	363 ± 13 ^{c}	153 ± 20 ^{c}	87 ± 19 ^{b}	0.49 ± 0.01 ^{d}	139 ± 3 ^{b}	89

[i] In the LVR tests, the subscript LVR is used to denote the mean values determined within the linear region.
[ii] Yield stress values obtained either by oscillatory tests or by Herschel–Bulkley fit are distinguished with subscripts $_{osc}$ and $_{HB}$, respectively.
[iii] In the 3ITT, the recovered G' was determined after 60 seconds as an average from 5 data points, whereas the recovered viscosity was determined with a single point after 30 seconds.

5.3 Printability assessment and process optimization

The printability assessment and 3D printing process optimization were conducted in publication **II** using the PLLGA microsphere-based inks. Additionally, 3D printing demonstrations can be found in publications **I** and **III**.

5.3.1 Filament formation and extrudate swell

The formation of a consistent and continuous filament is an essential requirement for sufficient printability.[118], [121] To evaluate the filament-forming capability of the inks, they were extruded through nozzles of varying sizes (D_p). Representative photographs of the extruded filaments are available in the supplementary material of publication **II**. All inks were extrudable through nozzles with D_p ranging from 200 to 580 µm. However, extruding the PLLGA50 ink through the 200 µm nozzle resulted in a granular and wavy filament. Previous studies have shown that concentrated microgel inks can be extruded through nozzles having diameters 2–4 times larger than the average microgel particle size.[180], [181] In contrast, when the ink contains solid particles, it is generally recommended to use nozzles with diameters over 10 times the average particle diameter.[14], [182] Since the sizes of the PLLGA microspheres (**Table 10**) and swollen Carbopol gel particles[158], [183] are comparable (mean size ≈ 25 µm), the solid PLLGA microspheres were the limiting factor. This is further supported by the observations with the PLLGA50 ink, where high microsphere concentrations led to increased particle-particle interactions, causing jamming in small nozzles.[184] Consequently, a 410 µm nozzle was selected for the tests presented in the following sections.

Measuring the width of deposited lines is a common method for evaluating processing parameters and printability.[121], [182] However, this approach is limited by ink spreading due to gravity, and even slight changes in layer height can affect the results.[141], [182] Because of these limitations, filaments were extruded in air, and their diameters (D) were measured using image analysis (**Figure 14**). The determined extrudate swell ratios (S) are provided in the supplementary material of publication **II**.

All D values were found to be larger than D_p, resulting in $S > 1$ for all ink-nozzle combinations. While D typically decreased with smaller nozzle sizes, the differences were minimal and statistically insignificant within the range of 250 to 410 µm for most inks. This phenomenon was unexpected and may originate from the elastic structure of the Carbopol gel: only when the nozzle becomes sufficiently small does the stress on the gel cause the microgel particles to slip past each, leading to unrecoverable deformation.

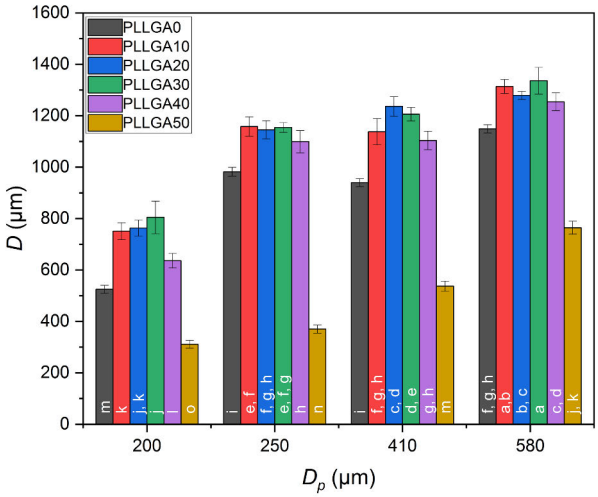

Figure 14. Filaments were extruded in air through nozzles of varying sizes (D_p) at a 1.5 µL/s extrusion rate, and their diameters (D) were measured using image analysis. The bars and error bars represent the mean values and standard deviations, respectively. Statistically significant differences ($p < 0.05$) are indicated by different letters. Adapted from publication **II** with permission from Elsevier.

Typically, extrudate swell increases with the elasticity of the ink but decreases with higher filler content.[14], [161], [185], [186]. Although **Figure 13a** showed an increase in G' with the rising microsphere concentration, the extrudate swell did not follow a similar trend (**Figure 14**). Firstly, PLLGA0 exhibited lower extrudate swell than the inks containing 10–40% (vol) microspheres. The lower values of PLLGA0 may have been influenced by the transparency of the gel, leading to a lower contrast in the image analysis. Additionally, gravitational pull may have elongated the freely hanging filament, particularly affecting PLLGA0, which had the lowest G'. Furthermore, the extrudate swell remained relatively stable at 10–30% (vol) microsphere concentration, with a decrease observed only when the concentration increased from 30% to 40% (vol) ($p < 0.05$). A more pronounced decrease occurred at a 50% (vol) microsphere concentration. For example, when using the 250 µm and 410 µm nozzles to extrude inks with 10–40% (vol) microsphere concentrations, the formed filaments had $D > 1{,}000$ µm, while for PLLGA50, $D < 600$ µm. The decrease in extrudate swell was indicated by the rheological analysis, which showed that the elasticity of the ink decreased with increasing microsphere concentration (**Figure 13a** and **Table 11**), leading to greater plastic deformation inside the nozzle and a subsequent reduction in the extrudate swell.[161], [186], [187] However, since this effect was only observed at high microsphere concentrations, the inks do not behave as simple systems. Their behavior is likely influenced by the competing effects of the

increased storage modulus and the reduced volume fraction of the elastically deformable gel component as the solid phase fraction increases.

The extrusion rate did not affect the extrudate swell (as shown in supplementary material of publication **II**), which contrasts with the typically observed increase in the extrudate swell at higher shear rates.[185], [186] Such behavior may again be attributed to the long relaxation time of the Carbopol gel, resulting in minimal relaxation within the nozzle during the extrusion process. Due to this lack of variation in the extrudate swell, it was feasible to use the average S and D values in the subsequent material flow optimization.

5.3.2 Printability index and filament collapse

Grid structures were printed to evaluate the differences between the PLLGA microsphere inks and their suitability for 3D printing of layered structures. In these tests, D_p and the nozzle size parameter (D_n) were set to 410 µm, while the layer height (h) was adjusted to 100%, 80%, or 50% of D_p. The printability index (P_r) values were calculated using **Equation 5**, following the image analysis of the pores. Perfectly shaped square pores yield P_r values of 1, while filament spreading and merging result in rounded pores with values below 1. Values above 1 are typically caused by irregular pores resulting from inconsistent filaments.[118], [154] Generally, P_r values in the range of 0.9–1.1 are considered adequate.[154]

Photographs from the printability index analysis are presented in **Figure 15**. The pores formed from inks containing 0–40% (vol) microspheres were rounded, as indicated by P_r values below 1.[155] In contrast, the PLLGA50 formulation yielded more rectangular pore structures, resulting in P_r values closer to 1. However, it was noted that the index values could be misleading, as some samples exhibited P_r values both above 1.1 and below 0.9, leading to average values close to 1. Therefore, qualitative analysis of the formed pores was necessary.

It was observed that the pores generally became more rectangular with increasing microsphere concentration or decreasing h. The effect of the microspheres can be attributed to the increased G' as the microsphere concentration within the ink increased (**Figure 13a** and **Table 11**), while lower h resulted in reduced extruded volumes, thereby decreasing the influence of gravity. Additionally, the spreading of the ink seems to be affected by extrudate swell, since the inks with the highest extrudate swell ratios also had the most deformed filaments and lower pore qualities. Consequently, the elastic recovery of the ink and the formation of thicker filaments impact the resulting pore quality.

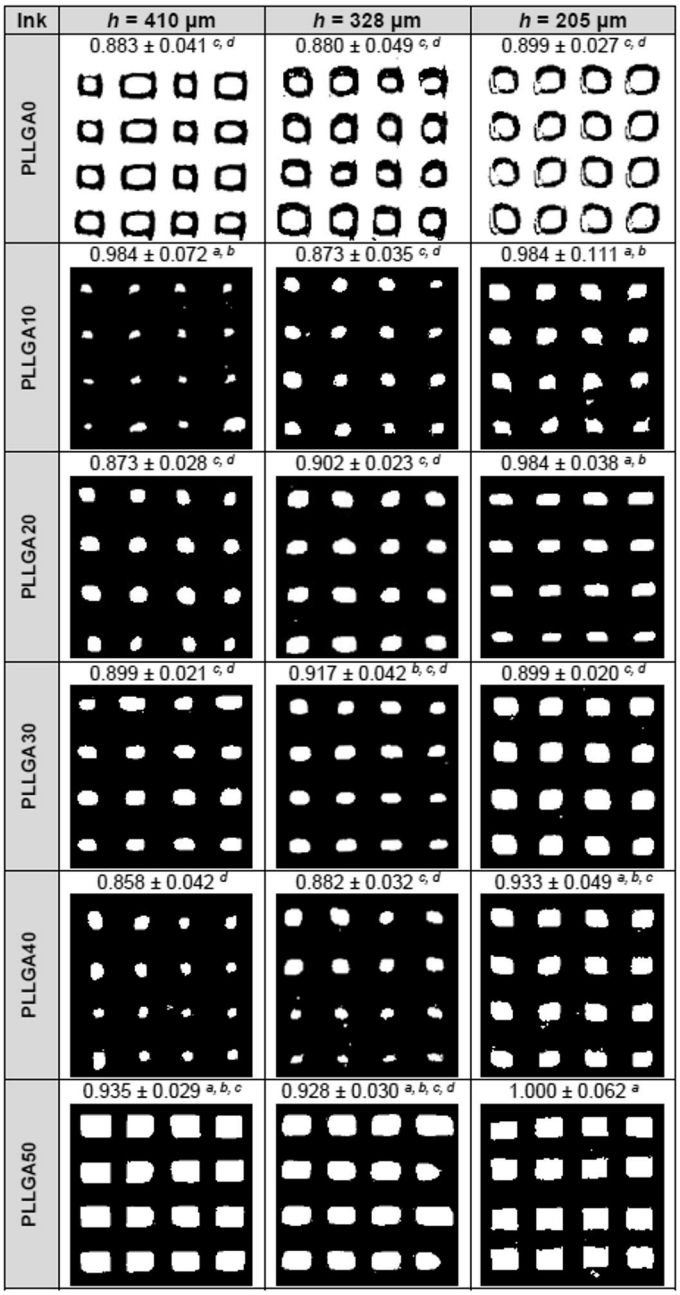

Figure 15. Representative thresholded photographs from the printability index analysis of inks with varying microsphere concentrations. Three different layer heights (h) were used, with D_p and D_n set to 410 µm. The resulting pore structures and printability indexes (mean ± standard deviation) are presented above the corresponding photographs. Statistically significant differences ($p < 0.05$) are indicated by different letters. The distance between the central points of the adjacent pores is approximately 1 mm. Reprinted from publication **II** with permission from Elsevier.

The filament collapse tests were conducted to evaluate the inks' ability to span gaps without collapsing. In contrast to the typically performed quantitative analysis of filaments spanning gaps of 1–16 mm[156], [188], [189], in publication **II** gaps up to 30 mm were tested, but only qualitative analysis was conducted.

In **Figure 16a**, a typical behavior in the test is illustrated using PLLGA30 ink as an example. As demonstrated in previous studies, filament deflection increases with the gap length due to more material being subjected to a gravitational pull.[156], [188] The ability of an ink to resist this deformation is influenced by its storage modulus and yield stress. In addition, controlling the extrusion rate is essential to prevent excessive sagging from over-extrusion or severe extension due to under-extrusion. For this reason, the effects of different D_n and h were assessed, with results shown in **Figure 16a** and **Figure 16b**.

When D_n and h were set equal to D_p, the inks containing 10–40% (vol) of microspheres failed to form stable filaments, and the maximum span distance of PLLGA0 also remained below 10 mm. In contrast, filaments extruded from the PLLGA50 ink successfully spanned gaps of ≥25 mm. This was due to the lower extrudate swell of PLLGA50, leading to a lower degree of extension with the set parameters. However, this slight extension was beneficial in reducing the filament deflection, as seen with PLLGA50 in publication **II** supplementary material.

When extrudate swell was taken into account in setting $D_n = D$, filament extension decreased, allowing all filaments to span longer gaps (10–30 mm). However, significant filament deflection occurred when also setting $h = D$, causing the filaments to contact the platform between the pillars. Extrusion rate calibration tests in publication **II** supplementary material confirmed that the extrusion rate is proportional to D_n and h, indicating that while the chosen parameters should have led to filament extrusion without extension or over-extrusion, further optimization is necessary for each ink. This can be achieved by quantifying the extrudate swell and also considering the spanning requirements when adjusting D_n. Overall, the results demonstrate that extrudate swell and extrusion rate significantly impact the outcome of the filament collapse test.

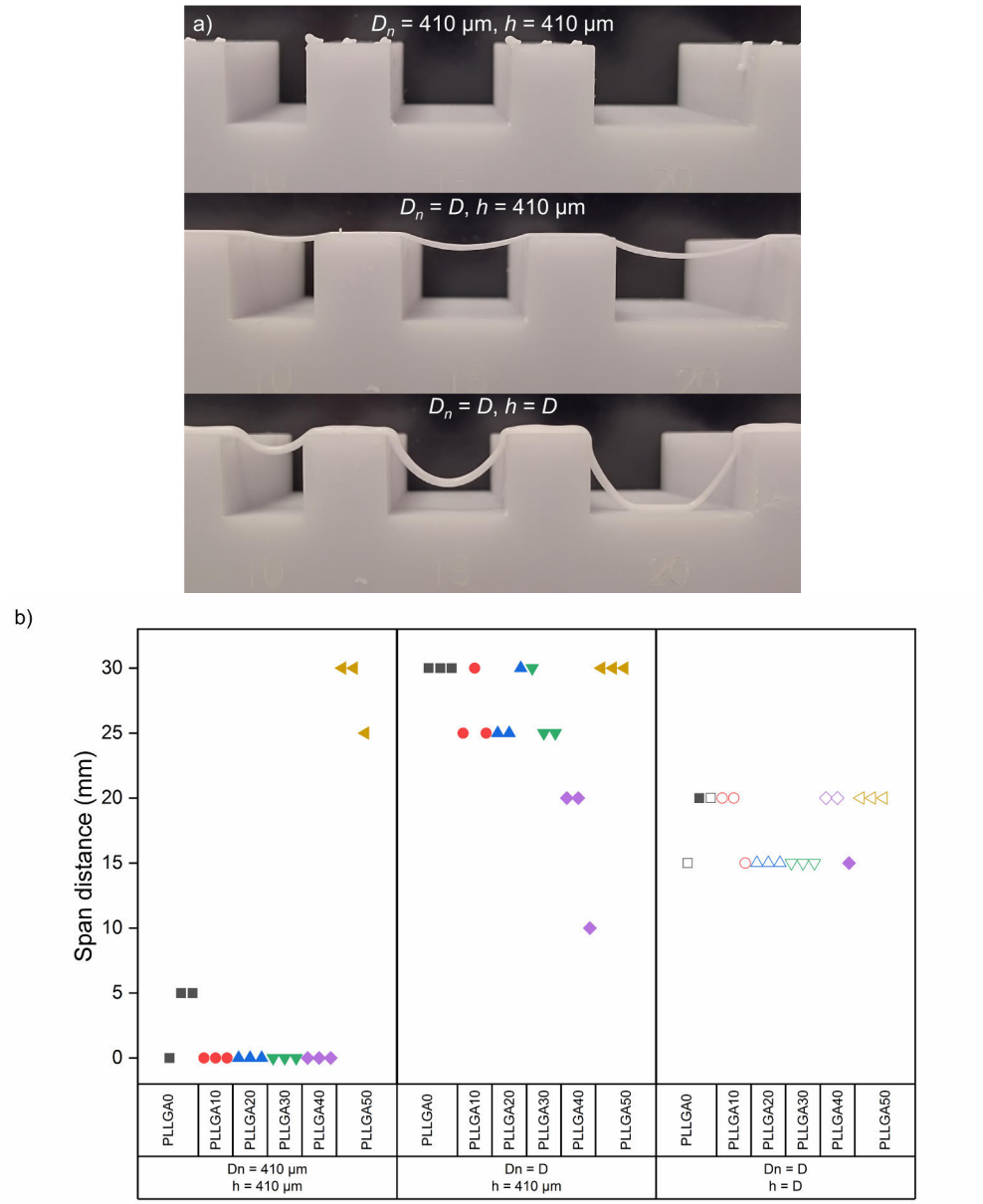

Figure 16. Photographs of the PLLGA30 ink in a) illustrate a typical behavior when a filament is deposited over different gaps (from left to right: 10, 15, and 20 mm), as well as the effects of different printing parameters on the maximum span length and filament deflection. In the grouped scatter plot b), the maximum filament span distances without breaking are presented with solid symbols, while the hollow symbols indicate the points after which the filaments touched the platform between the pillars due to sagging. In b), the results are shown for three parallel samples. For clarity, the *D* value is ink-specific. Adapted from publication **II** with permission from Elsevier.

5.3.3 Material flow optimization

Various printability assessment methods and the associated rheological requirements have been reported in the literature.[118], [121], [141], [188] While these serve as valuable guidelines in the ink development, it is essential to evaluate the practical effects of ink properties on the printing process and the quality of the resulting structures. For this reason, simple solid and hollow cylinders (diameter = 5 mm, height = 5 mm) were prepared in publication **II**.

The extrusion rate (Q) in the process depends on D_n, h, and v according to the formula:

$$Q \propto D_n \cdot h \cdot v \tag{9}$$

In addition, the extrusion factor (E) is used as a multiplying parameter to control the extrusion rate.[190] The following formula was used to calculate the E value that would allow for the deposition of a filament without extension:

$$E = \frac{Q_{swell}}{Q_{theoretical}} = \frac{D \cdot h \cdot v}{D_p \cdot h \cdot v} = \frac{D}{D_p} = S \tag{10}$$

In **Equation 10**, Q_{swell} and $Q_{theoretical}$ are the volumetric flow rates corresponding to the unextended and extended filaments, respectively. Q_{swell} is related to the extrusion of a filament affected by extrudate swell, whereas $Q_{theoretical}$ represents the theoretical situation without it. The equation reduces to the ratio of the measured filament diameter D, and the physical nozzle diameter D_p, i.e., the swell ratio S.

Figure 17 presents objects printed from the PLLGA0 and the PLLGA50 inks, while photographs of samples printed with other inks are shown in publication **II** supplementary material. In **Figure 17a**, the solid cylinders printed with varying D and h demonstrate that, as expected, the surfaces of the objects became smoother with lower h values. When h was set to 410 µm, changes in D did not significantly affect the resulting structures. Thus, while a larger nozzle typically leads to a decreased resolution[14], this effect can be mitigated by maintaining a low h[12]. However, a larger nozzle may result in suboptimal filling of small objects, as shown in publication **II** supplementary material. In contrast, the 410 µm nozzle (D_n) effectively filled the structures; however, the drag force of the deposited filament caused slight bending of the objects during printing, leading to ink accumulation in the center and the formation of rounded top layers (publication **II** supplementary material). Overall, the solid structure was able to withstand filament extension without catastrophic failure, indicating that extrudate swell had only minor effects on the quality of the solid cylinders. The PLLGA50 samples printed with $D_n = D$ and

$h = D$ suffered from poor contact formation between the layers and potential heterogeneity within the ink, decreasing the quality. Typically, printing is conducted with $h < D_n$[12], thereby reducing the risk of such failures.

In contrast to the solid cylinders, the hollow cylinders in **Figure 17b** demonstrate that neglecting extrudate swell significantly impacts object quality. When D_n was set to 410 µm, the cylinders became narrower, and the hollow structure disappeared as more layers were printed, primarily due to the drag force of the extended filament. Decreasing the h had only a negative effect on the quality, as lower h results in lower extrusion rate, leading to a more substantial extension of the filament. The results are in line with the observations of Wang and Shaw[191] who printed hollow cylinders using dental porcelain slurries. They calculated a critical nozzle height based on the extrusion rate, nozzle moving speed, and nozzle diameter, demonstrating that narrowing of the structure occurs when the nozzle height exceeds this critical value, i.e., when the extrusion rate does not correspond to the layer height.

However, as shown in **Figure 17b**, when $D_n = D$ was applied, the extrusion rate corresponded to the extrudate swell-affected filament, leading to the deposition of a filament without extension. This approach preserved the hollow structures and significantly improved object quality. In this case, decreasing h had positive effects, as the layer lines became less pronounced. For PLLGA50, h less than 80% of D_n was required to ensure proper contact formation between the different layers. These findings highlight the necessity of considering extrudate swell when printing hollow and thin-walled structures. Furthermore, this means that the final resolution of the object is not only limited by the physical nozzle size, but also by the extrudate swell.[122] When the data in **Figure 14** is considered, it might in fact be that, within a certain nozzle size range, the resolution remains relatively constant.

As indicated in **Equation 10**, the E corresponding to an unextended filament can be determined from S. To evaluate this approach, hollow cylinders were printed with varying E values, and the results are presented in **Figure 17c**. When E was set equal to S, the objects were practically identical to the ones shown in **Figure 17b** (when $D_n = D$). However, when $E < S$ was applied, the cylinders narrowed due to under-extrusion, whereas $E > S$ led to over-extrusion. While over-extrusion of PLLGA0 only led to the formation of thicker walls, buckling was observed with the PLLGA50 ink. This was likely due to the higher η, G', and σ_y of PLLGA50, which limited the filament's ability to be squeezed. Additionally, the lower S of PLLGA50 compared to the other inks caused a proportionally greater deviation from the ideal $E = S$ situation when the E was increased in specific increments. Overall, the results demonstrate the feasibility of optimizing E based on S. However, adjusting D_n instead of E was also feasible with the solid cylinders, making it a viable approach for producing more complex structures with both solid and thin-walled sections. This is because high E values can lead to significant over-extrusion and shape distortion

in the manufacturing of solid objects, as shown in publication **II** supplementary material.

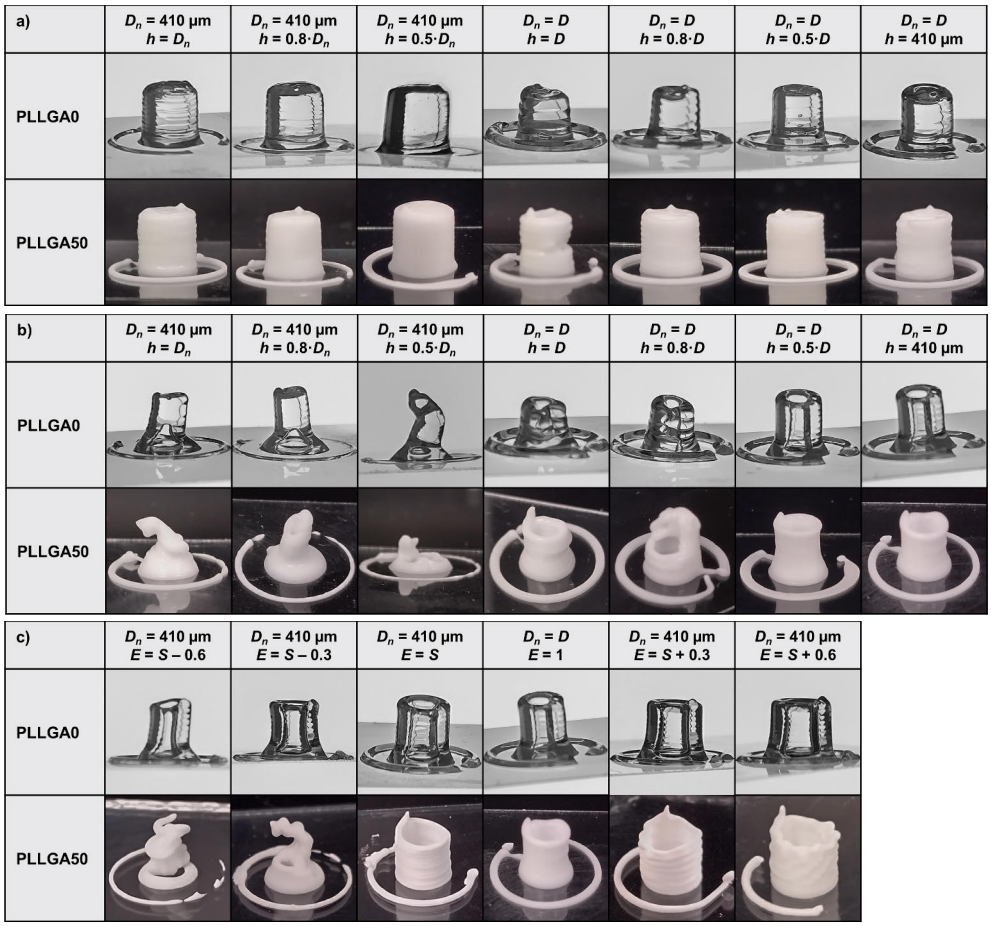

Figure 17. Representative photographs from the material flow optimization study. Objects printed from the PLLGA0 and PLLGA50 inks are shown as examples. Different D_n and h were used in the printing of a) solid and b) hollow cylinders. Hollow cylinders printed with h = 410 µm and different E are shown in c). For clarity, the D value is ink-specific. All objects have theoretical diameters and heights of 5 mm. In the tests, D_p = 410 µm. Reprinted from publication **II** with permission from Elsevier.

5.4 Effects of ink composition and post-processing parameters on the structure and properties of the printed objects

5.4.1 Ink composition effect on object shrinkage

Drying is a commonly required post-processing step for the objects manufactured by SSE 3D printing.[11] Since the aim in this thesis was to minimize exposure to high temperatures, a vacuum drying method was used in publications **I**, **II**, and **III**. Printed objects typically shrink during the drying process, which may cause unwanted deformations and dimensional inaccuracies.[12], [191] Thus, the phenomenon was evaluated in publication **II**.

The effect of ink composition on the volumetric shrinkage of the solid cylinders is presented in **Figure 18a** and **Figure 18b**. It was observed that the shrinkage was linearly dependent on the microsphere concentration in the ink, with higher microsphere concentration resulting in lower shrinkage (**Figure 18a**). The PLLGA0 cylinders, which contained only 0.5% (w/v) Carbopol gel, exhibited an extremely high shrinkage of 99.6%. In contrast, cylinders made from the PLLGA50 ink had shrinkages below 10%, which can be attributed to the microsphere concentration being only slightly below the close packing limit. All observed differences were statistically significant ($p < 0.05$). To achieve dimensions close to the original design, a high solid volume fraction is necessary. Alternatively, shrinkage must be taken into account during the design process.

The FE-SEM images of the hollow cylinders in **Figure 18c** show the effect of shrinkage on the wall thickness. The decrease in wall thickness (i.e. shrinkage in one dimension) was relative to the volumetric shrinkage, as shown in publication **II** supplementary material. Although the D_n was set significantly higher than D_p during printing (values listed in publication **II** supplementary material), the shrinkage upon drying had a counteracting effect on the final resolution and wall thickness. For instance, samples made from the PLLGA0 ink had a wall thickness of approximately 200 µm, which is less than 50% of D_p. These results demonstrate that controlled shrinkage by tailoring the ink composition is beneficial for enhancing precision in the printing process.

Previous studies have demonstrated that enhanced printing resolution can be achieved by using smaller nozzles[192] and slight under-extrusion[193]. However, the choice of nozzle size is limited by the size and concentration of the solid components within the ink. Furthermore, under-extrusion was shown to cause filament extension and deformation of the printed structures. Thus, post-printing shrinkage offers an advantage by overcoming these process-related limitations. Various methods for achieving shrinkage have been reported, including high-temperature pyrolysis[194],

gel scaffold collapse and dehydration[195], and solvent removal from cast objects[196]. Although these methods have been effective in certain applications for achieving high spatial resolution, they also possess limitations related to high temperatures[194], chemical reactions[195], and the use of molds[196], which may restrict their feasibility in the preparation of tailored drug delivery systems. In contrast, shrinkage resulting from the drying of semi-solid inks provides a straightforward method suitable for thermally sensitive materials.

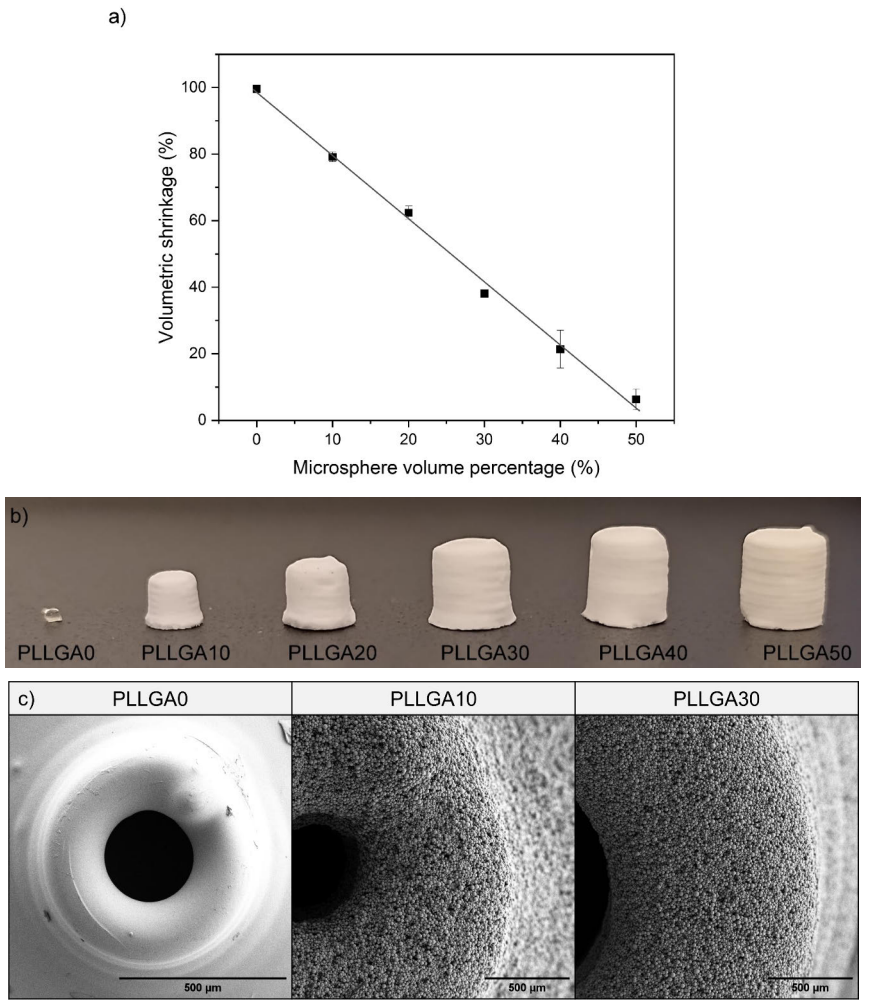

Figure 18. Volumetric shrinkage of the solid cylinders prepared with varying ink compositions is shown in a). In b) photographs of the printed and dried solid cylinders are shown. The FE-SEM images in c) show the PLLGA0, PLLGA10 and PLLGA30 hollow cylinders imaged from above. Scale bars in c) are 500 µm. D_p was 410 µm for all samples, while h depended on the sample type: 80% of D_p for solid cylinders and 50% of D_n *(D_n = D)* for hollow cylinders. Reprinted from publication **II** with permission from Elsevier.

5.4.2 Effect of post-processing on the microstructure and mechanical properties of the objects

Solvent vapor sintering was conducted as a post-processing step for the 3D printed structures in publications **I** and **III**. In the process, the objects were exposed to a solvent vapor-rich atmosphere at room temperature. The diffusion of solvent vapor into the objects resulted in a decrease in the T_g of the polymer, leading to increased polymer chain mobility and time-dependent fusing of the microspheres.[157], [197] To assess the potential of this method for tailoring the microstructure and mechanical strength of the printed objects, the solid cylinders were treated with either acetone (publications **I** and **III**) or a 1:3 mixture of acetone and water (publication **III**). Acetone was utilized for sintering structures consisting mainly of PLLGA and PMMA microspheres, while the acetone-water mixture was used for sintering structures containing PLGA microspheres, which dissolve more rapidly in acetone.

The effects of sintering time on the morphology and FD distribution within solid cylinders made from the $RG504_{FD}50$ ink were studied in publication **III**, and the results are shown in **Figure 19**. The samples without sintering (sintering time = 0 h) contained separate microspheres bound only by thin strands of dry gel, whereas the sintered samples show progressive fusing of the microspheres throughout the entire sample geometry as the sintering time increased. While individual microspheres remained detectable in the objects treated for up to 4 h, sintering times of ≥6 h resulted in nearly complete fusing of the particles. However, residual porosity was still observed within the samples even after 24 h of sintering (publication **III** supplementary material), which was attributed to entrapped air. The CLSM images also indicated that, although the microspheres fused during the process, the drug remained heterogeneously distributed. Similar sintering behavior was observed in publication **I** with solid cylinders made from the PLLGA50 ink (without the drug).

Particle fusing during sintering resulted in shrinking of the samples. This phenomenon was quantified in publication **I**, along with the changes in porosity and compressive strength of the solid cylinders made from the PLLGA50 ink. **Figure 20** shows that the porosity of the cylinders decreased from approximately 50% to 30% after sintering for 24 h, which also corresponded to a shrinkage of over 25%. As the contact area between the microspheres increased, the ultimate compressive strength increased from below 1 MPa in the untreated cylinders to approximately 9 MPa in the objects treated for 24 h. Overall, the compressive strengths of the cylinders fell within the range reported for trabecular bone[198], indicating their potential for load-bearing applications.

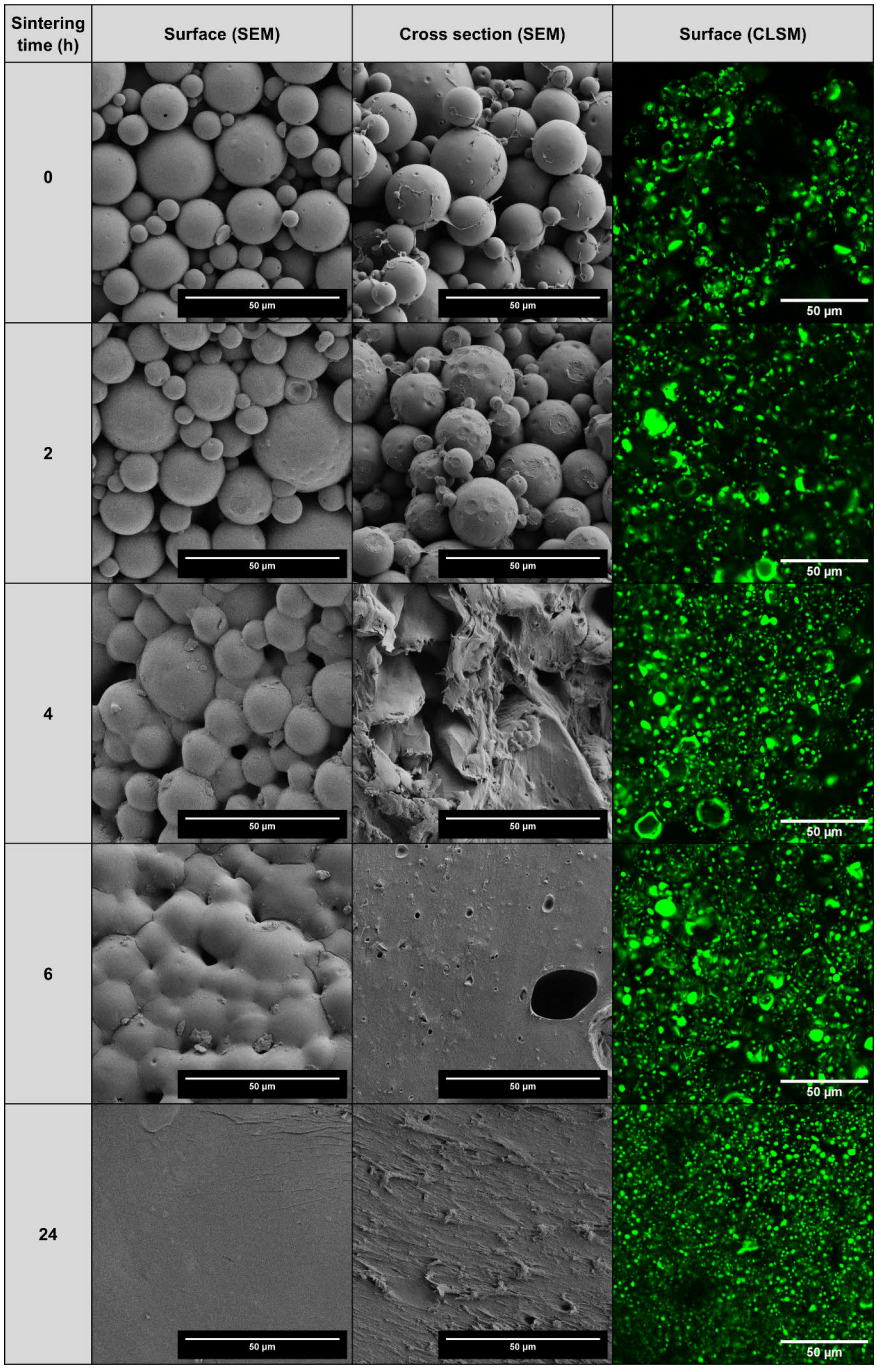

Figure 19. Effect of solvent vapor (acetone and water 1:3 mixture) sintering on the morphology and drug distribution within solid cylinders printed from the $RG504_{FD}50$ ink. Samples were treated for different times and imaged with FE-SEM (surface and cross-section) and CLSM (surface). All scale bars are 50 µm. Reprinted from publication **III** with permission from Elsevier.

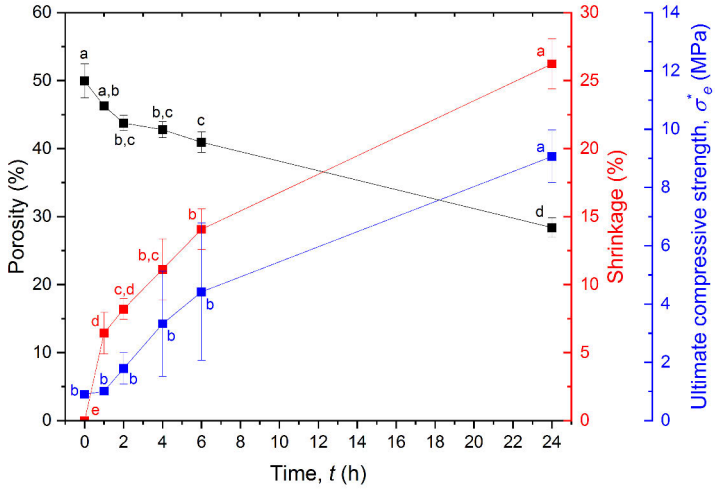

Figure 20. Porosity (black), shrinkage (red), and ultimate compressive strength (blue) evolution of solid cylinders printed from the PLLGA50 ink sintered for different times with acetone vapor. Statistically significant differences ($p < 0.05$) are indicated with different letters. Reprinted from publication **I** with permission from Elsevier.

5.5 *In vitro* drug release and polymer degradation

In vitro tests were conducted in publication **III** to study the effects of microsphere and ink formulations, as well as the sintering process, on drug release properties and polymer degradation. Solid cylinder samples (diameter = 5 mm, height = 5 mm) were printed and subjected to solvent vapor for varying durations, while the microspheres were used without further processing. The samples were immersed in PBS-Tween pH 7.4 buffer containing 0.02% (w/v) NaN_3 as a preservative and incubated for up to three months under constant stirring.

5.5.1 Microspheres

The release of FD from the different microspheres is presented in **Figure 21a**, showing significant differences between the formulations. Since the particle size distributions were identical for all microspheres (**Figure 10**), these differences can be attributed to the used polymers. Multi-phase release profiles were observed in the $RG502H_{FD}$ and $RG504_{FD}$ microspheres, whereas the $RG756S_{FD}$ microspheres displayed only an initial burst release followed by a long slow-release phase without complete release. The burst release is typically caused by the release of drug molecules located near the surface, while the later high release rate phase is attributed to polymer erosion.[30] The extent of the burst varied depending on the polymer, with the $RG502H_{FD}$ microspheres exhibiting a burst over 50%, whereas the

burst from the other microspheres was less than 10%. The high burst release observed in RG502H$_{FD}$ can be attributed to the acid end-capping of the polymer, which enhances water penetration and initial drug release.[199] Overall, the drug release rates were influenced by the degradation times of the polymers (RG 502 H < RG 504 < RG 756 S, as presented in **Figure 21b**), with the later high-release phases coinciding with significantly decreased molecular weights.[146], [199]

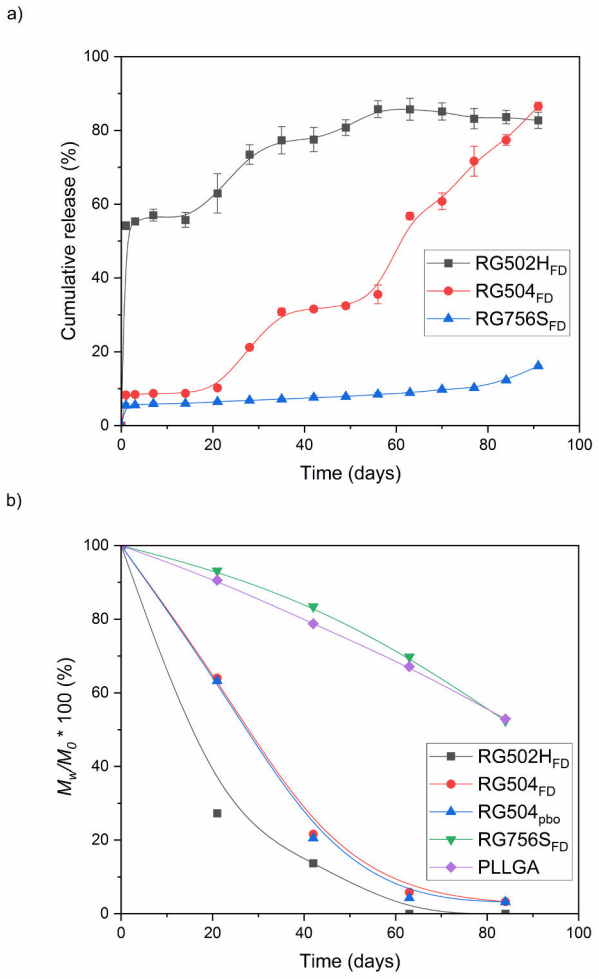

Figure 21. Cumulative *in vitro* FD release from the different microspheres is shown in a), whereas b) presents the relative molecular weight (M_w) decrease for the microspheres. Reprinted from publication **III** with permission from Elsevier.

5.5.2 3D printed systems

FD release from the printed $RG504_{FD}50$ cylinders after different sintering times is shown in **Figure 22a**. Sintering time significantly influenced the extent of burst release, which can be attributed to the decreased open porosity and surface area resulting from particle fusing. The burst decreased from over 20% in the unsintered samples to less than 5% after the cylinders were sintered for 24 h ($p < 0.05$). These results align with the observations of Elsner *et al*.[200], who studied drug-releasing wound dressings and concluded that the extent of burst release correlated with the porosity of the matrix. Notably, the unsintered samples exhibited a higher burst compared to the $RG504_{FD}$ microspheres (shown in **Figure 21a**), likely due to the aqueous ink formulation, which allowed partial drug release before the printed samples were dried. Unsintered samples also disintegrated within the first day due to the wetting of the hydrogel. Interestingly, while the sintering process affected the burst release, the release rates remained similar between days 1 and 21, regardless of the sintering time. Previous studies[199], [201] have demonstrated that higher porosities typically lead to increased drug release rates due to the greater number of diffusional channels[202], [203]. However, in the case of the $RG504_{FD}50$ cylinders, the drug was encapsulated within microspheres, which likely decreased the effect of porosity on the diffusional release during the initial weeks.

After 21 days, higher release rates were observed in the samples sintered for longer durations. Additionally, the onset of the high release rate phase between days 49 and 63 was slightly shifted to earlier time points for these samples. This can be attributed to the autocatalytic degradation of PLGA, where the accumulation of acidic degradation products in larger and denser structures accelerates the polymer degradation.[204]–[206] This phenomenon is also reflected in **Figure 22b**, showing a greater mass loss on day 63 in the cylinders sintered for ≥6 h ($p < 0.05$). However, such differences were less pronounced when considering the molecular weights (**Figure 22c**), likely due to the release of low molecular weight species during degradation, resulting in a lower effect of degradation on M_w during the active erosion phase.[207]

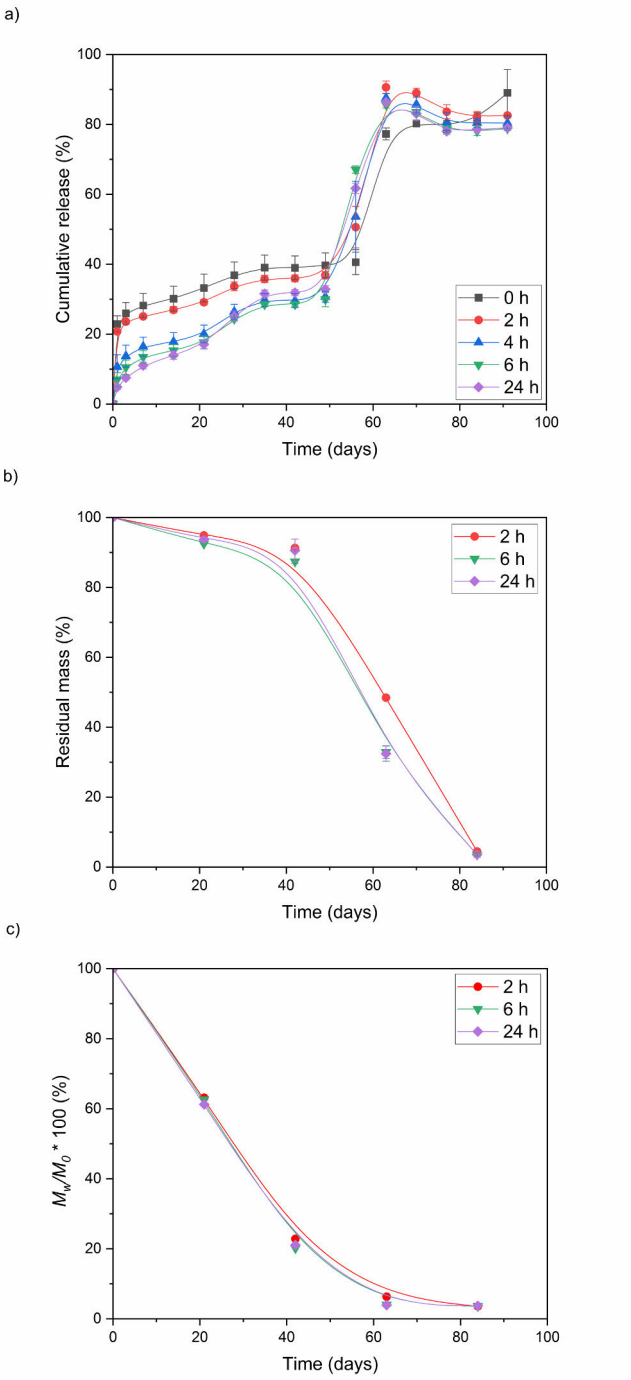

Figure 22. Cumulative *in vitro* a) FD release, b) mass loss, and c) molecular weight decrease of the $RG504_{FD}50$ cylinders sintered for different times. Reprinted from publication **III** with permission from Elsevier.

The effects of *in vitro* degradation on the internal and external morphology of the sintered $RG504_{FD}50$ cylinders are illustrated in **Figure 23**. No substantial changes were detected after 21 days, and the cylinders either contained intact individual microspheres or remained dense, depending on the sintering time. After 42 days, significant degradation had occurred. The microspheres in the cylinders sintered for 2 h became deformed and porous, while the samples sintered for ≥6 h developed a spongy texture. This change was also accompanied by significant swelling (publication **III** supplementary material). Swelling and pore formation during degradation have previously been observed in PLGA implants[208], [209] and microspheres[210]–[213]. Bassand *et al.*[208] showed that ibuprofen release rate from PLGA implants correlated with implant swelling, while Gasmi *et al.*[211] found that the swelling of PLGA microsphere and the rapid release of prilocaine free base were influenced by high water penetration into the degraded matrix. Similar observations were made by Gu *et al.*[212], who embedded dexamethasone-loaded PLGA microspheres in PVA hydrogel. In addition to microsphere swelling, they noted that the autocatalytic effect caused internal pore formation within the microspheres. The results of this thesis agree with these observations, as the high release rate phases were observed in swollen cylinders, although this occurred only after the onset of the active erosion phase. Finally, after 63 days, the 3D structures collapsed and became glassy (**Figure 23** and publication **III** supplementary material).

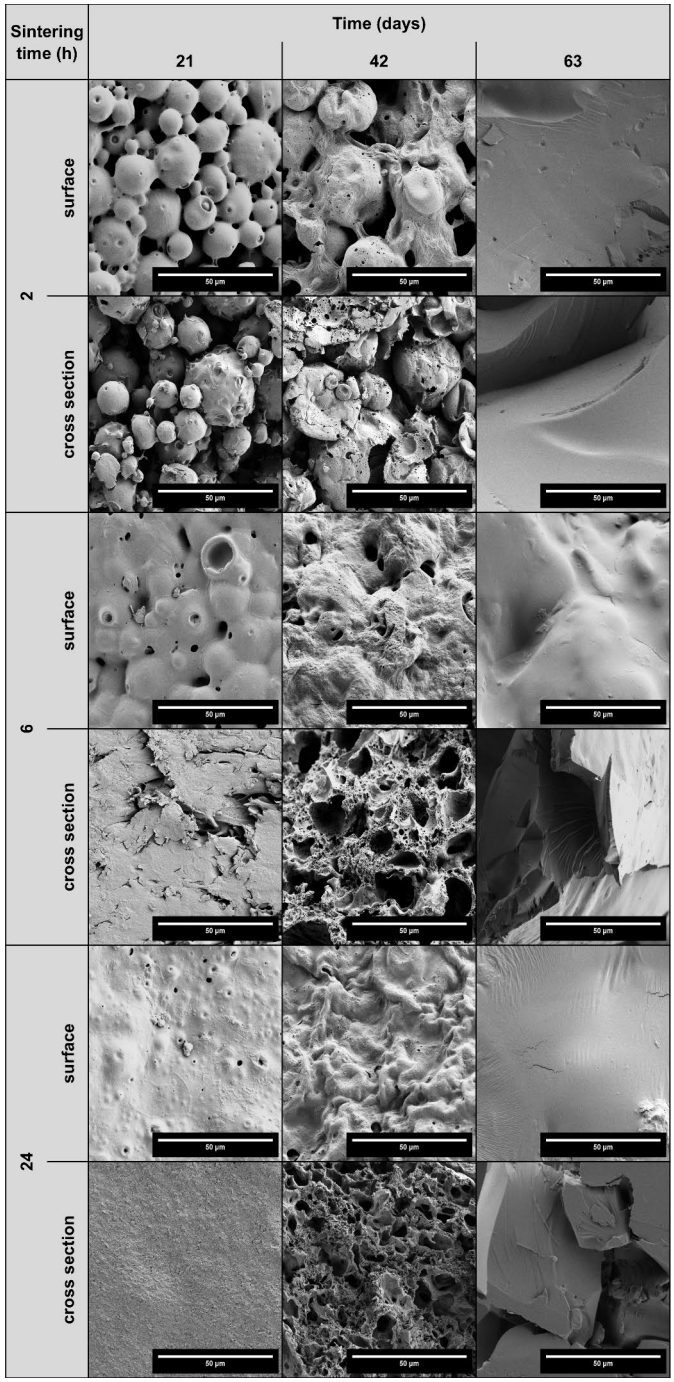

Figure 23. FE-SEM images of the surface or internal structure of the sintered RG504$_{FD}$50 cylinders after different *in vitro* degradation times. All scale bars are 50 µm. Reprinted from publication **III** with permission from Elsevier.

Cylinders having a drug-free microsphere matrix were printed using inks containing $RG504_{pbo}$ microspheres and various FD-loaded microspheres ($RG502H_{FD}$, $RG504_{FD}$, or $RG756S_{FD}$) at a 9:1 (vol) ratio. The cylinders were sintered for 4 h with a 1:3 mixture of acetone and water. The sintering time was selected based on the results presented in **Figure 19**, which indicated the presence of open porosity in $RG504_{FD}$ cylinders after such treatment. Comparable sintering behavior was later confirmed (publication **III** supplementary material). The effect of different polymer degradation times on the drug release was assessed, and the results are shown in **Figure 24**. All samples exhibited an initial burst release followed by a lag phase. However, the drug-free microsphere matrix influenced the drug release behavior, resulting in different release profiles compared to the pure microspheres (shown in **Figure 21a**).

While the $RG502H_{FD}$ microspheres exhibited a lag phase of approximately two weeks, the $RG504_{pbo}$45-$RG502H_{FD}$5 cylinders showed the second high release rate phase after 42 days, likely due to matrix degradation. Since substantial macromolecule release in nonporous systems primarily occurs as a results of polymer degradation[214], [215], the results suggest that a fraction of the $RG502H_{FD}$ microspheres was enclosed by the fused matrix microspheres, restricting the drug diffusion.

$RG504_{pbo}$45-$RG504_{FD}$5 cylinders exhibited a release profile similar to that of the $RG504_{FD}$50 cylinders sintered for 4 h, with the exception of having a higher burst. This difference is likely attributed to slight variations in the sintering behavior between the drug-free and drug-loaded microspheres, as **Figure 22a** demonstrated that the sintering process significantly affected the extent of the burst release.

The $RG504_{pbo}$45-$RG756S_{FD}$5 cylinders also exhibited the secondary high release rate phase, whereas the $RG756S_{FD}$ microspheres did not (**Figure 21a**). This can most likely be attributed to the degradation of the $RG504_{pbo}$ microsphere matrix, which also accelerated the degradation of RG 756 S. However, the higher molecular weight and longer degradation time of RG 756 S compared to the RG 504 caused the secondary burst to occur approximately two weeks later than in the $RG504_{pbo}$45-$RG504_{FD}$5 cylinders.

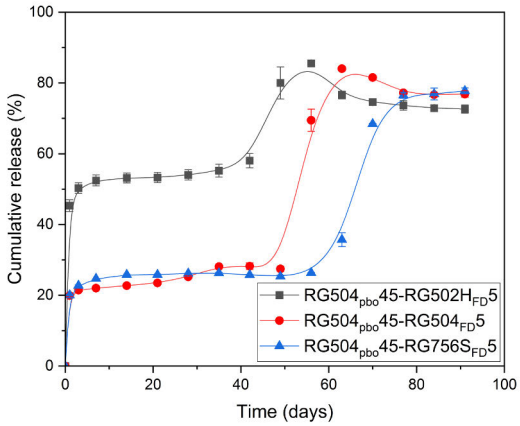

Figure 24. Cumulative *in vitro* FD release from the cylinders composed of a $RG504_{pbo}$ microsphere matrix and different FD-loaded microspheres. The samples were solvent vapor sintered with 1:3 mixture of acetone and water for 4 h. Reprinted from publication **III** with permission from Elsevier.

Additional cylinders were prepared by blending PLLGA or PMMA microspheres with $RG504_{FD}$ microspheres at a 9:1 (vol:vol) ratio, followed by sintering in acetone vapor for 2–6 h. PLLGA microspheres were selected due to their longer degradation time compared to $RG504_{FD}$ (**Figure 21b**), while PMMA microspheres were chosen due to their biostable nature, allowing for the investigation of possible enclosing of the FD-loaded microspheres by the matrix. Cylinder morphologies were analyzed by FE-SEM imaging (publication **III** supplementary material), and the drug release profiles are presented in **Figure 25**.

The PLLGA45-$RG504_{FD}$5 cylinders exhibited a significant burst of 30–40%, followed by a prolonged phase with an almost constant drug release rate (**Figure 25a**). The high burst was most likely caused by the harsher sintering conditions (using pure acetone) compared to the acetone:water mixtures used for the $RG504_{pbo}$45-$RG504_{FD}$5 cylinders. This resulted in greater deformation of the $RG504_{FD}$ microspheres, facilitating the separation of FD from the microsphere matrix at the particle surface. When the sintering time was extended from 2 to 6 h, the burst increased slightly from 37% to 39%. However, further prolonging the sintering time to 6 h resulted in a decrease in the burst to 30% ($p < 0.05$). Despite the lower burst observed in the samples sintered for 6 h, their drug release rate was the highest in the following days. This indicates that the extended sintering process primarily reduced the surface porosity, limiting drug diffusion during the first day while still allowing for continuous drug release for up to three months, due to the retention of diffusive channels throughout the cylinder structure. This is supported

by similar bulk porosity values regardless of the sintering time (publication **III** supplementary material).

In contrast, the PMMA45-RG504$_{FD}$5 cylinders exhibited an even higher burst of over 50%, with no further drug release occurring after the first week (**Figure 25b**). This indicates that, although the bulk porosities were slightly higher than those of the other cylinder types (publication **III** supplementary material), the PMMA microspheres enclosed a fraction of the RG504$_{FD}$ microspheres even during the shortest sintering time, thereby preventing complete drug release. This observation aligns with the previous speculation regarding the samples having a RG504$_{pbo}$ microsphere matrix.

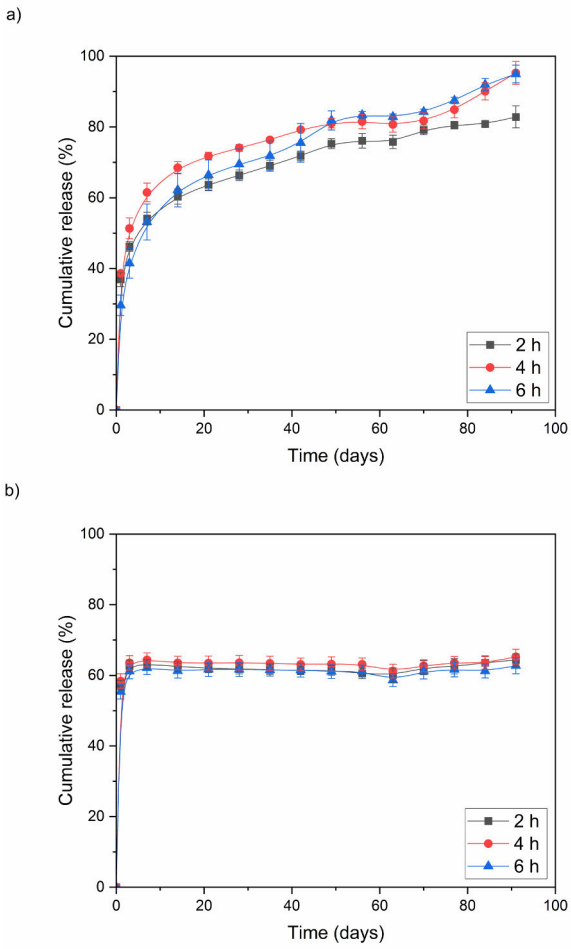

Figure 25. Cumulative *in vitro* FD release from the cylinders containing a) PLLGA, or b) PMMA microsphere matrix and the RG504$_{FD}$ microspheres. Samples were sintered with acetone vapor for different times. Reprinted from publication **III** with permission from Elsevier.

6 Conclusions

This thesis evaluated the potential of SSE 3D printing for the preparation of controlled release drug delivery systems. The research was motivated by limitations regarding the current therapeutic options: 1) the incompatibility of several therapeutic macromolecules with conventional heat-based processes, 2) limited diffusion of macromolecules through common biodegradable polymers, and 3) the potentially limited efficacy due to the "one size fits all" approach.

In the first study, extrudable inks were formulated by mixing PLLGA microspheres with a Carbopol gel at varying concentrations, and their rheological properties were analyzed. Additionally, 3D printing of the inks at ambient conditions was demonstrated and a solvent vapor-based sintering method was studied to control the microstructure of the printed objects. The rheological analysis revealed that increasing the microsphere concentration within the ink enhanced the viscoelastic moduli while narrowing the linear viscoelastic region. A different effect was observed during constant shear, where viscous properties of the gel matrix dominated, and the effect of microspheres was minimal. Overall, the inks exhibited adequate rheological properties for 3D printing, and manufacturing of constructs consisting almost entirely of the microspheres was feasible. Solvent vapor sintering resulted in gradual fusing of the particles, decreasing porosity and increasing mechanical strength, indicating potential for creating load-bearing systems and for controlling the drug release kinetics.

In the second study, the 3D printing process was optimized for the PLLGA microsphere-based inks, focusing on the extrudate swell phenomenon. It was found that the extrudate swell was significantly influenced by the microsphere concentration only close to the maximum packing density, likely due to the formation of a percolating particle network within the ink. The importance of taking extrudate swell into account during the printing process was demonstrated with different printability assessment techniques. Neglecting extrudate swell led to filament extension, which could result in catastrophic failures. However, quantifying extrudate swell allowed for flow rate corrections that improved print quality. While extrudate swell negatively impacted the object resolution, controlled shrinkage

through adjustments in the solid volume fraction within the ink had the opposite effect.

In the third study, PLGA microspheres encapsulating FITC-dextran were formulated for the SSE process. In addition, inks containing drug-free PLGA, PLLGA or PMMA microspheres blended with the drug-loaded ones were studied. The influence of ink composition and post-processing parameters on the degradation behavior and the drug release properties were evaluated, revealing that the release rate was affected by the ink formulation and the degree of particle fusing during the sintering process. The results demonstrated the feasibility of achieving tailored release profiles for FITC-dextran for up to three months. However, optimizing the post-processing conditions for different materials is essential to ensure proper drug release behavior.

Overall, this thesis demonstrates the manufacturing feasibility of polymer-based drug delivery systems for the long-term release of macromolecules via SSE 3D printing. It provides a comprehensive overview of the critical aspects to consider in the development of 3D printed drug delivery systems, including formulation selection and characterization, printing process optimization, and post-processing method development. By using extrudable inks composed of biodegradable polymer microspheres within a hydrogel matrix, 3D printing was possible at room temperature while maintaining the rheology-modifying excipient content in the final dry objects below 1% (wt). Furthermore, the inks were printable over a wide range of microsphere concentrations, which allowed for the use of controlled shrinkage in the printed parts. The solvent vapor-based post-processing method enabled tailoring of the porosity and mechanical strength of the printed objects at low temperatures, and controlled release of macromolecules for months was achieved.

Future implementation of the developed method would benefit from assessing the effects of different 3D structures to tailor the drug release properties, as well as from evaluating different materials to overcome the inherent limitations of PLGA. Finally, studying the release behavior of therapeutically relevant drugs would be necessary to ensure the feasibility of the technology.

Acknowledgements

This research was conducted at the Pharmaceutical Sciences function of Bayer Oy, Turku, during 2021-2025, as part of an industrial PhD track of the Doctoral Programme on Drug Research and Diagnostics (DRD) at the University of Turku, Department of Life Technologies, Biotechnology unit. I would like to express my gratitude to Bayer and all the company's stakeholders for their commitment to my personal development as a scientist.

I am sincerely thankful to my supervisors, Prof. Tero Soukka, DSc Mika Jokinen, and DSc Mikael Stolt, for their invaluable guidance and support over the past years. When I first considered pursuing doctoral studies, I had no connections with local universities or research groups and relied on the willingness of others to assist me. Tero, you volunteered as my academic supervisor and have been a constant source of support and expertise throughout this journey. Although we have only met in person a few times, I have always felt your availability and willingness to help. Mika, I appreciate your scientific insights and the challenging questions you posed about the gathered data. Your enthusiasm for rheology and 3D printing has positively influenced both this thesis and my personal growth in the field. I would also like to extend my heartfelt thanks to my principal supervisor, Mikael, from Bayer. Micke, although you were not the original industrial supervisor, your willingness to take on this role felt like winning the lottery. You have dedicated considerable time, even outside typical working hours, to provide detailed scientific input on my research and writing, particularly regarding the critical aspects of polymers and drug delivery systems.

I am also grateful to the members of my follow-up committee, Prof. Ullamari Pesonen and Adj. Prof. Vimalkumar Balasubramanian, for their professional guidance throughout this journey. Ullamari, you were my initial contact from the academic side, and I truly appreciate your assistance in arranging the DRD agreements between Bayer and the University, as well as your help in finding Tero as my supervisor. Your guidance through the University's bureaucratic processes has been invaluable.

Most of my work was conducted at Bayer, and I want to thank all my colleagues for creating such an inspiring work environment. Special thanks to Viljami for the

size exclusion chromatography, Harri for the mechanical testing, and Antti and Tarja for their help in gas chromatography analysis. Peggy, I am forever grateful for your help with proofreading my first two manuscripts and for teaching me so much about English grammar. Your positive spirit will be greatly missed.

3D printing was a crucial element of this thesis, and I want to thank Brinter AM Technologies Ltd. for providing access to their innovative technology. A special shout-out to Tomi and Dhayakumar (DK) for our collaboration; I look forward to exploring common interests and development initiatives also in the future! Thank you, Lari, for your assistance with occasional troubleshooting on the printers. I would also like to thank Ermei from the Materials Research Infrastructure (MARI) at the Department of Physics and Astronomy, University of Turku, for helping with the FE-SEM analysis, and Jouko from the Cell Imaging and Cytometry Core at the Turku Bioscience Centre for his guidance with CLSM imaging.

Finally, I want to express my deepest gratitude to my wife, Salla, for her unwavering support during these past few years. This thesis has required many evenings, weekends, and holidays, and your dedication to caring for our wonderful kids has made this work possible. I would also like to thank my other relatives for their interest in my studies and research.

Turku, August 2025

Juuso Pohjola

List of References

[1] S. Adepu and S. Ramakrishna, “Controlled drug delivery systems: current status and future directions,” *Molecules*, vol. 26, no. 19, Art. no. 5905, 2021, <https://doi.org/10.3390/molecules26195905>.

[2] L. Xiaoling, B. R. Jasti, V. P. Marasanapalle, and A. Kokate, “Physiological and biochemical barriers to drug delivery,” in *Design of Controlled Release Drug Delivery Systems*, X. Li and B. R. Jasti, Eds. New York, NY, USA: McGraw-Hill, 2006, pp. 41–74. <https://doi.org/10.1036/0071417591>.

[3] R. Chen, “Polymers in drug delivery: concepts, developments and potential,” in *Drug Delivery Systems: Advanced Technologies Potentially Applicable in Personalised Treatment*, J. Coelho, Ed. Dordrecht, Netherlands: Springer, 2013, pp. 1–34. <https://doi.org/10.1007/978-94-007-6010-3_1>.

[4] R. A. Bader and P. R. Wardwell, “Challenges of drug delivery,” in *Engineering Polymer Systems for Improved Drug Delivery*, R. A. Bader and D. A. Putnam, Eds. Hoboken, NJ, USA: Wiley, 2014, pp. 29–54. <https://doi.org/10.1002/9781118747896.ch2>.

[5] O. S. Fenton, K. N. Olafson, P. S. Pillai, M. J. Mitchell, and R. Langer, “Advances in biomaterials for drug delivery,” *Adv. Mater.*, vol. 30, no. 29, Art. no. 1705328, 2018, <https://doi.org/10.1002/adma.201705328>.

[6] S. J. Siegel and M. J. Rathbone, “Overview of controlled release mechanisms,” in *Fundamentals and Applications of Controlled Release Drug Delivery*, J. Siepmann, R. A. Siegel, and M. J. Rathbone, Eds. New York, NY, USA: Springer, 2012, pp. 19–43. <https://doi.org/10.1007/978-1-4614-0881-9_2>.

[7] K. Park, “Controlled drug delivery systems: past forward and future back,” *J. Control. Release*, vol. 190, pp. 3–8, 2014, <https://doi.org/10.1016/j.jconrel.2014.03.054>.

[8] L. Solorio, A. Carlson, H. Zhou, and A. A. Exner, “Implantable drug delivery systems,” in *Engineering Polymer Systems for Improved Drug Delivery*, R. A. Bader and D. A. Putnam, Eds. Hoboken, NJ, USA: Wiley, 2014, pp. 191–225. <https://doi.org/10.1002/9781118747896.ch7>.

[9] R. Bhujel, R. Maharjan, N. A. Kim, and S. H. Jeong, “Practical quality attributes of polymeric microparticles with current understanding and future perspectives,” *J. Drug Deliv. Sci. Technol.*, vol. 64, Art. no. 102608, 2021, <https://doi.org/10.1016/j.jddst.2021.102608>.

[10] S. Wang, R. Liu, Y. Fu, and W. J. Kao, “Release mechanisms and applications of drug delivery systems for extended-release,” *Expert Opin. Drug Deliv.*, vol. 17, no. 9, pp. 1289–1304, 2020, <https://doi.org/10.1080/17425247.2020.1788541>.

[11] S. Abdella *et al.*, “3D printing of thermo-sensitive drugs,” *Pharmaceutics*, vol. 13, no. 9, Art. no. 1524, 2021, <https://doi.org/10.3390/pharmaceutics13091524>.

[12] G. Auriemma, C. Tommasino, G. Falcone, T. Esposito, C. Sardo, and R. P. Aquino, “Additive manufacturing strategies for personalized drug delivery systems and medical devices: fused

filament fabrication and semi solid extrusion," *Molecules*, vol. 27, no. 9, Art. no. 2784, 2022, <https://doi.org/10.3390/molecules27092784>.

[13] S. J. Trenfield, C. M. Madla, A. W. Basit, and S. Gaisford, "The shape of things to come: emerging applications of 3D printing in healthcare," in *3D Printing of Pharmaceuticals*, 1st ed., A. W. Basit and S. Gaisford, Eds. Cham, Switzerland: Springer, 2018, pp. 1–19. <https://doi.org/10.1007/978-3-319-90755-0_1>.

[14] I. Seoane-Viaño, P. Januskaite, C. Alvarez-Lorenzo, A. W. Basit, and A. Goyanes, "Semi-solid extrusion 3D printing in drug delivery and biomedicine: personalised solutions for healthcare challenges," *J. Control. Release*, vol. 332, pp. 367–389, 2021, <https://doi.org/10.1016/j.jconrel.2021.02.027>.

[15] M. Askarizadeh, N. Esfandiari, B. Honarvar, S. A. Sajadian, and A. Azdarpour, "Kinetic modeling to explain the release of medicine from drug delivery systems," *ChemBioEng Rev.*, vol. 10, no. 6, pp. 1006–1049, 2023, <https://doi.org/10.1002/cben.202300027>.

[16] J. C. Near, "Active pharmaceutical ingredients," in *Good Manufacturing Practices for Pharmaceuticals*, 7th ed., G. P. Bunn, Ed. Boca Raton, FL, USA: CRC Press, 2019, pp. 217–226. <https://doi.org/10.1201/9781315120669>.

[17] A. Kar, N. Ahamad, M. Dewani, L. Awasthi, R. Patil, and R. Banerjee, "Wearable and implantable devices for drug delivery: applications and challenges," *Biomaterials*, vol. 283, Art. no. 121435, 2022, <https://doi.org/10.1016/j.biomaterials.2022.121435>.

[18] "Modification of drug release," in *Strategies to Modify the Drug Release from Pharmaceutical Systems*, 1st ed., Waltham, MA, USA: Woodhead Publishing, 2015, pp. 15–28. <https://doi.org/10.1016/B978-0-08-100092-2.00002-3>.

[19] Y. H. Yun, B. K. Lee, and K. Park, "Controlled drug delivery: historical perspective for the next generation," *J. Control. Release*, vol. 219, pp. 2–7, 2015, <https://doi.org/10.1016/j.jconrel.2015.10.005>.

[20] K. Park and H. Wen, "Introduction and overview of oral controlled release formulation design," in *Oral Controlled Release Formulation Design and Drug Delivery: Theory to Practice*, 1st ed., H. Wen and K. Park, Eds. Hoboken, NJ, USA: Wiley, 2010, pp. 1–20. <https://doi.org/10.1002/9780470640487.ch1>.

[21] M. Afzal *et al.*, "Introduction to molecular pharmacology: basic concepts," in *How Synthetic Drugs Work: Insights into Molecular Pharmacology of Classic and New Pharmaceuticals*, I. Kazmi, A. Shaharyar, F. A. Al-Abbasi, S. Karmakar, and M. Afzal, Eds. London, United Kingdom: Academic Press, 2023, pp. 1–25. <https://doi.org/10.1016/B978-0-323-99855-0.00001-4>.

[22] K. K. Jain, "An overview of drug delivery systems," in *Drug Delivery Systems*, 3rd ed., K. K. Jain, Ed. New York, NY, USA: Springer, 2020, pp. 1–54. <https://doi.org/10.1007/978-1-4939-9798-5_1>.

[23] H. A. Mohsen, "Routes of drug administration," in *Pharmaceutics: Basic Principles and Application to Pharmacy Practice*, 2nd ed., A. K. Dash and S. Singh, Eds. London, United Kingdom: Academic Press, 2024, pp. 537–554. <https://doi.org/10.1016/B978-0-323-99796-6.00006-0>.

[24] S. Mao, D. Cun, and Y. Kawashima, "Novel non - injectable formulation approaches of peptides and proteins," in *Delivery Technologies for Biopharmaceuticals: Peptides, Proteins, Nucleic Acids and Vaccines*, L. Jorgensen and H. M. Nielsen, Eds. Chichester, United Kingdom: Wiley, 2009, pp. 29–67. <https://doi.org/10.1002/9780470688397.ch3>.

[25] R. A. Bader, “Fundamentals of drug delivery,” in *Engineering Polymer Systems for Improved Drug Delivery*, R. A. Bader and D. A. Putnam, Eds. Hoboken, NJ, USA: Wiley, 2014, pp. 3–28. <https://doi.org/10.1002/9781118747896.ch1>.

[26] M. L. Bruschi, *Strategies to Modify the Drug Release from Pharmaceutical Systems*, 1st ed. Waltham, MA, USA: Woodhead Publishing, 2015. <https://doi.org/10.1016/C2014-0-02342-8>.

[27] H. Ravivarapu, R. Mahalingam, and B. R. Jasti, “Biodegradable polymeric delivery systems,” in *Design of Controlled Release Drug Delivery Systems*, New York, NY, USA: McGraw-Hill, 2006, pp. 271–304. <https://doi.org/10.1036/0071417591>.

[28] P. Wu and D. W. Grainger, “Drug/device combinations for local drug therapies and infection prophylaxis,” *Biomaterials*, vol. 27, no. 11, pp. 2450–2467, 2006, <https://doi.org/10.1016/j.biomaterials.2005.11.031>.

[29] M. Yang and S. Frokjaer, “Novel formulation approaches for peptide and protein injectables,” in *Delivery Technologies for Biopharmaceuticals: Peptides, Proteins, Nucleic Acids and Vaccines*, L. Jorgensen and H. M. Nielsen, Eds. Chichester, United Kingdom: Wiley, 2009, pp. 9–28. <https://doi.org/10.1002/9780470688397.ch2>.

[30] S. Fredenberg, M. Wahlgren, M. Reslow, and A. Axelsson, “The mechanisms of drug release in poly(lactic-co-glycolic acid)-based drug delivery systems—a review,” *Int. J. Pharm.*, vol. 415, no. 1–2, pp. 34–52, 2011, <https://doi.org/10.1016/j.ijpharm.2011.05.049>.

[31] Z. Wang and R. A. Shmeis, “Dissolution controlled drug delivery systems,” in *Design of Controlled Release Drug Delivery Systems*, New York, NY, USA: McGraw-Hill, 2006, pp. 139–172. <https://doi.org/10.1036/0071417591>.

[32] J. Siepmann, R. A. Siegel, and F. Siepmann, “Diffusion controlled drug delivery systems,” in *Fundamentals and Applications of Controlled Release Drug Delivery*, J. Siepmann, R. A. Siegel, and M. J. Rathbone, Eds. New York, NY, USA: Springer, 2012, pp. 127–152. <https://doi.org/10.1007/978-1-4614-0881-9_6>.

[33] P. Liu, T. Ju, and Y. Qiu, “Diffusion-controlled drug delivery systems,” in *Design of Controlled Release Drug Delivery Systems*, New York, NY, USA: McGraw-Hill, 2006, pp. 107–137. <https://doi.org/10.1036/0071417591>.

[34] J. Siepmann and F. Siepmann, “Swelling controlled drug delivery systems,” in *Fundamentals and Applications of Controlled Release Drug Delivery*, J. Siepmann, R. A. Siegel, and M. J. Rathbone, Eds. New York, NY, USA: Springer, 2012, pp. 153–170. <https://doi.org/10.1007/978-1-4614-0881-9_7>.

[35] S. Srikonda, P. Kotamraj, and B. Barclay, “Osmotic controlled drug delivery systems,” in *Design of Controlled Release Drug Delivery Systems*, New York, NY, USA: McGraw-Hill, 2006, pp. 203–230. <https://doi.org/10.1036/0071417591>.

[36] C. Fante and F. Greco, “Polymer-drug conjugates,” in *Engineering Polymer Systems for Improved Drug Delivery*, R. A. Bader and D. A. Putnam, Eds. Hoboken, NJ, USA: Wiley, 2014, pp. 57–83. <https://doi.org/10.1002/9781118747896.ch3>.

[37] Y. Fu and W. J. Kao, “Drug release kinetics and transport mechanisms of non-degradable and degradable polymeric delivery systems,” *Expert. Opin. Drug. Deliv.*, vol. 7, no. 4, pp. 429–444, 2010, <https://doi.org/10.1517/17425241003602259>.

[38] C. Aguzzi, P. Cerezo, I. Salcedo, R. Sánchez, and C. Viseras, “Mathematical models describing drug release from biopolymeric delivery systems,” *Mater. Technol.*, vol. 25, no. 3–4, pp. 205–211, 2010, <https://doi.org/10.1179/175355510X12723642365566>.

[39] P. Trucillo, “Drug carriers: A review on the most used mathematical models for drug release,” *Processes*, vol. 10, no. 6, Art. no. 1094, 2022, <https://doi.org/10.3390/pr10061094>.

[40] J. Siepmann and F. Siepmann, “Mathematical modeling of drug delivery,” *Int. J. Pharm.*, vol. 364, no. 2, pp. 328–343, 2008, <https://doi.org/10.1016/j.ijpharm.2008.09.004>.

[41] J. Siepmann and F. Siepmann, “Mathematical modeling of drug dissolution,” *Int. J. Pharm.*, vol. 453, no. 1, pp. 12–24, 2013, <https://doi.org/10.1016/j.ijpharm.2013.04.044>.

[42] S. D’Souza, “A review of *in vitro* drug release test methods for nano-sized dosage forms,” *Adv. Pharm.*, vol. 2014, Art. no. 304757, 2014, <https://doi.org/10.1155/2014/304757>.

[43] S. S. D’Souza and P. P. DeLuca, “Methods to assess *in vitro* drug release from injectable polymeric particulate systems,” *Pharm. Res.*, vol. 23, no. 3, pp. 460–474, 2006, <https://doi.org/10.1007/s11095-005-9397-8>.

[44] V. A. Gray, “Regulatory considerations,” in *In Vitro Drug Release Testing of Special Dosage Forms*, N. Fotaki and S. Klein, Eds. Hoboken, NJ, USA: Wiley, 2019, pp. 253–284. <https://doi.org/10.1002/9781118675748.ch10>.

[45] B. Wan, Q. Bao, and D. Burgess, “Long-acting PLGA microspheres: Advances in excipient and product analysis toward improved product understanding,” *Adv. Drug Deliv. Rev.*, vol. 198, Art. no. 114857, 2023, <https://doi.org/10.1016/j.addr.2023.114857>.

[46] N. Abbasnezhad, N. Zirak, S. Champmartin, M. Shirinbayan, and F. Bakir, “An overview of in vitro drug release methods for drug-eluting stents,” *Polymers*, vol. 14, no. 13, Art. no. 2751, 2022, <https://doi.org/10.3390/polym14132751>.

[47] D. J. Burgess, D. J. A. Crommelin, A. S. Hussain, and M.-L. Chen, “Assuring quality and performance of sustained and controlled release parenterals: EUFEPS workshop report,” *AAPS PharmSci*, vol. 6, no. 1, Art. no. 11, 2004, <https://doi.org/10.1208/ps060111>.

[48] J. Shen and D. J. Burgess, “Accelerated in-vitro release testing methods for extended-release parenteral dosage forms,” *J. Pharm. Pharmacol.*, vol. 64, no. 7, pp. 986–996, 2012, <https://doi.org/10.1111/j.2042-7158.2012.01482.x>.

[49] M. Jug *et al.*, “An overview of in vitro dissolution/release methods for novel mucosal drug delivery systems,” *J. Pharm. Biomed. Anal.*, vol. 147, pp. 350–366, 2018, <https://doi.org/10.1016/j.jpba.2017.06.072>.

[50] Y. Kim, E. J. Park, T. W. Kim, and D. H. Na, “Recent progress in drug release testing methods of biopolymeric particulate system,” *Pharmaceutics*, vol. 13, no. 8, Art. no. 1313, 2021, <https://doi.org/10.3390/pharmaceutics13081313>.

[51] P. Boyd *et al.*, “*In vitro* release testing methods for drug-releasing vaginal rings,” *J. Control. Release*, vol. 313, pp. 54–69, 2019, <https://doi.org/10.1016/j.jconrel.2019.10.015>.

[52] J. Shen and D. J. Burgess, “*In vitro–in vivo* correlation for complex non-oral drug products: where do we stand?,” *J. Control. Release*, vol. 219, pp. 644–651, 2015, <https://doi.org/10.1016/j.jconrel.2015.09.052>.

[53] K. E. Uhrich, S. M. Cannizzaro, R. S. Langer, and K. M. Shakesheff, “Polymeric systems for controlled drug release,” *Chem. Rev.*, vol. 99, no. 11, pp. 3181–3198, 1999, <https://doi.org/10.1021/cr940351u>.

[54] J. Tsung and D. J. Burgess, “Biodegradable polymers in drug delivery systems,” in *Fundamentals and Applications of Controlled Release Drug Delivery*, J. Siepmann, R. A. Siegel, and M. J. Rathbone, Eds. New York, NY, USA: Springer, 2012, pp. 107–123. <https://doi.org/10.1007/978-1-4614-0881-9_5>.

[55] O. A. Abu-Diak, G. P. Andrews, and D. S. Jones, “Hydrophobic polymers of pharmaceutical significance,” in *Fundamentals and Applications of Controlled Release Drug Delivery*, J. Siepmann, R. A. Siegel, and M. J. Rathbone, Eds. New York, NY, USA: Springer, 2012, pp. 47–73. <https://doi.org/10.1007/978-1-4614-0881-9_3>.

[56] W.-W. Yang and E. Pierstorff, “Reservoir-based polymer drug delivery systems,” *J. Lab. Autom.*, vol. 17, no. 1, pp. 50–58, 2012, <https://doi.org/10.1177/2211068211428189>.

[57] S. Borandeh, B. van Bochove, A. Teotia, and J. Seppälä, “Polymeric drug delivery systems by additive manufacturing,” *Adv. Drug Deliv. Rev.*, vol. 173, pp. 349–373, 2021, <https://doi.org/10.1016/j.addr.2021.03.022>.

[58] A. Bettencourt and A. J. Almeida, “Poly(methyl methacrylate) particulate carriers in drug delivery,” *J. Microencapsul.*, vol. 29, no. 4, pp. 353–367, 2012, <https://doi.org/10.3109/02652048.2011.651500>.

[59] E. B. Minelli and A. Benini, “PMMA as drug delivery system and *in vivo* release from spacers,” in *Infection and Local Treatment in Orthopedic Surgery*, E. Meani, C. Romanò, L. Crosby, G. Hofmann, and G. Calonego, Eds. Berlin, Germany: Springer, 2007, pp. 79–91. <https://doi.org/10.1007/978-3-540-47999-4_11>.

[60] G. Rivera-Hernández, M. Antunes-Ricardo, P. Martínez-Morales, and M. L. Sánchez, “Polyvinyl alcohol based-drug delivery systems for cancer treatment,” *Int. J. Pharm.*, vol. 600, Art. no. 120478, 2021, <https://doi.org/10.1016/j.ijpharm.2021.120478>.

[61] K. D. Dasse, M. J. Lander, and P. M. Novelli, “Chemoembolization with drug-eluting beads for the treatment of hepatocellular carcinoma,” *J. Adv. Pract. Oncol.*, vol. 7, no. 7, 2016, <https://doi.org/10.6004/jadpro.2016.7.7.8>.

[62] K. Malagari, A. Pomoni, D. Filippiadis, and D. Kelekis, “Chemoembolization of hepatocellular carcinoma with HepaSphere™,” *Hepat. Oncol.*, vol. 2, no. 2, pp. 147–157, 2015, <https://doi.org/10.2217/hep.15.2>.

[63] B. D. Ulery, L. S. Nair, and C. T. Laurencin, “Biomedical applications of biodegradable polymers,” *J. Polym. Sci. B Polym. Phys.*, vol. 49, no. 12, pp. 832–864, 2011, <https://doi.org/10.1002/polb.22259>.

[64] C. Wischke and S. P. Schwendeman, “Degradable polymeric carriers for parenteral controlled drug delivery,” in *Fundamentals and Applications of Controlled Release Drug Delivery*, J. Siepmann, R. A. Siegel, and M. J. Rathbone, Eds. New York, NY, USA: Springer, 2012, pp. 171–228. <https://doi.org/10.1007/978-1-4614-0881-9_8>.

[65] N. Kamaly, B. Yameen, J. Wu, and O. C. Farokhzad, “Degradable controlled-release polymers and polymeric nanoparticles: Mechanisms of controlling drug release,” *Chem. Rev.*, vol. 116, no. 4, pp. 2602–2663, 2016, <https://doi.org/10.1021/acs.chemrev.5b00346>.

[66] M. V. S. Varma, A. M. Kaushal, A. Garg, and S. Garg, “Factors affecting mechanism and kinetics of drug release from matrix-based oral controlled drug delivery systems,” *Am. J. Drug Deliv.*, vol. 2, no. 1, pp. 43–57, 2004, <https://doi.org/10.2165/00137696-200402010-00003>.

[67] S. P. Schwendeman, R. B. Shah, B. A. Bailey, and A. S. Schwendeman, “Injectable controlled release depots for large molecules,” *J. Control. Release*, vol. 190, pp. 240–253, 2014, <https://doi.org/10.1016/j.jconrel.2014.05.057>.

[68] S. Han and J. Wu, “Recent advances of poly(ester amide)s-based biomaterials,” *Biomacromolecules*, vol. 23, no. 5, pp. 1892–1919, 2022, <https://doi.org/10.1021/acs.biomac.2c00150>.

[69] J. Heller, J. Barr, S. Y. Ng, K. S. Abdellauoi, and R. Gurny, “Poly(ortho esters): synthesis, characterization, properties and uses,” *Adv. Drug Deliv. Rev.*, vol. 54, no. 7, pp. 1015–1039, 2002, <https://doi.org/10.1016/S0169-409X(02)00055-8>.

[70] S. Einmahl, S. Capancioni, K. Schwach-Abdellaoui, M. Moeller, F. Behar-Cohen, and R. Gurny, “Therapeutic applications of viscous and injectable poly(ortho esters),” *Adv. Drug Deliv. Rev.*, vol. 53, no. 1, pp. 45–73, 2001, <https://doi.org/10.1016/S0169-409X(01)00220-4>.

[71] M. Winnacker and B. Rieger, “Poly(ester amide)s: recent insights into synthesis, stability and biomedical applications,” *Polym. Chem.*, vol. 7, no. 46, pp. 7039–7046, 2016, <https://doi.org/10.1039/C6PY01783E>.

[72] I. Teasdale and O. Brüggemann, “Polyphosphazenes: multifunctional, biodegradable vehicles for drug and gene delivery,” *Polymers*, vol. 5, no. 1, pp. 161–187, 2013, <https://doi.org/10.3390/polym5010161>.

[73] N. K. Comolli and C. E. Clark, “Polymeric microparticles,” in *Engineering Polymer Systems for Improved Drug Delivery*, R. A. Bader and D. A. Putnam, Eds. Hoboken, NJ, USA: Wiley, 2014, pp. 85–116. <https://doi.org/10.1002/9781118747896.ch4>.

[74] P. Blasi, “Poly(lactic acid)/poly(lactic-co-glycolic acid)-based microparticles: an overview,” *J. Pharm. Investig.*, vol. 49, pp. 337–346, 2019, <https://doi.org/10.1007/s40005-019-00453-z>.

[75] M. Lengyel, N. Kállai-Szabó, V. Antal, A. J. Laki, and I. Antal, “Microparticles, microspheres, and microcapsules for advanced drug delivery,” *Sci. Pharm.*, vol. 87, no. 3, Art. no. 20, 2019, <https://doi.org/10.3390/scipharm87030020>.

[76] M. Ye, S. Kim, and K. Park, “Issues in long-term protein delivery using biodegradable microparticles,” *J. Control. Release*, vol. 146, no. 2, pp. 241–260, 2010, <https://doi.org/10.1016/j.jconrel.2010.05.011>.

[77] N. K. Varde and D. W. Pack, “Microspheres for controlled release drug delivery,” *Expert. Opin. Biol. Ther.*, vol. 4, no. 1, pp. 35–51, 2004, <https://doi.org/10.1517/14712598.4.1.35>.

[78] E. Lagreca, V. Onesto, C. Di Natale, S. La Manna, P. A. Netti, and R. Vecchione, “Recent advances in the formulation of PLGA microparticles for controlled drug delivery,” *Prog. Biomater.*, vol. 9, pp. 153–174, 2020, <https://doi.org/10.1007/s40204-020-00139-y>.

[79] S. Freiberg and X. X. Zhu, “Polymer microspheres for controlled drug release,” *Int. J. Pharm.*, vol. 282, no. 1–2, pp. 1–18, 2004, <https://doi.org/10.1016/j.ijpharm.2004.04.013>.

[80] A. Forigua, R. L. Kirsch, S. M. Willerth, and K. S. Elvira, “Recent advances in the design of microfluidic technologies for the manufacture of drug releasing particles,” *J. Control. Release*, vol. 333, pp. 258–268, 2021, <https://doi.org/10.1016/j.jconrel.2021.03.019>.

[81] W. Li *et al.*, “Microfluidic fabrication of microparticles for biomedical applications,” *Chem. Soc. Rev.*, vol. 47, no. 15, pp. 5646–5683, 2018, <https://doi.org/10.1039/C7CS00263G>.

[82] H. Zhong, G. Chan, Y. Hu, H. Hu, and D. Ouyang, “A comprehensive map of FDA-approved pharmaceutical products,” *Pharmaceutics*, vol. 10, no. 4, Art. no. 263, 2018, <https://doi.org/10.3390/pharmaceutics10040263>.

[83] H. Petersen, J.-C. Bizec, H. Schuetz, and M.-L. Delporte, “Pharmacokinetic and technical comparison of Sandostatin® LAR® and other formulations of long-acting octreotide,” *BMC Res. Notes*, vol. 4, Art. no. 344, 2011, <https://doi.org/10.1186/1756-0500-4-344>.

[84] A. C. Anselmo and S. Mitragotri, “An overview of clinical and commercial impact of drug delivery systems,” *J. Control. Release*, vol. 190, pp. 15–28, 2014, <https://doi.org/10.1016/j.jconrel.2014.03.053>.

[85] J. B. Wolinsky, Y. L. Colson, and M. W. Grinstaff, “Local drug delivery strategies for cancer treatment: gels, nanoparticles, polymeric films, rods, and wafers,” *J. Control. Release*, vol. 159, no. 1, pp. 14–26, 2012, <https://doi.org/10.1016/j.jconrel.2011.11.031>.

[86] I. Sivin *et al.*, “Levonorgestrel concentrations during 7 years of continuous use of Jadelle contraceptive implants☆,” *Contraception*, vol. 64, no. 1, pp. 43–49, 2001, <https://doi.org/10.1016/S0010-7824(01)00226-8>.

[87] J. Perry, A. Chambers, K. Spithoff, and N. Laperriere, “Gliadel wafers in the treatment of malignant glioma: a systematic review,” *Curr. Oncol.*, vol. 14, no. 5, pp. 189–194, 2007, <https://doi.org/10.3747/co.2007.147>.

[88] P. Darney, A. Patel, K. Rosen, L. S. Shapiro, and A. M. Kaunitz, “Safety and efficacy of a single-rod etonogestrel implant (Implanon): results from 11 international clinical trials,” *Fertil. Steril.*, vol. 91, no. 5, pp. 1646–1653, 2009, <https://doi.org/10.1016/j.fertnstert.2008.02.140>.

[89] “Additive Manufacturing — General Principles — Fundamentals and Vocabulary.” ISO/ASTM 52900, 2021. Accessed: Jan. 14, 2025. [Online]. Available: https://www.iso.org/obp/ui/en/#iso:std:iso-astm:52900:ed-2:v1:en

[90] C. M. Madla, S. J. Trenfield, A. Goyanes, S. Gaisford, and A. W. Basit, “3D printing technologies, implementation and regulation: an overview,” in *3D Printing of Pharmaceuticals*, A. W. Basit and S. Gaisford, Eds. Cham, Switzerland: Springer, 2018, pp. 21–40. <https://doi.org/10.1007/978-3-319-90755-0_2>.

[91] T. Auel, A. F. C. Mentrup, L. R. Oldfield, and A. Seidlitz, “3D printing of pharmaceutical dosage forms: recent advances and applications,” *Adv. Drug Deliv. Rev.*, vol. 217, Art. no. 115504, 2025, <https://doi.org/10.1016/j.addr.2024.115504>.

[92] S. Nikazar and S. Bahrololoumi, “3D-printing: a novel tool for personalized drug delivery,” in *Advanced and Modern Approaches for Drug Delivery*, 1st ed., A. K. Kayak, S. Hasnain, B. Laha, and S. Maiti, Eds. Advanced and Modern Approaches for Drug Delivery: Academic Press, 2023, pp. 621–647. <https://doi.org/10.1016/B978-0-323-91668-4.00006-X>.

[93] M. Cui, H. Pan, D. Fang, S. Qiao, S. Wang, and W. Pan, “Fabrication of high drug loading levetiracetam tablets using semi-solid extrusion 3D printing,” *J. Drug Deliv. Sci. Technol.*, vol. 57, Art. no. 101683, 2020, <https://doi.org/10.1016/j.jddst.2020.101683>.

[94] K. Elango *et al.*, “The effects of warfarin and direct oral anticoagulants on systemic vascular calcification: a review,” *Cells*, vol. 10, no. 4, Art. no. 773, 2021, <https://doi.org/10.3390/cells10040773>.

[95] N. Eriksson and M. Wadelius, “Prediction of warfarin dose: why, when and how?,” *Pharmacogenomics*, vol. 13, no. 4, pp. 429–440, 2012, <https://doi.org/10.2217/pgs.11.184>.

[96] G. Young, “Anticoagulation therapies in children,” *Pediatr. Clin. N. Am.*, vol. 64, no. 6, pp. 1257–1269, 2017, <https://doi.org/10.1016/j.pcl.2017.08.004>.

[97] M. Pandey *et al.*, “3D printing for oral drug delivery: a new tool to customize drug delivery,” *Drug Deliv. and Transl. Res.*, vol. 10, pp. 986–1001, 2020, <https://doi.org/10.1007/s13346-020-00737-0>.

[98] J. Wang *et al.*, “Emerging 3D printing technologies for drug delivery devices: current status and future perspective,” *Adv. Drug Deliv. Rev.*, vol. 174, pp. 294–316, 2021, <https://doi.org/10.1016/j.addr.2021.04.019>.

[99] S. F. Iftekar, A. Aabid, A. Amir, and M. Baig, “Advancements and limitations in 3D printing materials and technologies: a critical review,” *Polymers*, vol. 15, no. 11, Art. no. 2519, 2023, <https://doi.org/10.3390/polym15112519>.

[100] Z. Rahman, S. F. B. Ali, T. Ozkan, N. A. Charoo, I. K. Reddy, and M. A. Khan, “Additive manufacturing with 3D printing: progress from bench to bedside,” *AAPS J.*, vol. 20, Art. no. 101, 2018, <https://doi.org/10.1208/s12248-018-0225-6>.

[101] M. Deng, S. Wu, and M. Ning, “3D printing for controlled release pharmaceuticals: current trends and future directions,” *Int. J. Pharm.*, vol. 669, Art. no. 125089, 2025, <https://doi.org/10.1016/j.ijpharm.2024.125089>.

[102] S. J. Trenfield, C. M. Madla, A. W. Basit, and S. Gaisford, “Binder jet printing in pharmaceutical manufacturing,” in *3D Printing of Pharmaceuticals*, 1st ed., A. W. Basit and S. Gaisford, Eds. Cham, Switzerland: Springer, 2018, pp. 41–54. <https://doi.org/10.1007/978-3-319-90755-0_3>.

[103] J. Goole and K. Amighi, “3D printing in pharmaceutics: a new tool for designing customized drug delivery systems,” *Int. J. Pharm.*, vol. 499, no. 1–2, pp. 376–394, 2016, <https://doi.org/10.1016/j.ijpharm.2015.12.071>.

[104] P. R. Martinez, A. W. Basit, and S. Gaisford, “The history, developments and opportunities of stereolithography,” in *3D Printing of Pharmaceuticals*, 1st ed., A. W. Basit and S. Gaisford, Eds. Cham, Switzerland: Springer, 2018, pp. 55–79. <https://doi.org/10.1007/978-3-319-90755-0_4>.

[105] X. Xu, A. Awad, P. Robles-Martinez, S. Gaisford, A. Goyanes, and A. W. Basit, “Vat photopolymerization 3D printing for advanced drug delivery and medical device applications,” *J. Control. Release*, vol. 329, pp. 743–757, 2021, <https://doi.org/10.1016/j.jconrel.2020.10.008>.

[106] F. Fina, S. Gaisford, and A. W. Basit, “Powder bed fusion: the working process, current applications and opportunities,” in *3D Printing of Pharmaceuticals*, 1st ed., A. W. Basit and S. Gaisford, Eds. Cham, Switzerland: Springer, 2018, pp. 81–105. <https://doi.org/10.1007/978-3-319-90755-0_5>.

[107] M. A. Azad, D. Olawuni, G. Kimbell, A. Z. M. Badruddoza, M. S. Hossain, and T. Sultana, “Polymers for extrusion-based 3D printing of pharmaceuticals: a holistic materials–process perspective,” *Pharmaceutics*, vol. 12, no. 2, Art. no. 124, 2020, <https://doi.org/10.3390/pharmaceutics12020124>.

[108] M. Annaji *et al.*, “Application of extrusion-based 3D printed dosage forms in the treatment of chronic diseases,” *J. Pharm. Sci.*, vol. 109, no. 12, pp. 3551–3568, 2020, <https://doi.org/10.1016/j.xphs.2020.09.042>.

[109] S. Mohapatra, R. K. Kar, P. K. Biswal, and S. Bindhani, “Approaches of 3D printing in current drug delivery,” *Sens. Int.*, vol. 3, Art. no. 100146, 2022, <https://doi.org/10.1016/j.sintl.2021.100146>.

[110] J. Zhang, A. Q. Vo, X. Feng, S. Bandari, and M. A. Repka, “Pharmaceutical additive manufacturing: a novel tool for complex and personalized drug delivery systems,” *AAPS PharmSciTech*, vol. 19, no. 8, pp. 3388–3402, 2018, <https://doi.org/10.1208/s12249-018-1097-x>.

[111] F. Fina, C. M. Madla, A. Goyanes, J. Zhang, S. Gaisford, and A. W. Basit, “Fabricating 3D printed orally disintegrating printlets using selective laser sintering,” *Int. J. Pharm.*, vol. 541, no. 1–2, pp. 101–107, 2018, <https://doi.org/10.1016/j.ijpharm.2018.02.015>.

[112] F. Fina *et al.*, “3D printing of drug-loaded gyroid lattices using selective laser sintering,” *Int. J. Pharm.*, vol. 547, no. 1–2, pp. 44–52, 2018, <https://doi.org/10.1016/j.ijpharm.2018.05.044>.

[113] A. Awad, S. Gaisford, and A. W. Basit, “Fused deposition modelling: advances in engineering and medicine,” in *3D Printing of Pharmaceuticals*, 1st ed., A. W. Basit and S. Gaisford, Eds. Cham, Switzerland: Springer, 2018, pp. 107–132. <https://doi.org/10.1007/978-3-319-90755-0_6>.

[114] S. Bandari, D. Nyavanandi, N. Dumpa, and M. A. Repka, “Coupling hot melt extrusion and fused deposition modeling: critical properties for successful performance,” *Adv. Drug Deliv. Rev.*, vol. 172, pp. 52–63, 2021, <https://doi.org/10.1016/j.addr.2021.02.006>.

[115] P. Xu *et al.*, “Development of a quantitative method to evaluate the printability of filaments for fused deposition modeling 3D printing,” *Int. J. Pharm.*, vol. 588, Art. no. 119760, 2020, <https://doi.org/10.1016/j.ijpharm.2020.119760>.

[116] J. Firth, A. W. Basit, and S. Gaisford, “The role of semi-solid extrusion printing in clinical practice,” in *3D Printing of Pharmaceuticals*, 1st ed., A. W. Basit and S. Gaisford, Eds. Cham, Switzerland: Springer, 2018, pp. 133–151. <https://doi.org/10.1007/978-3-319-90755-0_7>.

[117] V. Domsta and A. Seidlitz, “3D-printing of drug-eluting implants: an overview of the current developments described in the literature,” *Molecules*, vol. 26, no. 13, Art. no. 4066, 2021, <https://doi.org/10.3390/molecules26134066>.

[118] A. Schwab, R. Levato, M. D’Este, S. Piluso, D. Eglin, and J. Malda, “Printability and shape fidelity of bioinks in 3D bioprinting,” *Chem. Rev.*, vol. 120, no. 19, pp. 11028–11055, 2020, <https://doi.org/10.1021/acs.chemrev.0c00084>.

[119] M. E. Cooke and D. H. Rosenzweig, “The rheology of direct and suspended extrusion bioprinting,” *APL Bioeng.*, vol. 5, no. 1, Art. no. 011502, 2021, <https://doi.org/10.1063/5.0031475>.

[120] S. Ramesh *et al.*, “Extrusion bioprinting: recent progress, challenges, and future opportunities,” *Bioprinting*, vol. 21, Art. no. e00116, 2021, <https://doi.org/10.1016/j.bprint.2020.e00116>.

[121] S. C. Lee, G. Gillispie, P. Prim, and S. J. Lee, “Physical and chemical factors influencing the printability of hydrogel-based extrusion bioinks,” *Chem. Rev.*, vol. 120, no. 19, pp. 10834–10886, 2020, <https://doi.org/10.1021/acs.chemrev.0c00015>.

[122] P. A. Amorim, M. A. d’Ávila, R. Anand, P. Moldenaers, P. van Puyvelde, and V. Bloemen, “Insights on shear rheology of inks for extrusion-based 3D bioprinting,” *Bioprinting*, vol. 22, Art. no. e00129, 2021, <https://doi.org/10.1016/j.bprint.2021.e00129>.

[123] G. Gillispie *et al.*, “Assessment methodologies for extrusion-based bioink printability,” *Biofabrication*, vol. 12, no. 2, Art. no. 022003, 2020, <https://doi.org/10.1088/1758-5090/ab6f0d>.

[124] I. El Aita, J. Breitkreutz, and J. Quodbach, “On-demand manufacturing of immediate release levetiracetam tablets using pressure-assisted microsyringe printing,” *Eur. J. Pharm. Biopharm.*, vol. 134, pp. 29–36, 2019, <https://doi.org/10.1016/j.ejpb.2018.11.008>.

[125] J. Conceição *et al.*, “Hydroxypropyl-β-cyclodextrin-based fast dissolving carbamazepine printlets prepared by semisolid extrusion 3D printing,” *Carbohydr. Polym.*, vol. 221, pp. 55–62, 2019, <https://doi.org/10.1016/j.carbpol.2019.05.084>.

[126] Y. Cheng, H. Qin, N. C. Acevedo, X. Jiang, and X. Shi, “3D printing of extended-release tablets of theophylline using hydroxypropyl methylcellulose (HPMC) hydrogels,” *Int. J. Pharm.*, vol. 591, Art. no. 119983, 2020, <https://doi.org/10.1016/j.ijpharm.2020.119983>.

[127] M. Cui *et al.*, “Effect of novel internal structures on printability and drug release behavior of 3D printed tablets,” *J. Drug Deliv. Sci. Technol.*, vol. 49, pp. 14–23, 2019, <https://doi.org/10.1016/j.jddst.2018.10.037>.

[128] A. Goyanes *et al.*, “Automated therapy preparation of isoleucine formulations using 3D printing for the treatment of MSUD: first single-centre, prospective, crossover study in patients,” *Int. J. Pharm.*, vol. 567, Art. no. 118497, 2019, <https://doi.org/10.1016/j.ijpharm.2019.118497>.

[129] T. Tagami, E. Ito, R. Kida, K. Hirose, T. Noda, and T. Ozeki, “3D printing of gummy drug formulations composed of gelatin and an HPMC-based hydrogel for pediatric use,” *Int. J. Pharm.*, vol. 594, Art.no. 120118, 2021, <https://doi.org/10.1016/j.ijpharm.2020.120118>.

[130] S. A. Khaled, J. C. Burley, M. R. Alexander, J. Yang, and C. J. Roberts, “3D printing of five-in-one dose combination polypill with defined immediate and sustained release profiles,” *J. Control. Release*, vol. 217, pp. 308–314, 2015, <https://doi.org/10.1016/j.jconrel.2015.09.028>.

[131] S. A. Khaled, J. C. Burley, M. R. Alexander, J. Yang, and C. J. Roberts, “3D printing of tablets containing multiple drugs with defined release profiles,” *Int. J. Pharm.*, vol. 494, no. 2, pp. 643–650, 2015, <https://doi.org/10.1016/j.ijpharm.2015.07.067>.

[132] M. S. Algahtani, A. A. Mohammed, J. Ahmad, M. M. Abdullah, and E. Saleh, “3D printing of dapagliflozin containing self-nanoemulsifying tablets: formulation design and in vitro

characterization," *Pharmaceutics*, vol. 13, no. 7, Art. no. 993, 2021, <https://doi.org/10.3390/pharmaceutics13070993>.

[133] H. Öblom, E. Sjöholm, M. Rautamo, and N. Sandler, "Towards printed pediatric medicines in hospital pharmacies: comparison of 2D and 3D-printed orodispersible warfarin films with conventional oral powders in unit dose sachets," *Pharmaceutics*, vol. 11, no. 7, Art. no. 334, 2019, <https://doi.org/10.3390/pharmaceutics11070334>.

[134] E. Sjöholm and N. Sandler, "Additive manufacturing of personalized orodispersible warfarin films," *Int. J. Pharm.*, vol. 564, pp. 117–123, 2019, <https://doi.org/10.1016/j.ijpharm.2019.04.018>.

[135] J. Elbl, J. Gajdziok, and J. Kolarczyk, "3D printing of multilayered orodispersible films with in-process drying," *Int. J. Pharm.*, vol. 575, Art. no. 118883, 2020, <https://doi.org/10.1016/j.ijpharm.2019.118883>.

[136] H.-G. Yi *et al.*, "A 3D-printed local drug delivery patch for pancreatic cancer growth suppression," *J. Control. Release*, vol. 238, pp. 231–241, 2016, <https://doi.org/10.1016/j.jconrel.2016.06.015>.

[137] M. Wu *et al.*, "Assisted 3D printing of microneedle patches for minimally invasive glucose control in diabetes," *Mater. Sci. Eng. C*, vol. 117, Art. no. 111299, 2020, <https://doi.org/10.1016/j.msec.2020.111299>.

[138] J. Holländer, R. Hakala, J. Suominen, N. Moritz, J. Yliruusi, and N. Sandler, "3D printed UV light cured polydimethylsiloxane devices for drug delivery," *Int. J. Pharm.*, vol. 544, no. 2, pp. 433–442, 2018, <https://doi.org/10.1016/j.ijpharm.2017.11.016>.

[139] A. J. Kyser *et al.*, "Formulation and characterization of pressure-assisted microsyringe 3D-printed scaffolds for controlled intravaginal antibiotic release," *Int. J. Pharm.*, vol. 641, Art. no. 123054, 2023, <https://doi.org/10.1016/j.ijpharm.2023.123054>.

[140] A. Khairuzzaman, "Regulatory perspectives on 3D printing in pharmaceuticals," in *3D Printing of Pharmaceuticals*, 1st ed., A. W. Basit and S. Gaisford, Eds. Cham, Switzerland: Springer, 2018, pp. 215–236. <https://doi.org/10.1007/978-3-319-90755-0_11>.

[141] S. Naghieh and X. Chen, "Printability–a key issue in extrusion-based bioprinting," *J. Pharm. Anal.*, vol. 11, no. 5, pp. 564–579, 2021, <https://doi.org/10.1016/j.jpha.2021.02.001>.

[142] H. Tong, J. Zhang, J. Ma, and J. Zhang, "Perspectives on 3D printed personalized medicines for pediatrics," *Int. J. Pharm.*, vol. 653, Art. no. 123867, 2024, <https://doi.org/10.1016/j.ijpharm.2024.123867>.

[143] L. Rodríguez-Pombo *et al.*, "Paediatric clinical study of 3D printed personalised medicines for rare metabolic disorders," *Int. J. Pharm.*, vol. 657, Art. no. 124140, 2024, <https://doi.org/10.1016/j.ijpharm.2024.124140>.

[144] I. Seoane-Viaño, S. J. Trenfield, A. W. Basit, and A. Goyanes, "Translating 3D printed pharmaceuticals: from hype to real-world clinical applications," *Adv. Drug Deliv. Rev.*, vol. 174, pp. 553–575, 2021, <https://doi.org/10.1016/j.addr.2021.05.003>.

[145] N. Beer *et al.*, "Scenarios for 3D printing of personalized medicines - a case study," *Explor. Res. Clin. Soc. Pharm.*, vol. 4, Art. no. 100073, 2021, <https://doi.org/10.1016/j.rcsop.2021.100073>.

[146] S. Mao, J. Xu, C. Cai, O. Germershaus, A. Schaper, and T. Kissel, "Effect of WOW process parameters on morphology and burst release of FITC-dextran loaded PLGA microspheres," *Int. J. Pharm.*, vol. 334, no. 1–2, pp. 137–148, 2007, <https://doi.org/10.1016/j.ijpharm.2006.10.036>.

[147] C. Wischke and S. P. Schwendeman, “Principles of encapsulating hydrophobic drugs in PLA/PLGA microparticles,” *Int. J. Pharm.*, vol. 364, no. 2, pp. 298–327, 2008, <https://doi.org/10.1016/j.ijpharm.2008.04.042>.

[148] F. Ito, H. Fujimori, and K. Makino, “Incorporation of water-soluble drugs in PLGA microspheres,” *Colloids Surf. B: Biointerfaces*, vol. 54, no. 2, pp. 173–178, 2007, <https://doi.org/10.1016/j.colsurfb.2006.10.019>.

[149] A. Dobhal, A. Srivastav, P. Dandekar, and R. Jain, “Influence of lactide vs glycolide composition of poly (lactic-co-glycolic acid) polymers on encapsulation of hydrophobic molecules: molecular dynamics and formulation studies,” *J. Mater. Sci.: Mater. Med.*, vol. 32, no. 10, p. 126, 2021, <https://doi.org/10.1007/s10856-021-06580-0>.

[150] J. Lange *et al.*, “Molecular dynamic simulation of oxaliplatin diffusion in poly(lactic acid- *co* -glycolic acid). Part A: parameterization and validation of the force-field CVFF: molecular dynamic simulation of oxaliplatin diffusion,” *Macromol. Theory Simul.*, vol. 25, no. 1, pp. 45–62, 2016, <https://doi.org/10.1002/mats.201500049>.

[151] P. R. de Souza Mendes, A. A. Alicke, and R. L. Thompson, “Parallel-plate geometry correction for transient rheometric experiments,” *Appl. Rheol.*, vol. 24, Art. no. 52721, 2014, <https://doi.org/10.3933/APPLRHEOL-24-52721>.

[152] S. Pawelczyk, M. Kniepkamp, S. Jesinghausen, and H.-J. Schmid, “Absolute rheological measurements of model suspensions: influence and correction of wall slip prevention measures,” *Materials*, vol. 13, no. 2, Art. no. 467, 2020, <https://doi.org/10.3390/ma13020467>.

[153] A.-M. Yousefi *et al.*, “Controlling the extrudate swell in melt extrusion additive manufacturing of 3D scaffolds: a designed experiment,” *J. Biomater. Sci. Polym. Ed.*, vol. 29, no. 3, pp. 195–216, 2018, <https://doi.org/10.1080/09205063.2017.1409022>.

[154] E. Naseri, H. Butler, W. MacNevin, M. Ahmed, and A. Ahmadi, “Low-temperature solvent-based 3D printing of PLGA: a parametric printability study,” *Drug Dev. Ind. Pharm.*, vol. 46, no. 2, pp. 173–178, 2020, <https://doi.org/10.1080/03639045.2019.1711389>.

[155] S. Kyle, Z. M. Jessop, A. Al-Sabah, and I. S. Whitaker, “‘Printability’ of candidate biomaterials for extrusion based 3D printing: state-of-the-art,” *Adv. Healthc. Mater.*, vol. 6, no. 16, Art. no. 1700264, 2017, <https://doi.org/10.1002/adhm.201700264>.

[156] D. Therriault, S. R. White, and J. A. Lewis, “Rheological behavior of fugitive organic inks for direct-write assembly,” *Appl. Rheol.*, vol. 17, no. 1, Art. no. 10112, pp. 1–8, 2007, <https://doi.org/10.1515/arh-2007-0001>.

[157] A. Jaklenec, E. Wan, M. E. Murray, and E. Mathiowitz, “Novel scaffolds fabricated from protein-loaded microspheres for tissue engineering,” *Biomaterials*, vol. 29, no. 2, pp. 185–192, 2008, <https://doi.org/10.1016/j.biomaterials.2007.09.017>.

[158] Z. Jaworski, T. Spychaj, A. Story, and G. Story, “Carbomer microgels as model yield-stress fluids,” *Rev. Chem. Eng.*, vol. 38, no. 7, pp. 881–919, 2022, <https://doi.org/10.1515/revce-2020-0016>.

[159] M. L. Houchin and E. M. Topp, “Chemical degradation of peptides and proteins in PLGA: a review of reactions and mechanisms,” *J. Pharm. Sci.*, vol. 97, no. 7, pp. 2395–2404, 2008, <https://doi.org/10.1002/jps.21176>.

[160] H. K. Makadia and S. J. Siegel, “Poly lactic-co-glycolic acid (PLGA) as biodegradable controlled drug delivery carrier,” *Polymers*, vol. 3, no. 3, pp. 1377–1397, 2011, <https://doi.org/10.3390/polym3031377>.

[161] H. A. Barnes, “A review of the rheology of filled viscoelastic systems,” *Rheol. Rev.*, pp. 1–36, 2003.

[162] É. Guazzelli and O. Pouliquen, “Rheology of dense granular suspensions,” *J. Fluid Mech.*, vol. 852, 2018, <https://doi.org/10.1017/jfm.2018.548>.

[163] M. Li, O. Rouaud, and D. Poncelet, “Microencapsulation by solvent evaporation: state of the art for process engineering approaches,” *Int. J. Pharm.*, vol. 363, no. 1–2, pp. 26–39, 2008, <https://doi.org/10.1016/j.ijpharm.2008.07.018>.

[164] P. R. Varges, C. M. Costa, B. S. Fonseca, M. F. Naccache, and P. R. de Souza Mendes, “Rheological characterization of Carbopol® dispersions in water and in water/glycerol solutions,” *Fluids*, vol. 4, no. 1, Art. no. 3, 2019, <https://doi.org/10.3390/fluids4010003>.

[165] Z. Chen *et al.*, “3D printing of multifunctional hydrogels,” *Adv. Funct. Mater.*, vol. 29, no. 20, Art. no. 1900971, 2019, <https://doi.org/10.1002/adfm.201900971>.

[166] T. F. Tadros, *Rheology of dispersions: principles and applications*. Weinheim, Germany: Wiley, 2010. <https://doi.org/10.1002/9783527631568>.

[167] C. R. Wildemuth and M. C. Williams, “Viscosity of suspensions modeled with a shear-dependent maximum packing fraction,” *Rheol. Acta*, vol. 23, pp. 627–635, 1984, <https://doi.org/10.1007/BF01438803>.

[168] H. Woods *et al.*, “Rheological considerations for binder development in direct ink writing of energetic materials,” *Propellants, Explos. Pyrotech.*, vol. 45, no. 1, pp. 26–35, 2020, <https://doi.org/10.1002/prep.201900159>.

[169] S. Migliozzi, G. Meridiano, P. Angeli, and L. Mazzei, “Investigation of the swollen state of Carbopol molecules in non-aqueous solvents through rheological characterization,” *Soft Matter*, vol. 16, no. 42, pp. 9799–9815, 2020, <https://doi.org/10.1039/D0SM01196G>.

[170] B. Nan, P. Gołębiewski, R. Buczyński, F. J. Galindo-Rosales, and J. M. F. Ferreira, “Direct ink writing glass: a preliminary step for optical application,” *Materials*, vol. 13, no. 7, Art. no. 1636, 2020, <https://doi.org/10.3390/ma13071636>.

[171] G. J. Donley, P. K. Singh, A. Shetty, and S. A. Rogers, “Elucidating the G″ overshoot in soft materials with a yield transition via a time-resolved experimental strain decomposition,” *Proc. Natl. Acad. Sci. U.S.A.*, vol. 117, no. 36, pp. 21945–21952, 2020, <https://doi.org/10.1073/pnas.2003869117>.

[172] M. Dinkgreve, J. Paredes, M. M. Denn, and D. Bonn, “On different ways of measuring ‘the’ yield stress,” *J. Non-Newton. Fluid Mech.*, vol. 238, pp. 233–241, 2016, <https://doi.org/10.1016/j.jnnfm.2016.11.001>.

[173] A. C. K. Sato, Perrechil, Fabiana A., and R. L. Cuncha, “Rheological behavior of suspensions dispersed in non-Newtonian matrix,” *Appl. Rheol.*, vol. 23, Art. no. 45397, 2013, <https://doi.org/10.3933/APPLRHEOL-23-45397>.

[174] M. R. Kamal and A. Mutel, “Rheological properties of suspensions in Newtonian and non-Newtonian fluids,” *J. Polym. Eng.*, vol. 5, no. 4, 1985, <https://doi.org/10.1515/POLYENG.1985.5.4.293>.

[175] M. Kroupa, M. Soos, and J. Kosek, “Slip on a particle surface as the possible origin of shear thinning in non-Brownian suspensions,” *Phys. Chem. Chem. Phys.*, vol. 19, no. 8, pp. 5979–5984, 2017, <https://doi.org/10.1039/C6CP07666A>.

[176] P. Wilms, J. Hinrichs, and R. Kohlus, “Macroscopic rheology of non-Brownian suspensions at high shear rates: the influence of solid volume fraction and non-Newtonian behaviour of the liquid phase,” *Rheol. Acta*, vol. 61, pp. 123–138, 2022, <https://doi.org/10.1007/s00397-021-01320-1>.

[177] L. Zhang *et al.*, “High internal phase pickering emulsion stabilized by sea bass protein microgel particles: food 3D printing application,” *Food Hydrocoll.*, vol. 131, Art. no. 107744, 2022, <https://doi.org/10.1016/j.foodhyd.2022.107744>.

[178] P. Lidon, L. Villa, and S. Manneville, “Power-law creep and residual stresses in a carbopol gel,” *Rheol. Acta*, vol. 56, pp. 307–323, 2017, <https://doi.org/10.1007/s00397-016-0961-4>.

[179] M. R. Sommer, L. Alison, C. Minas, E. Tervoort, P. A. Rühs, and A. R. Studart, “3D printing of concentrated emulsions into multiphase biocompatible soft materials,” *Soft Matter*, vol. 13, no. 9, pp. 1794–1803, 2017, <https://doi.org/10.1039/C6SM02682F>.

[180] S. Xin, D. Chimene, J. E. Garza, A. K. Gaharwar, and D. L. Alge, “Clickable PEG hydrogel microspheres as building blocks for 3D bioprinting,” *Biomater. Sci.*, vol. 7, no. 3, pp. 1179–1187, 2019, <https://doi.org/10.1039/C8BM01286E>.

[181] S. Xin *et al.*, “Generalizing hydrogel microparticles into a new class of bioinks for extrusion bioprinting,” *Sci. Adv.*, vol. 7, no. 42, Art. no. eabk3087, 2021, <https://doi.org/10.1126/sciadv.abk3087>.

[182] S. Jang *et al.*, “Effect of material extrusion process parameters on filament geometry and inter-filament voids in as-fabricated high solids loaded polymer composites,” *Addit. Manuf.*, vol. 47, Art. no. 102313, 2021, <https://doi.org/10.1016/j.addma.2021.102313>.

[183] C. Oelschlaeger, J. Marten, F. Péridont, and N. Willenbacher, “Imaging of the microstructure of Carbopol dispersions and correlation with their macroelasticity: a micro- and macrorheological study,” *J. Rheol.*, vol. 66, no. 4, pp. 749–760, 2022, <https://doi.org/10.1122/8.0000452>.

[184] B. Xia and P. S. Krueger, “Rheology of particulate suspensions with non-Newtonian fluids in capillaries,” *Proc. R. Soc. A: Math. Phys. Eng. Sci.*, vol. 478, no. 2262, Art. no. 20210615, 2022, <https://doi.org/10.1098/rspa.2021.0615>.

[185] J. Z. Liang, “Effects of extrusion conditions on die-swell behavior of polypropylene/diatomite composite melts,” *Polym. Test.*, vol. 27, no. 8, pp. 936–940, 2008, <https://doi.org/10.1016/j.polymertesting.2008.08.001>.

[186] A. K. Mehrjerdi, T. Bashir, and M. Skrifvars, “Melt rheology and extrudate swell properties of talc filled polyethylene compounds,” *Heliyon*, vol. 6, no. 5, Art. no. e04060, 2020, <https://doi.org/10.1016/j.heliyon.2020.e04060>.

[187] A. Zidan *et al.*, “Extrudability analysis of drug loaded pastes for 3D printing of modified release tablets,” *Int. J. Pharm.*, vol. 554, pp. 292–301, 2019, <https://doi.org/10.1016/j.ijpharm.2018.11.025>.

[188] A. Ribeiro *et al.*, “Assessing bioink shape fidelity to aid material development in 3D bioprinting,” *Biofabrication*, vol. 10, no. 1, Art. no. 014102, 2017, <https://doi.org/10.1088/1758-5090/aa90e2>.

[189] F. Cai, S. Heid, and A. R. Boccaccini, “Potential of Laponite® incorporated oxidized alginate–gelatin (ADA-GEL) composite hydrogels for extrusion-based 3D printing,” *J. Biomed. Mater. Res. - B Appl. Biomater.*, vol. 109, no. 8, pp. 1090–1104, 2021, <https://doi.org/10.1002/jbm.b.34771>.

[190] J. Ghorbani, P. Koirala, Y.-L. Shen, and M. Tehrani, “Eliminating voids and reducing mechanical anisotropy in fused filament fabrication parts by adjusting the filament extrusion rate,” *J. Manuf. Process.*, vol. 80, pp. 651–658, 2022, <https://doi.org/10.1016/j.jmapro.2022.06.026>.

[191] J. Wang and L. L. Shaw, “Rheological and extrusion behavior of dental porcelain slurries for rapid prototyping applications,” *Mater. Sci. Eng. A.*, vol. 397, no. 1–2, pp. 314–321, 2005, <https://doi.org/10.1016/j.msea.2005.02.045>.

[192] G. Vozzi, A. Previti, D. de Rossi, and A. Ahluwalia, “Microsyringe-based deposition of two-dimensional and three-dimensional polymer scaffolds with a well-defined geometry for application to tissue engineering,” *Tissue Eng.*, vol. 8, no. 6, pp. 1089–1098, 2002, <https://doi.org/10.1089/107632702320934182>.

[193] H. Yuk and X. Zhao, “A new 3D printing strategy by harnessing deformation, instability, and fracture of viscoelastic inks,” *Adv. Mater.*, vol. 30, no. 6, Art. no. 1704028, 2018, <https://doi.org/10.1002/adma.201704028>.

[194] J. Bauer, A. Schroer, R. Schwaiger, and O. Kraft, “Approaching theoretical strength in glassy carbon nanolattices,” *Nat. Mater.*, vol. 15, pp. 438–443, 2016, <https://doi.org/10.1038/nmat4561>.

[195] D. Oran *et al.*, “3D nanofabrication by volumetric deposition and controlled shrinkage of patterned scaffolds,” *Science*, vol. 362, no. 6420, pp. 1281–1285, 2018, <https://doi.org/10.1126/science.aau5119>.

[196] E. Davoodi, H. Montazerian, A. Khademhosseini, and E. Toyserkani, “Sacrificial 3D printing of shrinkable silicone elastomers for enhanced feature resolution in flexible tissue scaffolds,” *Acta Biomater.*, vol. 117, pp. 261–272, 2020, <https://doi.org/10.1016/j.actbio.2020.10.001>.

[197] J. Pohjola, M. Jokinen, T. Soukka, and M. Stolt, “Polymer microsphere inks for semi-solid extrusion 3D printing at ambient conditions,” *J. Mech. Behav. Biomed. Mater.*, vol. 160, Art. no. 106783, 2024, <https://doi.org/10.1016/j.jmbbm.2024.106783>.

[198] L.-C. Gerhardt and A. R. Boccaccini, “Bioactive glass and glass-ceramic scaffolds for bone tissue engineering,” *Materials*, vol. 3, no. 7, pp. 3867–3910, 2010, <https://doi.org/10.3390/ma3073867>.

[199] C. Cai *et al.*, “Influence of morphology and drug distribution on the release process of FITC-dextran-loaded microspheres prepared with different types of PLGA,” *J. Microencapsul.*, vol. 26, no. 4, pp. 334–345, 2009, <https://doi.org/10.1080/02652040802354707>.

[200] J. J. Elsner, A. Shefy-Peleg, and M. Zilberman, “Novel biodegradable composite wound dressings with controlled release of antibiotics: microstructure, mechanical and physical properties,” *J. Biomed. Mater. Res. - B Appl. Biomater.*, vol. 93B, no. 2, pp. 425–435, 2010, <https://doi.org/10.1002/jbm.b.31599>.

[201] J. J. Elsner and M. Zilberman, “Antibiotic-eluting bioresorbable composite fibers for wound healing applications: microstructure, drug delivery and mechanical properties,” *Acta Biomater.*, vol. 5, no. 8, pp. 2872–2883, 2009, <https://doi.org/10.1016/j.actbio.2009.04.007>.

[202] W. D. Rhine, D. S. T. Hsieh, and R. Langer, “Polymers for sustained macromolecule release: procedures to fabricate reproducible delivery systems and control release kinetics,” *J. Pharm. Sci.*, vol. 69, no. 3, pp. 265–270, 1980, <https://doi.org/10.1002/jps.2600690305>.

[203] T. Ehtezazi and C. Washington, “Controlled release of macromolecules from PLA microspheres: using porous structure topology,” *J. Control. Release*, vol. 68, no. 3, pp. 361–372, 2000, <https://doi.org/10.1016/S0168-3659(00)00270-4>.

[204] C. Berkland, K. Kyekyoon, and D. W. Pack, “PLG microsphere size controls drug release rate through several competing factors,” *Pharm. Res.*, vol. 20, pp. 1055–1062, 2003, <https://doi.org/10.1023/A:1024466407849>.

[205] K. Fu, D. W. Pack, A. M. Klibanov, and R. Langer, “Visual evidence of acidic environment within degrading poly(lactic-co-glycolic acid) (PLGA) microspheres,” *Pharm. Res.*, vol. 17, pp. 100–106, 2000, <https://doi.org/10.1023/A:1007582911958>.

[206] J. Siepmann, K. Elkharraz, F. Siepmann, and D. Klose, “How autocatalysis accelerates drug release from PLGA-based microparticles: a quantitative treatment,” *Biomacromolecules*, vol. 6, no. 4, pp. 2312–2319, 2005, <https://doi.org/10.1021/bm050228k>.

[207] M. Stolt, K. Krasowska, M. Rutkowska, H. Janik, A. Rosling, and A. Södergård, “More on the poly(L-lactide) prepared using ferrous acetate as catalyst,” *Polym. Int.*, vol. 54, no. 2, pp. 362–368, 2005, <https://doi.org/10.1002/pi.1691>.

[208] C. Bassand, J. Verin, M. Lamatsch, F. Siepmann, and J. Siepmann, "How agarose gels surrounding PLGA implants limit swelling and slow down drug release," *J. Control. Release*, vol. 343, pp. 255–266, 2022, <https://doi.org/10.1016/j.jconrel.2022.01.028>.

[209] F. Yang *et al.*, "Development of poly (lactic-co-glycolic acid) (PLGA) based implants using hot melt extrusion (HME) for sustained release of drugs: the impacts of PLGA's material characteristics," *Int. J. Pharm.*, vol. 663, Art. no. 124556, 2024, <https://doi.org/10.1016/j.ijpharm.2024.124556>.

[210] H. Gasmi, F. Danede, J. Siepmann, and F. Siepmann, "Does PLGA microparticle swelling control drug release? New insight based on single particle swelling studies," *J. Control. Release*, vol. 213, pp. 120–127, 2015, <https://doi.org/10.1016/j.jconrel.2015.06.039>.

[211] H. Gasmi, J.-F. Willart, F. Danede, M. C. Hamoudi, J. Siepmann, and F. Siepmann, "Importance of PLGA microparticle swelling for the control of prilocaine release," *J. Drug Deliv. Sci. Technol.*, vol. 30, Part A, pp. 123–132, 2015, <https://doi.org/10.1016/j.jddst.2015.10.009>.

[212] B. Gu, X. Sun, F. Papadimitrakopoulos, and D. J. Burgess, "Seeing is believing, PLGA microsphere degradation revealed in PLGA microsphere/PVA hydrogel composites," *J. Control. Release*, vol. 228, pp. 170–178, 2016, <https://doi.org/10.1016/j.jconrel.2016.03.011>.

[213] C. E. Rapier, K. J. Shea, and A. P. Lee, "Investigating PLGA microparticle swelling behavior reveals an interplay of expansive intermolecular forces," *Sci. Rep.*, vol. 11, Art. no. 14512, 2021, <https://doi.org/10.1038/s41598-021-93785-6>.

[214] R. A. Siegel and R. Langer, "Controlled release of polypeptides and other macromolecules," *Pharm. Res.*, vol. 1, pp. 2–10, 1984, <https://doi.org/10.1023/A:1016318423563>.

[215] S. Fredenberg, M. Reslow, and A. Axelsson, "Encapsulated zinc salt increases the diffusion of protein through PLG films," *Int. J. Pharm.*, vol. 370, no. 1–2, pp. 47–53, 2009, <https://doi.org/10.1016/j.ijpharm.2008.11.017>.

TURUN
YLIOPISTO
UNIVERSITY
OF TURKU

Painosalama, Turku, Finland 2025

ISBN 978-952-02-0386-3 (PRINT)
ISBN 978-952-02-0387-0 (PDF)
ISSN 2736-9390 (Print)
ISSN 2736-9684 (Online)